UAB

Universitat Autònoma de Barcelona

Department of Telecommunications and Systems Engineering

Direct Bandpass Methodology for Synthesis and Design of Stand-Alone Filters and Duplexers Based on Acoustic Wave Technologies

Ph.D. Dissertation in Electrical and Telecommunications Engineering by

Iuliia Evdokimova
E-mail: Iuliia.Evdokimova@uab.cat

Thesis Advisor: Prof. Pedro de Paco Sánchez
E-mail: Pedro.depaco@uab.cat
Universitat Autònoma de Barcelona (UAB)
Escola d'Enginyeria

May, 2018

UAB
Universitat Autònoma de Barcelona

The undersigned, Dr. Pedro de Paco Sánchez, Professor of the Department of Telecommunications and Systems Engineering (Engineering School) of the Universitat Autònoma de Barcelona (UAB),

CERTIFIES:
that the thesis entitled "Direct Bandpass Methodology for Synthesis and Design of Stand-Alone Filters and Duplexers Based on Acoustic Wave Technologies" has been written by Iuliia Evdokimova under his supervision.

And hereby to acknowledge the above, sign the present.

Dr. Pedro de Paco Sánchez   Iuliia Evdokimova

Ph.D. in Electrical and Telecommunication Engineering
Department of Telecommunications and Systems Engineering
Universitat Autònoma de Barcelona (UAB)

Bellaterra (Cerdanyola del Vallès), May 2018

iv

Abstract

Today, constant end-user demands have become the engine of technological progress. Evolution of mobile phones and telecommunication standards is a clear example of fast technological breakthrough which continues to be improved. Nowadays, it is impossible to imagine our life without a mobile phone. Thanks to mobile Internet development, we have got unlimited opportunities. In order to maintain an ever-increasing data exchange, high data rates, reduced latency, and broadband data services have become objects of constant technological improvement. Emerged 4G network standard in deployment and upcoming 5G standard will require even more challenging enhancement of these key characteristics, affecting the entire mobile handset, but especially filtering systems.

The main objective of this thesis is to provide an advanced synthesis techniques for ladder-type acoustic filters, duplexers, and multiplexers, taking into account technological constraints which become more stringent in course of time. Classical synthesis methodologies may not be sufficient in order to tackle future technological innovations. Even optimization techniques, mostly used in industry of acoustic filters, can be very time consuming in these new conditions. In order to provide an accurate result compatible with advanced technology on the whole frequency range, direct bandpass synthesis methodology is developed in this work. The method is particularly useful for intra-band and inter-band Carrier Aggregation where phase evaluation at frequency far away from the passband has to be of the highest accuracy in order to avoid interferences between multiple transmitter and receiver channels.

One of the most important aspects of acoustic filter' design is accommodation of technological constraints and mask specification fulfillment. This thesis takes into account such important technological parameters as effective coupling coefficient of each resonator, resonant frequencies, stored energy, occupied filter area, and quality factor. Described synthesis techniques analytically analyze and manage these constraints so as to provide the best possible result within the range of specified parameters.

Special attention is paid to quality factor management of acoustic resonator. When quality factor is taken into account directly in synthesis procedure, special features of transmission and reflection response can be obtained. In this case, designed filter is called "lossy" and it is characterized by finite dimensions. Certain distribution of quality factor of each resonator can maintain the flatness of passband and avoid edge rounding, thus maintaining the transmitted and received information. Proposed methodology of lossy acoustic filter synthesis accommodates the technological constraints and manage losses of every resonator so that an optimum filter based on acoustic waves can be obtained.

Resumen

Hoy en día, constantes exigencias del usuario han llegado a ser el motor del progreso tecnológico. La evolución de los teléfonos móviles y de los estándares de telecomunicaciones es un claro ejemplo de rápido avance tecnológico que continúa mejorando. Actualmente, es imposible imaginar nuestra vida sin un teléfono móvil. Gracias al desarrollo de Internet móvil, ahora tenemos variedad de oportunidades sin límites. Para mantener el nivel de intercambio de datos cada vez mayor, la alta velocidad, la latencia reducida y los servicios de banda ancha se han convertido en los objetos de constante mejora tecnológica. Emergido estándar de red 4G en el estado de difusión y próximo estándar 5G requerirán una mejora aún más desafiante de estas características clave, afectando a todo el dispositivo móvil, pero especialmente a los sistemas de filtrado.

El objetivo principal de esta tesis es proporcionar técnicas avanzadas de síntesis para diseño de filtros de topología en escalera, duplexores y multiplexores, teniendo en cuenta las limitaciones tecnológicas que se vuelven más estrictas en el transcurso del tiempo. Las clásicas metodologías de síntesis pueden no ser suficientes para abordar innovaciones tecnológicas futuras. Incluso las técnicas de optimización frecuentemente utilizadas en la industria de filtros acústicos pueden consumir mucho tiempo en estas nuevas condiciones. Con el fin de proporcionar un resultado de alta precisión compatible con tecnología avanzada en todo el rango de frecuencias, en esta tesis se desarrolla la metodología de síntesis directa en paso banda. El método es especialmente útil para *Carrier Aggregation* de bandas contiguas y no contiguas, donde la evaluación de fase a una frecuencia alejada de la banda de paso debe ser de mayor precisión para evitar interferencias entre múltiples canales de transmisores y receptores.

Uno de los aspectos más importantes del diseño del filtro acústico es la adaptación de las restricciones tecnológicas y el cumplimiento de máscara. Esta tesis tiene en cuenta diferentes parámetros tecnológicos como el coeficiente de acoplamiento efectivo de cada resonador, frecuencias de resonancia, energía almacenada, área de filtro ocupada y factor de calidad. Las técnicas de síntesis descritas analizan y gestionan estas restricciones para proporcionar el mejor resultado posible dentro del rango de parámetros especificados.

Se presta especial atención a la gestión de factor de calidad del resonador acústico. Cuando el factor de calidad se tiene en cuenta directamente en el procedimiento de síntesis, se puede obtener características especiales de la respuesta en transmisión y reflexión. En este caso, el filtro diseñado se denomina "lossy" y se caracteriza por dimensiones finitas. Cierta distribución del factor de calidad de cada resonador puede mantener la planitud de la banda de paso y evitar el redondeo de los bordes, manteniendo así la información transmitida y recibida. La metodología propuesta de síntesis de filtro acústico lossy acomoda las restricciones tecnológicas y gestiona las pérdidas de cada resonador de tal manera que se puede obtener un filtro óptimo.

x

Acknowledgements

I am very pleased of having passed the Ph.D. program in Department of Telecommunications and Systems Engineering of Universitat Autònoma de Barcelona. I was very lucky to join the research group of Antennas and Microwave Systems, and to have Prof. Pedro de Paco as my supervisor. My first special thanks goes to him for his valuable advices, dedicated time, guidance and encouragement in tough moments. His professional and personal qualities helped me to grow as a specialist in micro-acoustic technology.

Also, I would like to express my gratitude to all members of Antennas and Microwave Systems group, especially to Dr. Jordi Verdú, Prof. Josep Parrón, and Prof. Gary Junkin for sharing their professional and educational experience with me. Moreover, I would like to mention Ernesto Díaz for great technical assistance.

In addition, I would like to give my sincere thanks to my past and current roommates: Mercedes, Alfred, Ángel, and Patricia for our endless conversations and laugh. Also, I would like to extend my gratitude to my other colleagues: Alex, Yi, Dani, Vicente, Toni, Guillem, Ivan, Edwar, Giulio, Edith, and Dani. Special thanks goes to Sergi for his support, understanding, and constant jokes.

Work apart, I would like to express my exceptional gratitude to Albert for his kind support and motivation, especially in tough moments, and to my "spanish family", Ana, Juan, Inma, and Pedro, for their sincere interest and encouragement throughout these years.

Moreover, I would like to thank my dear family for their unconditional support that I felt at a distance. My parents, Nursiia and Alexandr, and my brother Valentin, thank you for helping and believing in me. Also, I would like to mention my close friends: Anatoliy, Viktor, Konstantin, Ilya, Evgeniy, Margarita, and Liliya, for being always there and for sending me encouraging messages. Special acknowledgement goes to Prof. V.B. Yankevich for his advices, support, and interest in my career.

Finally, I thank everybody who influenced on my research activity directly and indirectly, without you my professional progress would not be possible. Thanks.

Contents

List of Figures

List of Tables

Introduction

Nowadays, mobile personal devices have an extreme popularity. People use their phones to consume not only messaging and social media services but also entertainment content, e-commerce, educational and government assistance, and others. Responding to consumer demand, the mobile industry has constantly been improving mobile technologies, presenting 2G (GSM, GPRS, EDGE), 3G (W-CDMA, HSDPA) and 4G (LTE, LTE-A) networks including mobile Internet and smartphones' propagation.

In 2017 more than 5 billion people were connected to mobile services, and it is expected that this number will reach 5.9 billion by 2025 which is equivalent to 71% of the world's population [1]. Here, the most important growth will lie in mobile Internet, providing 1.75 billion new users over the next eight years.

The 4G network technology will take the leading position in 2019 with more than 3 billion connections. Meanwhile, the mobile industry continues to advance in next generation of mobile networks, 5G, making successful pilot testing. In December 2017 new radio specifications for non-standalone 5G were approved in the 3rd Generation Partnership Project (3GPP) Release 15 [2], and throughout next three years USA and major markets of Asia and Europe will launch first 5G technology connections. By the end of 2025, it is expected more than 1.2 billion 5G connections around the world. At the same time, smartphones will become the most popular handset growing by 20% in period from 2017 to 2025.

According to Ericsson [3], global mobile data traffic for all devices will increase eightfold between 2017 and 2023, achieving 110 exabytes (1 exabyte = 10^{18} bytes) per month. Video-based content consumption is constantly increasing, and by 2023 video will be performed by 75% of world mobile data traffic. Advanced video technologies such as 4K and 8K UHD, 360-degree video would also have more influence on traffic since data will become more intensive.
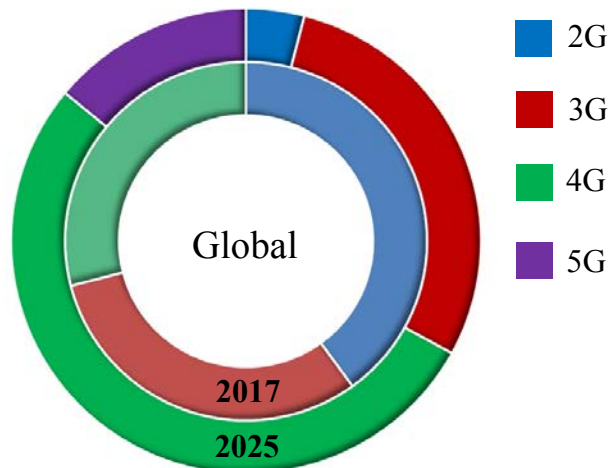
Figure 1.1: Network technology mix in 2017 and 2025. Source: GSMA Intelligence data, December 2017 [1].

Initially, 4G networks with new advanced functionalities, such as Carries Aggregation (CA) and Multiple Input Multiple Output (MIMO), are expected to continue providing Gbit/s download speeds in response to increasing demands. However, in order to provide higher data rates needed for future broadband services and applications, an additional spectrum available to support 5G subscription growth has to be involved. Two principal bandwidths in 26 GHz band (24.25 – 27.50 GHz) and in 28 GHz band (26.5 – 29.5 GHz) are assigned for 5G connections. The 38 GHz and 42 GHz bands are also being considered as additional resources to support 5G requirements. Nevertheless, an intermediate network generation 4.5G (LTE-Advanced Pro) operating on frequency bands below 6 GHz, and preparing a smooth transition to 5G standard has been also considered to be implemented [4]. As a result, 4G, 4.5G, and 5G will represent the majority of connections in 2025 illustrated in Figure 1.1.

Multiple MIMO technology (M-MIMO) will play an important role in 5G communications, improving end-user experience, increasing network capacity and coverage, and reducing interference. Instead of 4×4 or 8×8 MIMO technology of 4G networks, in M-MIMO antenna system for 5G a number of antennas of the order of a hundred or more are expected to transmit the same signal. It will be a good solution for better spatial diversity providing reliable communication and high energy efficiency [5]. Multibeam antennas (MBAs) serve as key hardware for M-MIMO technology. At high operating frequencies of 5G and much smaller wavelength, more antennas can be implemented into an aperture with the same physical area, providing a higher gain, high-speed data transmission, and more compact device form factor [6].

Exponentially growing demand for higher data rates requires additional spectrum for efficient performance. Therefore, 3GPP introduced CA as a key technology in LTE-A [7], which allowed to increase transmission bandwidth by 20 to 100 MHz, using fragmented spectrum from different

bands. In LTE-A a component carrier (CC) can be of 1.4, 3, 5, 10, or 20 MHz, and a maximum of five CCs can be aggregated. Further 4.5G and 5G network connections will be able to combine up to 32 CCs (massive CA) of larger bandwidths for both downlink and uplink paths [8, 9].

Radio frequency (RF) filters have always been a major part of mobile phone. State-of-the-art smartphones now contain more than 60 filters [4] because of increased number of frequency bands and CA technology implementation. Further 5G networks will require even larger number of filters in addition to the difficult specifications. The best suited filters to accomplish mobile communications' requirements have always been surface acoustic wave (SAW) filters and bulk acoustic wave (BAW) filters. Unlike ceramic, dielectric and lumped element filters, acoustic wave filter technology presents high performance, small form factor, and low costs simultaneously. Typically, SAW filters are used for mobile communications from 600 MHz to 2 GHz and BAW filters operate from 1.5 GHz to 3.5 GHz. For frequencies more than 2 GHz SAW filters exhibit high parasitic losses, whereas filters based on BAW get larger in size below 1.5 GHz, so both technologies coexist in order to provide better performance in certain frequency range.

CA technology evolution complicates filter's design since each filter cannot influence on other CCs' bands to avoid interference. Therefore, increased number of CCs leads to designing multiplexers instead of duplexers [10, 11] which can be a challenging task for 4.5G and 5G network standards. Another issue to deal with is operating frequency. Starting from 5 GHz, BAW filters' losses begin to increase exponentially, and filter's size becomes unrealistically small [4]. Improved micro-acoustic technology (BAW) will likely cover the 3.5 − 6.0 GHz range, whereas SAW filters will continue to dominate lower frequencies. Thus, acoustic filters will keep their leading positions in 4G and 4.5G mobile networks. Some of the acoustic technologies could probably be implemented for 5G high frequency applications; however, filter's characteristics have to be greatly improved. Therefore, it is possible that for frequencies above 26 GHz other filtering solution, comprising high performance and form factor compatible with mobile device, has to be found.

1.1 Micro-Acoustic Technology in Cellular System

Filters based on acoustic waves are widely implemented in mobile communications thanks to their high performance which is characterized by high quality factor (Q), low insertion loss (IL), high return loss level (RL), sharp transition slopes and high rejection at out-of-band frequencies. These features are achieved by converting electromagnetic wave with a high propagation velocity to an acoustic wave with low propagation velocity, using a piezoelectric material. This fact makes possible submillimeter-sized resonators needed for reduced in size mobile phones. Two different technologies are available for communication systems: SAW and BAW, which are distinguished by direction of acoustic wave propagation in piezoelectric slab.
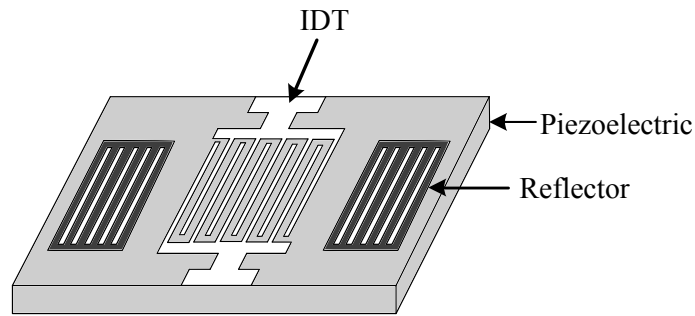
Figure 1.2: Structure of SAW resonator.

SAW RF Resonator

SAW device consists of metallic interdigital transducers (IDTs) and reflection gratings placed on piezoelectric substrate of lithium tantalate (LiTaO$_3$), as depicted in Figure 1.2 [12]. An electromagnetic signal applied to the input IDT provokes an acoustic wave which propagates along the SAW surface. The piezoelectric effect stimulates the generation of electromagnetic signal at output IDT. Thus, the achievable operating frequency of SAW resonator is limited by separation of each IDT finger. At frequencies higher than 2.5 GHz, a lithography resolution lower than 0.25 μm has to be applied to produce IDTs of needed dimensions [13], which is a challenging task for manufacturers.

Alternative IDT electrodes arrangement presented in [14] provides improved frequency response characteristics. Advanced SAW resonators with enhanced performance also include piston mode technique which improves wave guidance in a longitudinal direction and reduces losses in the bulk of the substrate [15]. An additional silicon dioxide (SiO$_2$) layer on top of IDT of temperature compensated SAW device (TC-SAW) reduces temperature variation of frequency, and in this case a piezoelectric material lithium niobate (LiNbO$_3$) has to be implemented since it provides larger resonator bandwidth [16,17]. In addition, an Incredible High Performance-SAW (IHP-SAW) device was reported in [18] which exhibits very high $Q = 3500$, low temperature coefficient of frequency (TCF), and improvement of total transmission loss in multiplexer device. Implementation of new materials such as ScAlN described in [19] offers anomalously strong piezoelectricity and low acoustic and dielectric losses in GHz range. Thus, it can be applicable to wideband and low-loss SAW filters operating over 3 GHz, where current SAW technologies may not be feasible.

BAW RF Resonator

A BAW resonator consists of a piezoelectric crystal of aluminium nitride (AlN) sandwiched between two metallic electrodes. When voltage is applied to the electrodes, the piezoelectric
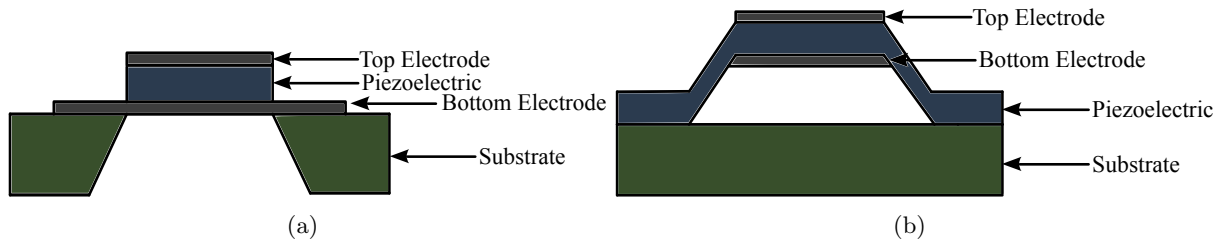
Figure 1.3: Structure of FBARs (a) with pothole membrane and (b) air gap membrane.
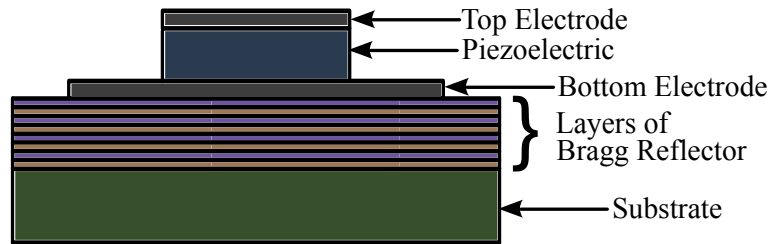
Figure 1.4: Structure of SMR.

effect provokes a vertical propagation of acoustic wave in the bulk of the structure. The resonant frequency is defined by thickness of piezoelectric film. BAW filters have lower IL and good out-of-band rejection capability, which is particularly suitable for multiplexer applications in mobile phones [13]. BAW resonators have much more complex fabrication process than in SAW technology consisting of several lithographic and deposited layers [20]. There are two types of BAW resonator which are widely used in telecommunications.

The first structure is film bulk acoustic resonator (FBAR). Depending on fabrication method, two options are possible by using pothole membrane depicted in Figure 1.3 (a) or undercut air gap membrane illustrated in Figure 1.3 (b) [21]. Here, piezoelectric film with top and bottom electrodes is acoustically isolated from a silicon (Si) carrier substrate so that the acoustic wave is reflected at the air boundaries. Additional implementation of mass adjustment structure presented in [22] improves the quality factor of the resonator. FBARs present the highest Q (up to 5000) af all acoustic filters [23]. Implementation of ruthenium (Ru) instead of molybdenum (Mo) as electrode material for high frequency applications was reported in [24], which allowed to design a filter with $Q = 3500$ at 5 GHz. Another alternative solution was proposed in [25] where single crystal AlN-on-SiC is used so that compact, low loss, wideband and high power filter can be fabricated at 3.7 GHz.

Filters based on air-gap type FBAR from Figure 1.3 (b) operating at 19 GHz and 24/29 GHz were presented in [26, 27]. These filters could be possibly implemented for 5G high frequency bands; however, an improvement of poor out-of-band rejection and IL level will be required.
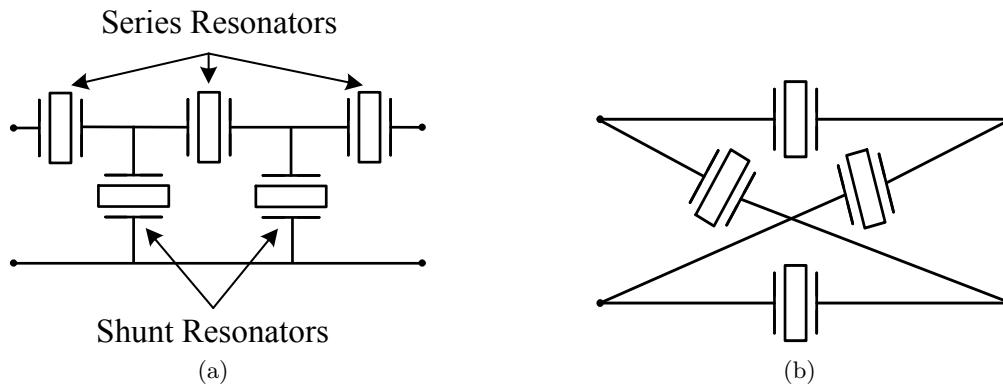
Figure 1.5: Electrically coupled filters: (a) ladder and (b) lattice topologies.

The second type of BAW technology is solidly mounted resonator (SMR) illustrated in Figure 1.4. Here, in order to confine the acoustic energy in the piezoelectric slab, the bottom electrode sits on a reflector (Bragg reflector) and the top electrode is exposed to air. Reflector is composed by oxide and metal layers of characteristic impedances and quarter-wavelength ($\lambda/4$) thicknesses to make the overall impedance close to air [28]. For high frequency applications a resonator was proposed in [29] which consists of a well-textured AlN thin film on platinum (Pt) electrodes and SiO_2/AlN Bragg reflector. The device was successfully fabricated at 8 GHz; however, its quality factor was very small (360). In the same year, an improved Bragg reflector was described in [30] where optimized layers' thicknesses different to $\lambda/4$ permitted to increase the quality factor up to 2000.

As well as in SAW technology, there is a TC-BAW fabrication methods where oxide layers of SiO_2 can be positioned below or above the electrodes, or in the middle of piezoelectric slab. Advantages and disadvantages of every SiO_2 layer position are discussed in [20, 31].

A brief review of the progress in filtering performance improvement of acoustic technology has been presented. Filters based on acoustic waves are object of constant enhancement in order to provide better service and fulfill specific requirements of developing communication networks. Thanks to their characteristics, acoustic filters will keep the leading position in mobile phones industry for at least next 10 years.

1.2   Acoustic Wave Filter Configurations

There are number of acoustic filter topologies suitable for high frequency applications, which are designed to provide certain filter characteristics [32]. Depending on the nature, two types of connection can be implemented resulting in electrically and acoustically coupled filters.

Electrically coupled bandpass networks include lattice and ladder configurations presented

in Figure 1.5, which can be used for both SAW and BAW technologies. Thanks to its low IL and symmetric passband, the most commonly used network for acoustic filters is ladder-type topology, although lattice configuration can be applied for specific implementations [33]. As it is demonstrated in Figure 1.5 (a), ladder filter consists of a number of acoustic resonators positioned in series and shunt. This type of networks provides a high selectivity since every resonator introduces a finite transmission zero (TZ) below or above the passband; however, out-of-band attenuation level is relatively poor. By increasing the number of resonators and adding reactive external elements, the rejection level can be improved. Finally, a mixed ladder-lattice topology can be elaborated providing filters with high selectivity, high out-of-band rejection, and low IL [34].

Stacked Crystal Filters (SCFs) and Coupled Resonator Filters (CRFs) topologies represent acoustically coupled BAW networks [20,35], whereas Double Mode SAW (DMS) and Multi-Mode SAW (MMS) are acoustically coupled filters in SAW technology. Since only all-pole transmission response can be obtained in such filters, they exhibit a poor selectivity, and therefore, are not used in congested spectrum of current telecommunication standards; however, CRF filters are implemented for less stringent Wi-Fi and GPS technologies [36]. Another drawback is narrow passband because of weak coupling between resonators. In [37] a solution for passband widening was proposed; however, the problem of selectivity kept on persisting. In [38] a combined ladder-DMS structure was described which exhibited a wide passband, sharp selectivity, and high rejection level, although the number of resonators and reactive elements was very large for mobile applications.

1.3 Motivation and Purpose of the Thesis

Design of acoustic filters is performed mainly to accomplish key characteristics so as to provide a perfect end-user experience. Nowadays, modern smartphones contains more than 60 filters and this number will increase with 5G standard introduction. Each time, more frequency bands are got involved and they are placed closer to each other, especially with CA technology exploitation. Use of multiplexers instead of duplexers has become a new trend in mobile filtering system. The higher communication quality becomes, the more expectations acoustic filters will have to fulfill such as better performance, smaller form factor, and cheaper price.

Manufacturers of SAW and BAW acoustic filters design stand-alone and multiplexer devices from technological point of view. That is, considering physical parameters such as material quality, layers' and electrodes' dimensions, electromagnetic and temperature influence, and package, they achieve a high performance network. A good knowledge of physical phenomena inside the filtering device and the procedures of thin film fabrication is required for the efficient use of time and resources. Therefore, in all stages of filter's design different methods of optimization are

widely used which allow to fulfill technological constraints and mask specifications within the specified range of parameters. Generally, there is a trade-off between filter's performance and complexity and costs of fabrication procedure, which has to be always taken into account.

On the other hand, simpler from the technological point of view cavity, waveguide, and other kinds of filters' technology are designed using well-established synthesis procedures, since mathematical prototype is easily matched with dimensions of the manufactured filter. Synthesis is based on mathematical lowpass prototype of the filter, choice and application of suited filtering function, calculation of characteristic polynomials, and elements' extraction procedure. Generally, aforementioned types of technology do not have a high level of fabrication complexity nor stringent technological constraints as they are designed for different fields of application.

In order to simplify and accelerate design of filters based on acoustic waves, our research group created a holistic methodology combining synthesis, topology, and technology in one mathematical tool [39]. Here, a lowpass prototype of acoustic filter is firstly elaborated taking into account mask specifications, which then is complemented with technological constraints. Unlike optimization methods, mathematical synthesis procedure takes minimum time and computational effort. A number of various solutions can be checked within some minutes since no physical prototype is required. Moreover, filters can be designed to meet a variety of requirements, thus providing different circuit values. Resulting network can then be checked for electromagnetic radiation and adjusted in order to meet needed specifications. Package influence is another aspect that has to be evaluated afterwards. In this case optimization methods can be used as an additional tool. Since suitable initial seed from the synthesis has already been found, the optimization procedure becomes fast and provides small values' variation.

The purpose of this thesis is to elevate the methodology to even higher level by presenting a direct bandpass synthesis technique with acoustic technological constraints accommodation. Lowpass approach exhibits calculation simplicity and speed, and it works well for narrowband filters. However, it also has its inherent drawbacks which can lead to impossibility of wideband filters' and multiplexers' design for 5G communication networks with their intrinsic stringent requirements. Direct bandpass technique is based on consideration that all network's elements are frequency dependent which leads to new features of transmission and reflection response. This makes the bandpass methodology more complex and numerically more instable so that an additional effort has to be directed to calculation accuracy improvement. Despite these difficulties, the bandpass approach exhibits precision of both transmission and reflection response (magnitude and phase) at any frequency, even far away from the passband. A novel bandpass phase correction methodology elaborated in this thesis allows to synthesize duplexers and multiplexers, containing both intra-band and inter-band aggregations. Taking into consideration the fast development of new network standard, 5G, bandpass synthesis methodology can be a good solution to tackle upcoming stringent specifications.

Another important aspect, which has to be taken into account in 4G and 5G communications, is flatness of IL level. When real filter with finite quality factor is considered, the edges of the passband become more rounded and the passband itself turns to be narrower. This leads to a serious problem since part of the information is lost and valuable frequency spectrum is not used efficiently. Widening the passband of filters with low-Q resonators improves IL problem but reduces selectivity. For future demanding 5G applications this selectivity degradation will not be acceptable any more. Existing techniques of lossy filter synthesis were elaborated for different kinds of technology but not for acoustic wave ladder-type filters. In this dissertation a solution for this type of filters is proposed which links flat IL level and required quality factor of every resonator by combining coupling matrix approach and optimization procedure.

1.4 Thesis Outline

In this section a brief outline of the dissertation is presented. The work consists of six chapters and reflects the research results throughout the Ph.D. program.

Chapter 1 is dedicated to the technological progress of telecommunications, especially in mobile sector. Future expectations and difficulties of new network standard, 5G, have been summarized by means of a number of recent papers, industry reports, and patents. Special attention has been paid to acoustic filter technologies, SAW and BAW, and their important role in mobile communications. A concise description of different types of acoustic resonator and their technological improvement has been presented. The main filter topologies have been described as well. Finally, the chapter concludes with motivation and main purposes of the thesis, and scientific contributions.

Chapter 2 presents the basics of lowpass methodology for ladder-type acoustic filter's and duplexer's design. At the beginning, bandpass and two corresponding lowpass models of acoustic resonator are outlined, which compound a lowpass nodal representation of ladder-type topology. Then, important features of scattering parameters are introduced. Description of lowpass synthesis procedure by means of Chebyshev filtering function and characteristic polynomials follows afterwards. Then, ladder-type network is realized by input admittance function obtaining and elements extraction procedure. The main constraints of acoustic technology are reviewed and their inclusion in filter's design is described. Finally, two examples of stand-alone acoustic filter and duplexer are presented in order to demonstrate the functionalities of the methodology.

Chapter 3 describes direct bandpass synthesis technique which allows to overcome the inherent drawbacks of lowpass approach. Updated nodal representation of acoustic resonators, positioned in series and shunt, consists of only frequency dependent nodes, and it is outlined at the beginning. Two different cases of capacitive and inductive matching elements at input and output ports lead to four possible ladder-type networks. Frequency behavior of each topology is

analyzed, paying special attention to TZs at the origin and infinity. Chebyshev filtering function is modified in order to include these TZs and provide a correct mathematical description of the bandpass ladder-type network. A corresponding modification of characteristic polynomials' calculation is also presented. Extraction procedure of basic blocks of bandpass inline representation gives real and positive circuit elements, which after denormalization constitute a real ladder-type filter. An important issue about numerical instabilities in polynomials synthesis of high-order filters and following it extraction procedure, which always occurs in direct bandpass synthesis, is also discussed. A proposed solution to this problem is implementation of additional toolbox for MATLAB which allows to pass from double to quadruple precision. Finally, after accommodation of technological constraints, two examples are presented in order to demonstrate the possibilities of bandpass methodology, comparing with lowpass approach.

In Chapter 4 a novel bandpass phase correction technique is described. Phase adaptation is an important condition for successful duplexers' and multiplexers' design since by phase modification a balanced common port of the device is achieved, decreasing the interference between frequency bands. Implementation of the same phase modification method as in lowpass approach gives complex bandpass elements, and therefore, cannot be applied in direct bandpass synthesis technique. Until now, no solution to this problem has been found in our best of knowledge, and a possible approach is introduced in this thesis. A corresponding filtering function modification for each ladder-type network is presented, leading to input reactive elements variation, which, in turn, influence on input phase. Intrinsic and technological limitations of the method are also discussed. Finally, a numerical example of duplexer with phase adaptation is shown in order to validate the method.

Chapter 5 is dedicated to lossy synthesis technique elaborated specially for ladder-type acoustic filters. An overview of existing techniques for lossy filtering networks of other technologies is presented at the beginning. A lossy coupling matrix of ladder-type filter is then described, specifying the constraints of parameters to optimize. An elaborated cost function is capable to provide two solutions. The former is flat passband IL level obtaining from given Q-vector of the resonators, and the latter is finding the distribution of Q of every resonator which corresponds to a predetermined by manufacturers flat IL level. Two following examples show the method's capabilities, depending on the choice of optimized parameters.

Finally, main conclusions of the dissertation and future work recommendations are given in Chapter 6.

It has to be noted that elaborated examples of designed filters serve to demonstrate the functionality, suitability, and flexibility of proposed methodologies, rather than providing definitive solutions which are limited by intellectual property and industrial secret.

1.5   Research Contributions

Throughout the Ph.D. program a number of papers have been elaborated which have taken part in this dissertation. The list of scientific contributions includes:

- A. Gimenez, I. Evdokimova, J. Verdú, and P. de Paco, "Extended Synthesis Technique for the Design of Ladder-Type Acoustic Filters in the Bandpass Domain," in *IEEE Trans. on Microwave Theory and Techniques*, (Submitted).

- I. Evdokimova, J. Verdú, and P. de Paco, "Bandpass Phase Correction Methodology for Ladder-Type Acoustic Filters," in *European Microwave Week*, September 2018, Madrid (Spain), (Accepted).

- I. Evdokimova, J. Verdú, and P. de Paco, "Direct Bandpass Synthesis of High-Order Ladder-Type Filters," in 7th *International Workshop on Microwave Filters*, April 2018, Noordwijk (The Netherlands).

- I. Evdokimova, A. Gimenez, J. Verdú, and P. de Paco, "Synthesis of Ladder-Type Acoustic Filters in the Band-Pass Domain," in *European Microwave Week*, October 2017, Nuremberg (Germany).

- J. Verdú, I. Evdokimova, and P. de Paco, "Systematic Synthesis Methodology for the Design of Acoustic Wave Stand-Alone Ladder Filters, Duplexers and Multiplexers," in *Int. Ultrasonic Symp.*, September 2017, Washington, D.C. (USA).

- I. Evdokimova, J. Verdú, and P. de Paco, "Lossy Acoustic Filter Synthesis by Gradient-Based Optimization Technique," in *Progress In Electromagnetics Research Symp. (PIERS 2017)*, May 2017, Saint Petersburg (Russia).

- J. Verdú, A. Gimenez, A. Triano, I. Evdokimova, P. Silveira, and P. de Paco, "Distortion of the Bandpass Filter Response Under Heterogeneous Temperature Distribution," in *Microwave Technology and Techniques Workshop*, April 2017, Noordwijk (The Netherlands).

Synthesis and Design Fundamentals of Acoustic Filter in Lowpass Domain

A holistic methodology for synthesis and design of ladder-type acoustic filters, duplexers, and multiplexers is presented in this chapter. Classical lowpass approach with further lowpass-to-bandpass elements' transformation is applied in order to achieve a feasible filtering network. The methodology links traditional mathematical tools of filters' synthesis with micro-acoustic technological constraints, thus allowing to reduce the use of optimization methods and increase computational efficiency.

In order to operate in lowpass frequency domain, an equivalent model of acoustic resonator, consisted of frequency invariant reactances, is presented in the first part of the chapter. Applying well-known Chebyshev filtering function and further elements' extraction procedure, a mathematical prototype of ladder-type acoustic filter is obtained. By implementing of automatic search engine, input parameters of the synthesis are chosen so as to fulfill mask specifications and technological constraints. In the end, denormalization of the circuit's elements provides bandpass filtering network. At this stage, quality factor influence, power handling, total chip size, and other technological parameters can be evaluated.

Connection of two or several filters to the common port provides duplexer or multiplexer network, respectively. In this case, the management of input phase becomes important. Presented methodology adapts the phase value in order to reduce the loading effect from one channel to other. Thus, stand-alone filters are synthesized separately with updated phase condition in such a way that when they are connected together their frequency performance is almost maintained. Finally, two examples of stand-alone filter and duplexer are presented in order to demonstrate the functionalities of the proposed methodology.
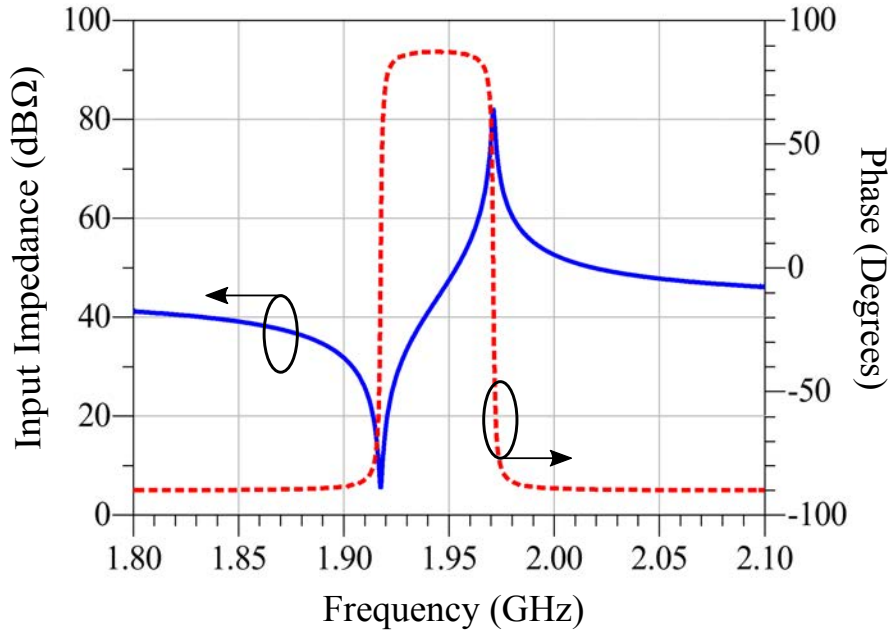
Figure 2.1: Input impedance magnitude and phase of acoustic resonator.

2.1 Equivalent Electrical Circuit in Lowpass Domain

In order to perform mathematical description of ladder-type acoustic network, bandpass circuit and its lowpass equivalence have to be found. In this section a brief discussion of possible filter models is presented, paying special attention to the most suitable one. Lowpass-to-bandpass transformation for lumped network elements is derived, and the most important features of acoustic resonator and ladder topology are discussed as well.

2.1.1 Acoustic Resonator

As it has been mentioned in Introduction, voltage application on piezoelectric slab provokes the generation of mechanic wave. Resulting complex impedance, i.e., its magnitude and phase, of the resonator exhibits both series and parallel resonances which can be observed in Figure 2.1 [40]. At frequencies outside the resonances, resonator's phase is near $-90°$, which means that the resonator behaves as capacitor. At series resonant frequency, f_s, the impedance reaches its minimum value and becomes resistive if resonator has finite Q. In ideal lossless situation $Z_{in} = 0$ at f_s. Between two resonances the resonator behaves as inductor with phase near $90°$. Then, at parallel resonant frequency, f_p, the impedance has very large value and again becomes resistive for lossy resonator. In case of ideal resonator, $Z_{in} = \infty$ at f_p.

In order to design the acoustic resonator, different approaches can be applied [41]. The first is
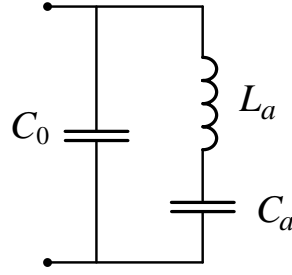
Figure 2.2: Butterworth-Van Dyke equivalent model of acoustic resonator.

Mason Model where each layer of resonator stack, including electrodes and reflector in case of a SMR, are represented by transmission line sections [42–44]. It is a physical-based one-dimensional (1D) approach where a single-mode operation is assumed. Using 2D and 3D numerical Finite Element Method (FEM) instead of 1D Mason Model allows to take into account spurious and non-trapped modes, resulting from lateral wave propagation, and resistive losses in the electrodes [45] for both SAW and BAW technologies [46, 47]. This approach has a good accuracy, dealing with resonator's geometry and physical constants directly; however, the computational cost is also increased.

In this thesis we implement the third approach, i.e., Butterworth-Van Dyke equivalent circuit representation illustrated in Figure 2.2 [48], which is suitable for both SAW and BAW resonators. Here, static capacitance C_0 represents parallel electrodes of BAW resonator or IDT of SAW resonator, and acoustic path is performed by L_a and C_a. It is a simpler model since higher order harmonics are neglected and only lossless lumped elements are used to describe the electroacoustic behavior of the resonator. A lossy network is characterized by modified BVD (mBVD) model where three resistors are added in order to provide a more realistic functionality [49]. This type of networks is discussed in Section 2.4.2 and Chapter 5.

The input impedance of the network from Figure 2.2 has the following expression:

$$Z_{in}(\omega) = \frac{j\left(\omega L_a - 1/(\omega C_a)\right)}{1 - \omega^2 C_0 L_a + C_0/C_a}. \tag{2.1}$$

Series and parallel resonant frequencies can be found by establishing $Z_{in}(\omega) = 0$ and $Z_{in}(\omega) = \infty$, respectively, so that

$$f_s = \frac{1}{2\pi\sqrt{L_a C_a}} \tag{2.2}$$

and

$$f_p = \frac{1}{2\pi}\sqrt{\frac{C_a + C_0}{L_a C_a C_0}} = f_s \cdot \sqrt{1 + \frac{C_a}{C_0}}. \tag{2.3}$$

From these equations it can be seen that $(f_p - f_s)$ is proportional to the ratio C_a/C_0.
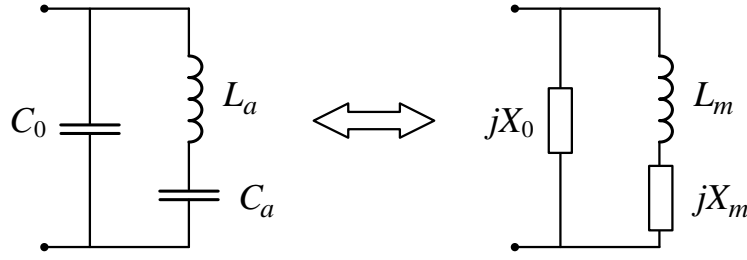
Figure 2.3: Bandpass-to-lowpass transformation of Butterworth-Van Dyke acoustic resonator model.

Acoustic Resonator Model in Lowpass Domain

In order to apply lowpass synthesis techniques for acoustic filter design, the equivalent circuit from Figure 2.2 has to be modified. Resulting lowpass BVD model is illustrated in Figure 2.3 where capacitors are replaced by Frequency Invariant Reactances (FIRs) first introduced in [50]. FIR is a mathematical tool which allows to synthesize an asymmetric response in lowpass domain. The circuit equivalence presented in Figure 2.3 is possible since purely imaginary FIRs act as frequency detuning elements, providing thereby two resonant frequencies Ω_s and Ω_p in lowpass domain below and above zero central frequency, respectively.

FIR approximation is widely used in filter's synthesis in situations where asymmetric bandpass response is required. It is suitable for any kind of filter technology where equivalent lowpass network is made up of lossless lumped inductors and capacitors terminated in a matching resistor [51–53]. Generally, including FIRs into the circuit means frequency shifts from the bandpass filter's nominal central frequency, providing required asymmetric response [54].

Observing the lowpass equivalent circuit of acoustic resonator from Figure 2.3, its input impedance is found to be

$$Z_{in}\left(\Omega\right) = \frac{jX_0\left(\Omega L_m + X_m\right)}{\Omega L_m + X_m + X_0}, \tag{2.4}$$

where Ω is a normalized frequency variable for unity bandwidth and zero central frequency, which takes part in lowpass-to-bandpass transformation by means of mapping formula

$$\Omega = j\alpha\left(\frac{\omega}{\omega_0} - \frac{\omega_0}{\omega}\right). \tag{2.5}$$

Here, ω is a frequency variable in bandpass domain, $\omega_0 = \sqrt{\omega_1\omega_2}$ is bandpass central frequency, and α is a parameter defined by fractional or relative bandwidth so that

$$\alpha = \frac{\omega_0}{\omega_2 - \omega_1}. \tag{2.6}$$

In order to establish the relationship between lowpass and bandpass elements, an accordance between acoustic and static paths of both circuits is used [39]. Thus, considering acoustic branch

and applying (2.5), we get:

$$j\alpha \left(\frac{\omega}{\omega_0} - \frac{\omega_0}{\omega} \right) L_m + jX_m = j\omega L_a + \frac{1}{j\omega C_a}. \tag{2.7}$$

This equation has two variables L_a and C_a, so a second equation is required which is obtained by determination of the first derivative of (2.7) with respect to ω:

$$j\alpha \left(\frac{1}{\omega_0} - \frac{\omega_0}{\omega^2} \right) L_m = jL_a + \frac{1}{j\omega^2 C_a}. \tag{2.8}$$

By establishing $\omega = \omega_0$, lowpass elements L_m and X_m are found to be

$$L_m = \frac{\omega_0 L_a}{2\alpha} + \frac{1}{2\alpha \omega_0^2 C_a}, \tag{2.9a}$$

$$X_m = \omega_0 L_a - \frac{1}{\omega_0 C_a}. \tag{2.9b}$$

The remaining FIR X_0 is straightforwardly determined by

$$X_0 = -\frac{1}{\omega_0 C_0}. \tag{2.10}$$

Bandpass circuit elements L_a, C_a, and C_0 can be found by the same equations (2.7) and (2.8) as a functions of the lowpass L_m, X_m, and X_0 so that

$$L_A = \frac{Z_0}{2} \left(\frac{2\alpha L_m + X_m}{\omega_0} \right),$$

$$C_A = \frac{2}{Z_0} \frac{1}{\omega_0 \left(2\alpha L_m - X_m \right)}, \tag{2.11}$$

$$C_0 = -\frac{1}{Z_0} \frac{1}{\omega_0 X_0},$$

where Z_0 is the reference impedance.

It has to be mentioned that derived relationships (2.9), (2.10), and (2.11) between lowpass and bandpass elements of acoustic resonator are based on an evaluation at central frequency ω_0, which means that they are valid only at a narrowband frequency range at vicinity of ω_0. Since FIRs X_m and X_0 are frequency independent, they represent the frequency behavior of dependent reactive capacitors C_a and C_0 only at central frequency ω_0. This feature of lowpass-to-bandpass transformation makes the following synthesis easier to perform, but at the same time, it exhibits lack of precision at out-of-band frequencies, which represents a serious drawback for filters with wide passband and duplexers and multiplexers.

Upcoming filter synthesis in lowpass domain, and following chapters of the thesis are based on resonator nodal representation, named dangling resonator, which is particularly useful in elements' extraction procedure. Model description and mathematical relation between lowpass BVD and dangling resonator are described hereafter.
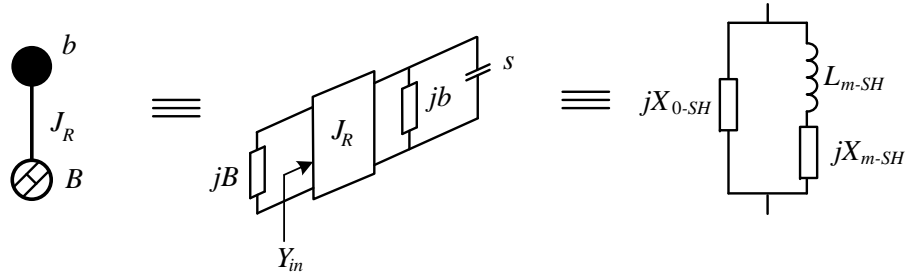
Figure 2.4: Equivalence between dangling and BVD lowpass acoustic resonator positioned in shunt.

Dangling Resonator

In Section 1.2 it has been mentioned that every resonator of ladder-type filter introduces a finite TZ below or above the passband, thus providing a high selectivity. This means that one of the two resonant frequencies of the resonator, f_s or f_p, has to perform a notch in filter transmission response, i.e., a TZ.

Presented in Figure 2.4 dangling resonator model is a classical realization of arbitrarily placed TZ [55]. It consists of a Resonant Node (RN) b depicted as black circle, Non-Resonating Node (NRN) B which is represented by dashed circle, and admittance inverter J_R between them. At the same time, RN is performed by unitary capacitor s in parallel with FIR jb which performs a frequency tuning so that resulting TZ $j\Omega_k = -jb$. Described first in [56], NRN is represented by FIR jB connected to ground and acts independently from unit capacitor. The proposed model of dangling resonator represents BVD lowpass equivalent circuit of shunt connected resonator.

Input admittance at the point where admittance inverter connects to the NRN is derived as

$$Y_{in} = \frac{J_R^2}{s + jb}, \tag{2.12}$$

which corresponds to input impedance

$$Z_{in} = \frac{s}{J_R^2} + j\frac{b}{J_R^2}. \tag{2.13}$$

It can be noticed that at $s = -jb$ input admittance becomes infinite and input impedance equals to zero, thus guiding all signal to the ground through shunt connected resonator and providing a finite TZ at frequency $\Omega_k = -b$. In case of shunt resonator b has to be positive so as to place the TZ below the passband, i.e., series resonant frequency f_s of shunt resonator performs the TZ in lowpass domain. Therefore, by establishing equivalence between two networks, lowpass
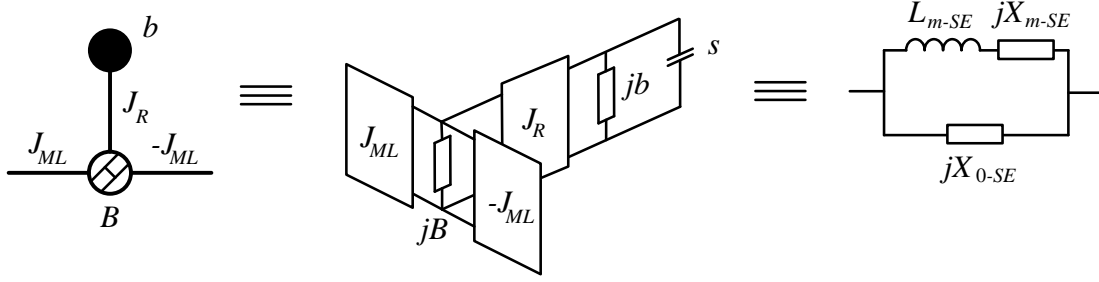
Figure 2.5: Equivalence between dangling and BVD lowpass acoustic resonator positioned in series.

BVD elements can be found as

$$L_{m-SH} = \frac{1}{J_R^2},$$

$$X_{m-SH} = \frac{b}{J_R^2}, \tag{2.14}$$

$$X_{0-SH} = -\frac{1}{B}.$$

In order to obtain an equivalent circuit of resonator positioned in series, dangling resonator from Figure 2.4 is serialized by adding two side inverters $\pm J_{ML}$. Resulting network is depicted in Figure 2.5. Since side inverters serve only to serialize the shunt resonator, they are not physically implemented in the network. Therefore, they cannot introduce any additional changes in transmission and reflection response either in magnitude or in phase. Thus, these admittance inverters have to be equal in value but with opposite signs in order to maintain zero phase variation.

Impedance parameter of series connected resonator can be written as

$$Z = j\frac{B}{J_{ML}^2} + \frac{1}{\frac{s}{J_R^2}J_{ML}^2 + j\frac{b}{J_R^2}J_{ML}^2}. \tag{2.15}$$

At $s = -jb$ input impedance becomes infinite, thus reflecting all signal passing through series connected resonator and providing a finite TZ at lowpass frequency $\Omega_k = -b$. When series connected resonator is considered, b has to have negative value so as to place the TZ above the passband, i.e., parallel resonant frequency f_p of series resonator is responsible of the TZ in lowpass domain. Established relationship between lowpass BVD model and series connected
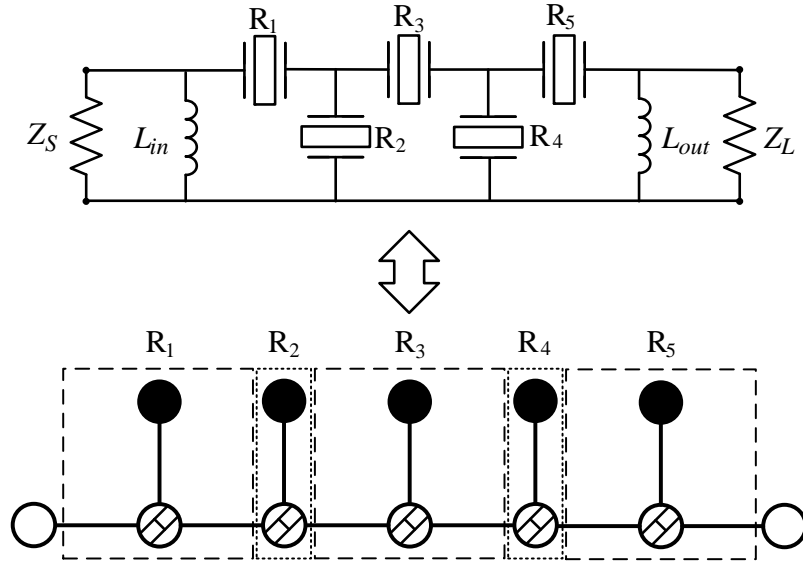
Figure 2.6: Equivalence between ladder-type and inline topologies for filter with first resonator positioned in series.

dangling resonator is found to be

$$L_{m-SE} = \frac{B^2}{J_R^2 J_{ML}^2},$$

$$X_{m-SE} = \frac{bB^2}{J_R^2 J_{ML}^2} - \frac{B}{J_{ML}^2}, \tag{2.16}$$

$$X_{0-SE} = \frac{B}{J_{ML}^2}.$$

In order to provide a feasible network, the sign of NRN B has to be positive for shunt resonator and negative for series one since it is directly related with static capacitance. Together with sign alternation of FIR b, they represent first constraints imposed by micro-acoustic technology.

Dangling resonator model, as a part of ladder-type topology, perfectly represents frequency behavior of acoustic resonator in lowpass domain. Its major advantage is modularity since every TZ is controlled independently by one resonator, i.e., each dangling resonator generates and controls its own TZ.

2.1.2   Acoustic Ladder-Type Filter

Concatenation of electrically coupled acoustic resonators positioned in series and shunt provides ladder-type filter topology suitable for both SAW and BAW technologies. Two possible networks
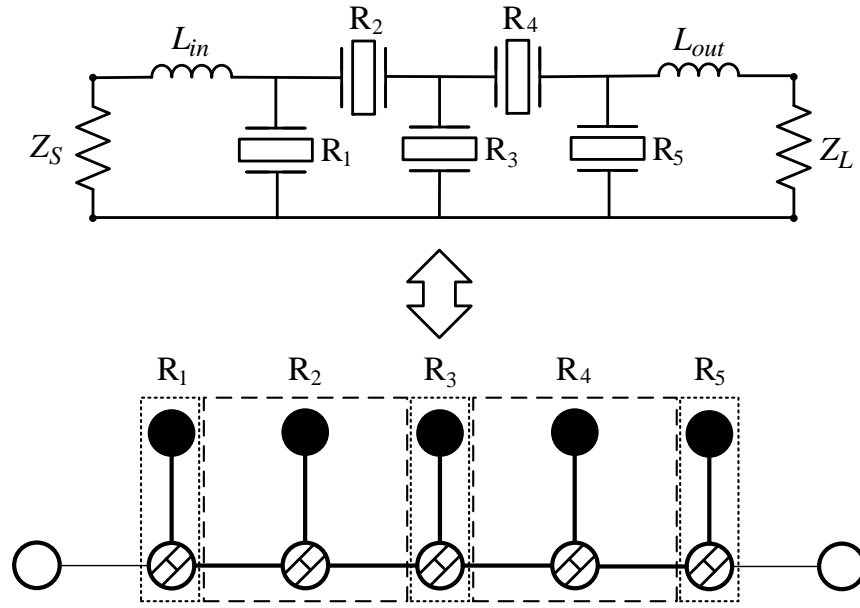
Figure 2.7: Equivalence between ladder-type and inline topologies for filter with first resonator positioned in shunt.

can be obtained started either with series or shunt resonator. The first option is illustrated in Figure 2.6. Here, ladder-type topology contains shunt connected matching inductors at source and load which may be required in extraction procedure. Equivalent inline nodal representation consists of alternation of series and shunt dangling resonators. Here, inductors are included in source and load terminations as FIRs.

Another possible topology is presented in Figure 2.7. Here, the first resonator is positioned in shunt, and therefore, matching inductors at input and output ports have to be series connected for correct extraction procedure. Also, it has to be noticed that there is no inverter between source/load node and the first/last resonator.

Since each dangling resonator introduces TZ at finite frequency, ladder-type filter topology, and consequently, its inline nodal representation performs a fully canonical network, i.e., number of finite TZs of Nth order filter is $n_{fz} = N$. This important feature allows to place TZs close to passband so as to fulfill high selectivity requirements. It is well-known that in order to provide fully canonical network, a direct source-load coupling is required [57]. However, including NRNs implements source-load coupling through the reactive path of static capacitors. Moreover, such source-load coupling representation has an advantage over the standard one since in this case TZs become inter-independent and can be controlled independently which provides modularity and flexibility. Inclusion of cross-couplings allows to obtain other filter topologies, maintaining the same transmission and reflection response. However, in this case, finite TZs will be affected since they will depend on couplings' strength. Also, additional cross-couplings can simulate
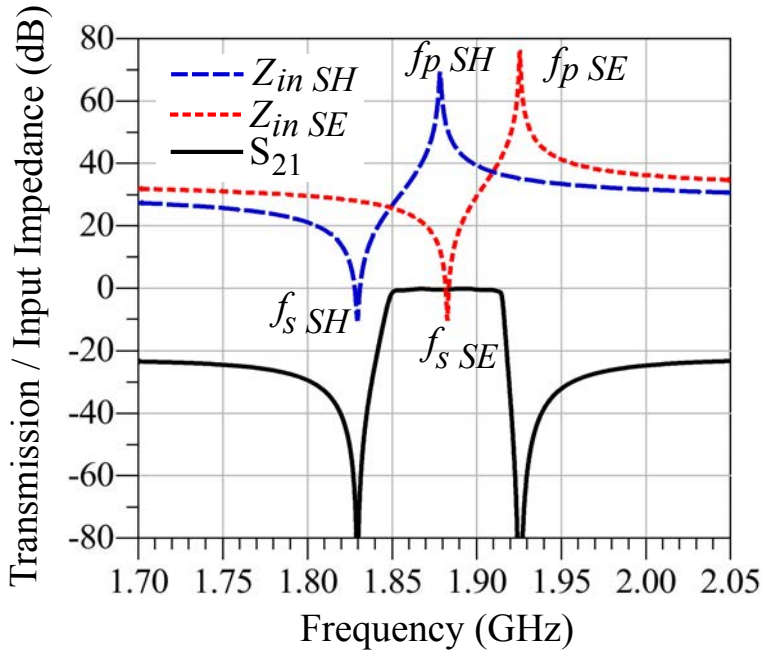
Figure 2.8: Operation principle of ladder-type filter.

electromagnetic interaction between resonators or source-load leakage effects [58].

The typical frequency behavior of ladder-type acoustic filter is presented in Figure 2.8. Here, the transmission response of the whole filter and input impedance of a shunt and series connected resonators demonstrate the operational principle. As it has been explained above, series resonant frequency of shunt resonator $f_{s\ SH}$ and parallel resonant frequency of series resonator $f_{p\ SE}$ are responsible of finite TZs below and above the passband, respectively. At parallel resonant frequency $f_{p\ SH}$ the shunt resonator behaves as open-circuit network and the signal is transmitted towards output port. Similarly, at series resonant frequency $f_{s\ SE}$ series connected resonator turns to have low impedance, thus passing the signal [59].

Rejection at out-of-band frequencies is a weakness of ladder topology and it is a serious problem for duplexers' and multiplexers' design. Since at frequencies below $f_{s\ SH}$ and above $f_{p\ SE}$ both shunt and series resonators behave as capacitors, the attenuation level is controlled by the capacitive voltage divider nature of the ladder-type filter. By increasing the number of acoustic resonators, composing the ladder network, a better out-of-band rejection level can be achieved; however, it also negatively affects on in-band IL level. Arranging external shunt or series inductors to the resonators, additional TZs appear at out-of-band frequencies, thus providing a complementary attenuation [60]. However, the overall number of external elements and their values are limited by technological constraints. Moreover, the transmission response is sensitive to inductors' low quality factor.

2.2 Synthesis of a General Class of Chebyshev Filtering Function

Once an equivalent circuit of filtering network based on acoustic waves has been determined, we proceed to its mathematical description. For this purpose, scattering parameters, which are widely used in microwave circuits, and their important relations are considered in this section. Then, general kind of Chebyshev function is derived suited for symmetric and asymmetric filter response with arbitrary distribution of TZs. Finally, characteristic polynomials of ideal filter in lowpass domain are obtained.

2.2.1 Transfer and Reflection Parameters for Two-Port Network

Filter circuit is a two-port network which can be described by a 2×2 scattering matrix by means of [61]

$$\begin{bmatrix} b_1 \\ b_2 \end{bmatrix} = \begin{bmatrix} S_{11} & S_{12} \\ S_{21} & S_{22} \end{bmatrix} \cdot \begin{bmatrix} a_1 \\ a_2 \end{bmatrix}, \tag{2.17}$$

where b_1 and b_2 are reflected power waves from ports 1 and 2, respectively, and a_1 and a_2 are incident power waves at ports 1 and 2, respectively.

For passive, lossless, reciprocal network, i.e., $S_{12}(s) = S_{21}(s)$, two equations of energy conservation for $s = j\Omega$

$$S_{11}(s)S_{11}(s)^* + S_{21}(s)S_{21}(s)^* = 1, \tag{2.18a}$$

$$S_{22}(s)S_{22}(s)^* + S_{21}(s)S_{21}(s)^* = 1, \tag{2.18b}$$

and one equation of orthogonality

$$S_{11}(s)S_{21}(s)^* + S_{21}(s)S_{22}(s)^* = 0 \tag{2.19}$$

can be established, where symbol * defines operation of paraconjugation so as $A(s)^* = A^*(-s)$. Rewriting equations from (2.18) in polar coordinates and dropping s, it can be stated that

$$|S_{11}| = |S_{22}|, \tag{2.20a}$$

$$|S_{21}|^2 = 1 - |S_{11}|^2. \tag{2.20b}$$

Applying polar form representation to (2.19), we obtain

$$|S_{11}| |S_{21}| \left(e^{j(\theta_{11} - \theta_{21})} + e^{j(\theta_{21} - \theta_{22})} \right) = 0. \tag{2.21}$$

Therefore, the condition of orthogonality can be satisfied only if $e^{j(\theta_{11} - \theta_{21})} = -e^{j(\theta_{21} - \theta_{22})}$ or

$$-\theta_{21} + \frac{(\theta_{11} + \theta_{22})}{2} = \frac{\pi}{2} \left(2k \pm 1 \right). \tag{2.22}$$

At the same time, reflection and transmission parameters of Nth-order filter can be defined by characteristic polynomials as follows [62]:

$$S_{21}(s) = \frac{P(s)/\varepsilon}{E(s)}, \qquad S_{11}(s) = \frac{F(s)/\varepsilon_R}{E(s)}. \tag{2.23}$$

Here, polynomial $P(s)$ is calculated from finite normalized TZs and its coefficients alternate between purely real and purely imaginary as the power of s increases. This is a necessary condition for purely reactive filter elements realization. Nth-degree polynomial $F(s)$ has the same behavior in relation to its coefficients. Since this is a lossless passive network, $E(s)$ is strictly Hurwitz, i.e., all the roots of $E(s)$ are in the left half of the complex plane. ε and ε_R are normalizing constants.

Taking into consideration (2.23), angles of scattering parameters can be represented as

$$\theta_{21} = \theta_P - \theta_E, \tag{2.24a}$$

$$\theta_{11} = \theta_F - \theta_E, \tag{2.24b}$$

$$\theta_{22} = \theta_{F_{22}} - \theta_E, \tag{2.24c}$$

and substituting them into expression (2.22) the following relationship is obtained:

$$-\theta_P + \frac{(\theta_F + \theta_{F_{22}})}{2} = \frac{\pi}{2}(2k \pm 1). \tag{2.25}$$

Derived expression states that the difference between phase of polynomial $P(s)$ and average of phases of $F(s)$ and $F_{22}(s)$ must be an odd multiple of $\pi/2$ radians; that is, angle difference between scattering parameter $S_{21}(s)$ and $(S_{11}(s) + S_{22}(s))/2$ has to be orthogonal for any value of s. Therefore, from this rule two important constraints on zeros' position of $P(s)$, $F(s)$, and $F_{22}(s)$ can be derived:

1. $P(s)$ must have zeros either on the imaginary axis of the complex s plane or in mirror-image pairs symmetrically arranged about the imaginary axis.
2. Zeros of $F(s)$ and zeros of $F_{22}(s)$ must either be coincident on the imaginary axis or arranged in mirror-image pairs about the imaginary axis, i.e., $s_{22_i} = -s_{11_i}^*$.

From these constraints the following conclusion can be made. If an Nth-order filter with n_{fz} finite TZs is considered, the integer quantity $(N - n_{fz})$ must be odd in order to fulfill the condition of orthogonality. For cases where $(N - n_{fz})$ is even, an extra $\pi/2$ radians must be added to θ_P in equation (2.25), which is equivalent of multiplying polynomials $P(s)$ by j. By this way the condition of orthogonality will always be satisfied.

2.2.2 Relationship Between ε and ε_R

Real coefficients ε and ε_R presented in (2.23) serve to normalize polynomials $P(s)$ and $F(s)$ so that $|S_{21}(s)|$ and $|S_{11}(s)|$ are ≤ 1 at any value of s.

Normalizing constant ε is defined by evaluating $P(s)/E(s)$ at $s = \pm j$, where equiripple RL level for Chebyshev filters is known, by means of

$$\varepsilon = \frac{1}{\sqrt{1 - 10^{-RL/10}}} \left| \frac{P(s)}{E(s)} \right|_{s = \pm j}, \tag{2.26}$$

or

$$\frac{\varepsilon}{\varepsilon_R} = \frac{1}{\sqrt{10^{RL/10} - 1}} \left| \frac{P(s)}{F(s)} \right|_{s = \pm j}. \tag{2.27}$$

This sets the maximum level of $|S_{21}(s)|$ to 1, and for networks with at least one TZ at infinity, i.e., $n_{fz} < N$, $|S_{21}(\pm j\infty)| = 0$. Therefore, at $s = j\infty$ the condition of energy conservation becomes

$$S_{11}(j\infty) = \frac{1}{\varepsilon_R} \left| \frac{F(j\infty)}{E(j\infty)} \right| = 1, \tag{2.28}$$

where it can be seen that $\varepsilon_R = 1$ since both $F(s)$ and $E(s)$ are monic polynomials, i.e., their highest-degree coefficients equal to one.

In case of fully canonical network, where all available TZs are at finite frequencies ($n_{fz} = N$), the attenuation level at $s = \pm j\infty$ is finite and ε_R is found by means of energy conservation condition as

$$S_{11}(j\infty)S_{11}(j\infty)^* + S_{21}(j\infty)S_{21}(j\infty)^* = 1, \tag{2.29a}$$

$$\frac{F(j\infty)F(j\infty)^*}{\varepsilon_R^2 E(j\infty)E(j\infty)^*} + \frac{P(j\infty)P(j\infty)^*}{\varepsilon^2 E(j\infty)E(j\infty)^*} = 1. \tag{2.29b}$$

Considering that $P(s)$, $F(s)$, and $E(s)$ are monic polynomials, we obtain

$$\frac{1}{\varepsilon_R^2} + \frac{1}{\varepsilon^2} = 1, \qquad \varepsilon_R = \frac{\varepsilon}{\sqrt{\varepsilon^2 - 1}}. \tag{2.30}$$

Resulting coefficient ε_R is slightly greater that one since $\varepsilon > 1$.

2.2.3 Synthesis Methodology

Each filtering network has to be described by mathematical function which completely characterizes frequency behavior of the prototype. Among different known filtering functions, the Chebyshev one is the best suited for acoustic ladder-type filters since it has an equiripple passband and monotonically rising attenuation band which provides a high rejection level. Moreover,
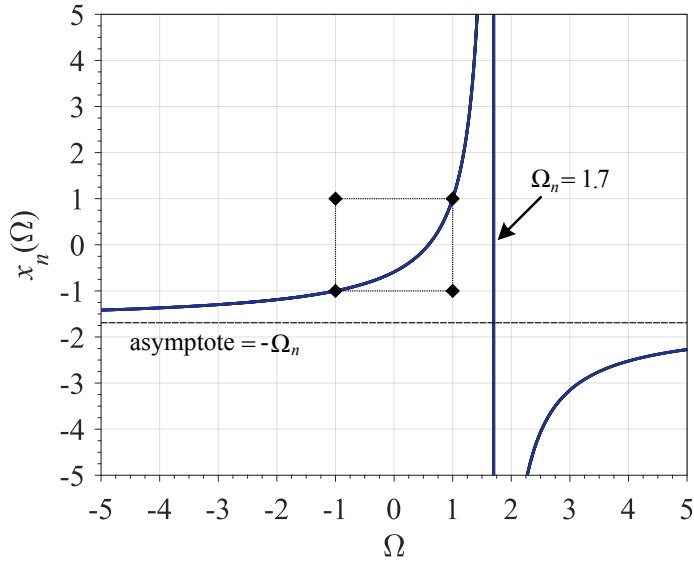
Figure 2.9: Graphical representation of function $x_n(\Omega)$ with prescribed TZ at $\Omega_n = 1.7$.

it permits to synthesize symmetric and asymmetric filters of even or odd degree with any set of prescribed finite TZs.

For $\Omega = s/j$ general Chebyshev function for Nth-order filter has the following expression [63]:

$$C_N(\Omega) = \cosh\left[\sum_{n=1}^{N} \cosh^{-1}(x_n(\Omega))\right]. \tag{2.31}$$

Term $x_n(\Omega)$ contains N TZs at finite frequency or infinity and N reflection zeros (RZs) inside the passband, and it has to fulfill following requirements in order to represent a Chebyshev function correctly:

1. $x_n(\Omega_n) = \pm\infty$, where Ω_n is a normalized finite TZ or TZ at infinity.
2. At $\Omega = \pm 1$, $x_n(\Omega) = \pm 1$.
3. Inside the passband, i.e., between $\Omega = -1$ and $\Omega = 1$, $1 \geq x_n(\Omega) \geq -1$.

Therefore, taking into consideration these requirements, the term $x_n(\Omega)$ is derived as

$$x_n(\Omega) = \frac{\Omega - 1/\Omega_n}{1 - \Omega/\Omega_n}, \tag{2.32}$$

where $\Omega_n = s_n/j$ is the position of nth TZ in the complex frequency plane. Figure 2.9 shows frequency behavior of function $x_n(\Omega)$ with normalized finite TZ positioned at 1.7, making $x_n(1.7) = \pm\infty$, where rectangular area represents in-band variation of $x_n(\Omega)$ demonstrating all conditions fulfillment.

Definition of Characteristic Polynomials

Chebyshev filtering function can be also derived by characteristic polynomials so that

$$C_N(\Omega) = \frac{F(\Omega)}{P(\Omega)}. \tag{2.33}$$

Therefore, its poles and zeros are the roots of $P(\Omega)$ and $F(\Omega)$, respectively.

Inline topology described in previous section for ladder-type acoustic filters contains only finite TZs. Such network is defined as fully-canonical, when number of finite TZs equals to filter's order, i.e., $n_{fz} = N$. Thus, polynomial $P(\Omega)$ can be easily derived from set of prescribed TZs by means of

$$P(\Omega) = j \prod_{n=1}^{N} (1 - \Omega/\Omega_n), \tag{2.34}$$

where multiplication by j is a necessary action in order to satisfy the condition of orthogonality since $(N - n_{fz}) = 0$ is an even integer quantity.

To determine the coefficients of polynomial $F(\Omega)$ of fully canonical network, filtering function $C_N(\Omega)$ is rewritten, applying mathematical steps from [54], and its alternative expression results to be

$$C_N(\Omega) = \frac{1}{2} \frac{\prod_{n=1}^{N} (c_n + d_n) + \prod_{n=1}^{N} (c_n - d_n)}{j \prod_{n=1}^{N} (1 - \Omega/\Omega_n)}, \tag{2.35}$$

where

$$c_n = \left(\Omega - \frac{1}{\Omega_n} \right), \tag{2.36a}$$

$$d_n = \Omega' \sqrt{1 - \frac{1}{\Omega_n^2}}. \tag{2.36b}$$

Ω' is a transformed frequency variable which is defined as $\Omega' = \sqrt{\Omega^2 - 1}$. Terms c_n and d_n are then used in recursive technique for computing coefficients of $F(\Omega)$, where the solution for the nth degree is built up from the results of the $(n-1)$th degree. Polynomials $U_N(\Omega)$ and $V_N(\Omega)$ are implemented for this purpose so that after the last iteration roots of polynomial $U_N(\Omega)$ equal to roots of $F(\Omega)$.

The recursive procedure starts with the terms corresponding to the first finite TZ at Ω_1 so that

$$U_1(\Omega) = \Omega - \frac{1}{\Omega_1}, \tag{2.37a}$$

$$V_1(\Omega) = \Omega' \sqrt{\left(1 - \frac{1}{\Omega_1^2} \right)}. \tag{2.37b}$$

Then the cycle is repeated for all remaining finite TZs Ω_i ($i = 2...N$) using the following expressions:

$$U_i(\Omega) = \Omega U_{i-1}(\Omega) - \frac{U_{i-1}(\Omega)}{\Omega_i} + \Omega'\sqrt{\left(1 - \frac{1}{\Omega_i^2}\right)}V_{i-1}(\Omega), \tag{2.38a}$$

$$V_i(\Omega) = \Omega V_{i-1}(\Omega) - \frac{V_{i-1}(\Omega)}{\Omega_i} + \Omega'\sqrt{\left(1 - \frac{1}{\Omega_i^2}\right)}U_{i-1}(\Omega). \tag{2.38b}$$

Once $P(s)$ and $F(s)$ (for $s = j\Omega$) have been defined, the remaining polynomial $E(s)$ is calculated, using equation of energy conservation:

$$E(s)E(s)^* = \frac{F(s)F(s)^*}{\varepsilon_R^2} + \frac{P(s)P(s)^*}{\varepsilon^2}. \tag{2.39}$$

Determined characteristic polynomials $P(s)$, $F(s)$, and $E(s)$ completely describe the frequency behavior of ladder-type acoustic filter.

2.3 Ladder-Type Network Realization

Extraction procedure based on NRN technique by means of input admittance function allows to obtain a lowpass prototype of ladder-type filter based on acoustic waves in accordance with its mathematical description through Chebyshev filtering function. In this section, a detailed procedure of elements' obtaining is provided taking into account necessary phase adjustment for stand-alone filters and duplexers.

2.3.1 Lowpass Prototype Elements Extraction

As it has been explained in Section 2.2.1, scattering parameters derived by (2.23) have to fulfill the orthogonality condition. However, their phase values are not specified, although the synthesis success depends on them. In extraction procedure presented here only reflection coefficient $S_{11}(s)$ is needed. Therefore, taking into consideration its phase term the expression from (2.23) is rewritten as

$$S_{11}(s) = e^{j\theta_{11}}\frac{F(s)/\varepsilon_R}{E(s)}. \tag{2.40}$$

Here, phase term multiplication does not affect on transmission and reflection filtering response since θ_{11} is purely real.

General inline configuration of ladder-type acoustic filter in lowpass domain is presented in Figure 2.10 where $G_S = G_L = 1$ are normalized conductances and $jb_i = -j\Omega_i$ represents
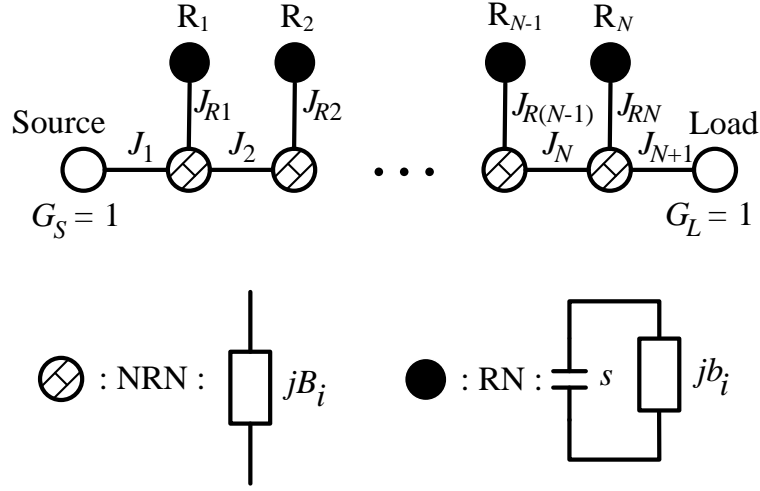
Figure 2.10: General nodal representation of ladder-type filter with N finite TZs.

position of prescribed finite TZ. Extraction procedure applied for ladder-type acoustic filters adopts the strategy from [55, 64]. The input admittance function of this network is derived as

$$Y_{in}(s) = \frac{1 - S_{11}(s)}{1 + S_{11}(s)} = \frac{\varepsilon_R E(s) - e^{j\theta_{11}} F(s)}{\varepsilon_R E(s) + e^{j\theta_{11}} F(s)}. \tag{2.41}$$

Considering only the first resonator, the input admittance takes the following form:

$$Y_{in}(s) = \frac{J_1^2}{jB_1 + \dfrac{J_{R1}^2}{s + jb_1} + \dfrac{J_2^2}{y\prime(s)}}, \tag{2.42}$$

where $y\prime(s)$ defines the rest of the circuit. Since at $s = -jb_1$, the admittance reaches zero and $|S_{11}(s)| = 1$, then

$$e^{j\theta_{11}} = \left. \frac{E(s)}{F(s)/\varepsilon_R} \right|_{s=-jb_1}. \tag{2.43}$$

Modification of phase value gives additional advantages in design process of duplexer and multiplexer module, which will be explained further.

Once phase term has been evaluated, the extraction process of dangling resonators can be performed. Unfolded form of admittance function for network depicted in Figure 2.10 is obtained as

$$Y_{in}(s) = \frac{J_1^2}{jB_1 + \dfrac{J_{R1}^2}{s + jb_1} + \dfrac{J_2^2}{jB_2 + \dfrac{J_{R2}^2}{s + jb_2} + \ldots + \dfrac{J_N^2}{jB_N + \dfrac{J_{RN}^2}{s + jb_N} + J_{N+1}^2}}}. \tag{2.44}$$

Since phase term $e^{j\theta_{11}}$ has been already included in admittance parameter, FIR of source node $B_S = 0$. In case of symmetric filtering network ($\Omega_1 = \Omega_N$, $\Omega_2 = \Omega_{N-1}$, and so on) FIR of load node B_L also equals to 0; however, if asymmetric topology is considered, an additional matching element has to be extracted. Introduction of $e^{j\theta_{11}}$ at the beginning of extraction procedure prepares the annihilation of finite TZ of the first resonator.

As inline topology is made up of cascaded dangling resonators, the extraction procedure of ith resonator is repeated N times until input admittance is completely removed. Thus, $y_{in}(s)$ for ith resonator is defined as

$$y_{in}(s) = \frac{J_i^2}{jB_i + \dfrac{J_{Ri}^2}{s + jb_i} + y\prime(s)}, \tag{2.45}$$

which is the same as

$$\frac{J_i^2}{y_{in}(s)} = \frac{J_{Ri}^2}{s + jb_i} + jB_i + y\prime(s). \tag{2.46}$$

It is interesting to notice that it is not possible to determine both J_i and J_{Ri} but only their ratio. This useful property can lead to multiple solutions suitable for different types of technologies, providing the same transmission and reflection response. However, for micro-acoustic technology allowed values of J_i can be only ± 1 because these inverters do not exist physically and serve only to serialize shunt connected resonator. The sign alternation of side inverters among the path between source and load is a necessary condition for further lowpass-to-bandpass elements' transformation. From the expression (2.46) it can be seen that J_{Ri} is related to the residue of the left-hand side at $s = -jb_i$, i.e.,

$$J_{Ri}^2 = J_i^2 \text{ residue} \left(\frac{1}{y_{in}(s)} \right) \Big|_{s=-jb_i}. \tag{2.47}$$

Taking into account $J_i^2 = 1$, dangling inverter is found to be

$$J_{Ri}^2 = (s + jb_i) \left. \frac{1}{y_{in}(s)} \right|_{s=-jb_i}. \tag{2.48}$$

After inverter extraction the remaining admittance function has to be updated by means of

$$y_{in}(s) \longleftarrow \frac{J_i^2}{y_{in}(s)} - \frac{J_{Ri}^2}{s + jb_i} = jB_i + y\prime(s). \tag{2.49}$$

The last element of ith resonator to be extracted is NRN B_i. FIR B_i prepares the extraction of the next finite TZ of $(i+1)$th dangling resonator; therefore, admittance parameter has to be evaluated at $-jb_{i+1}$ so that

$$jB_i = y_{in}(s)|_{s=-jb_{i+1}}, \tag{2.50}$$

and updated admittance function is obtained as

$$y_{in}(s) \longleftarrow y_{in}(s) - jB_i. \tag{2.51}$$

Now, all elements of dangling resonator are defined. RN is composed by unitary capacitor and FIR $b_i = -\Omega_i$, whose value is given from set of finite TZs, $J_i = \pm 1$ in order to fulfill technological requirements, and inverter J_{Ri} and FIR B_i are found from extraction procedure. It is interesting to notice that series connected resonators exhibit negative values of FIRs b_i and B_i, whereas in shunt resonators they are positive. This is the aforementioned constraint of lowpass-to-bandpass transformation.

After extraction of all resonators, the remaining elements of the network B_N and B_L (in case of asymmetric network) have to be defined. Therefore, the input admittance of final subnetwork is derived as

$$y_{in} = jB_N + \frac{J_{N+1}^2}{jB_L + G_L}. \tag{2.52}$$

Assuming that $J_{N+1}^2 = 1$, this expression can be separated into a real and imaginary parts as

$$\text{Re}\,[y_{in}] = \frac{G_L}{B_L^2 + G_L^2}, \tag{2.53a}$$

$$\text{Im}\,[y_{in}] = B_N - \frac{B_L}{B_L^2 + G_L^2}. \tag{2.53b}$$

Since $G_L = 1$, FIRs B_N and B_L can be found as

$$B_L = \pm\sqrt{\frac{G_L - G_L^2\,\text{Re}[y_{in}]}{\text{Re}[y_{in}]}} \tag{2.54}$$

and

$$B_N = \ \text{Im}[y_{in}] + \frac{B_L}{B_L^2 + G_L^2}. \tag{2.55}$$

Sign choice of B_L leads to different element's realization in bandpass domain providing shunt connected capacitor if B_L is positive, and shunt connected inductor if load FIR has negative value. Thus, definitive value of B_L will be set up by micro-acoustic technological constraints such as filter area and material system. Moreover, the real part of remaining admittance function $\text{Re}[y_{in}]$ must be smaller than 1. Otherwise, load FIR becomes purely imaginary, thus providing a resistive element. This undesirable situation can be solved by additional reactive element introduced at load port or by changing load conductance [65].

In this thesis the extraction procedure follows from source to load node since computational accuracy is not affected when filters of order from five to nine are considered in lowpass domain. However, for larger inline topologies a simultaneous extraction from source and load may be a

better choice in order to maintain numerical precision. In this case scattering parameter $S_{22}(s)$ has to be also implemented so that

$$S_{22}(s) = e^{j\theta_{22}} \frac{F(s)/\varepsilon_R}{E(s)}. \tag{2.56}$$

and

$$e^{j\theta_{22}} = \left. \frac{E(s)}{F(s)/\varepsilon_R} \right|_{s=-jb_N}. \tag{2.57}$$

Thus, secondary admittance parameter for extraction from output port is found to be

$$Y_{out}(s) = \frac{1 - S_{22}(s)}{1 + S_{22}(s)} = \frac{\varepsilon_R E(s) - e^{j\theta_{22}} F(s)}{\varepsilon_R E(s) + e^{j\theta_{22}} F(s)}. \tag{2.58}$$

The extraction procedure of dangling resonators from output port is performed by the same expressions as described above. It has to be mentioned that in case of asymmetric network, characteristic polynomial $F(s)$ in expressions (2.56), (2.57), and (2.58) has to be replaced by $F_{22}(s)$. Moreover, the fulfillment of orthogonality condition between θ_{11}, θ_{22}, and θ_{21} has to be checked. Methodologies of asymmetric filter synthesis can be found in [66, 67].

2.3.2   Phase Correction in Lowpass Domain

As it has been demonstrated above, phase introduction into characteristic polynomials provides $0°$ phase value of $S_{11}(s)$ at frequency of the first finite TZ which means that no external element at input port is required. This approach is much more useful than application of phase shifters in extracted pole technique [68] or advanced unified method [69] since these phase blocks are not suitable in micro-acoustic technology because of limited chip size.

When duplexer network design is considered, the condition of $0°$ phase at frequency of the first finite TZ is changed. Since duplexer is a three-port device consisted of antenna port, transmitter path (Tx), and receiver path (Rx), a high isolation between Tx and Rx filters is required. This means that duplexers are designed so that the passbands of each filter do not load the other filter, shifting its impedance value to open position. Thus, the interference cancellation is achieved by correction of input phase of reflection parameter $S_{11}(s)$ so that the phase equals to $0°$ at counterband central frequency f_{dual}. That is, in case of Rx filter design, f_{dual} is a central frequency of Tx path, and vice versa, if Tx filter is synthesized, f_{dual} equals to a central frequency of Rx filter. Therefore, the phase evaluation is performed by using (2.43) but substituting $\theta_{11} = \theta_{dual}$ and $-b_1 = \Omega_{dual}$ so that

$$e^{j\theta_{dual}} = \left. \frac{E(s)}{F(s)/\varepsilon_R} \right|_{s=j\Omega_{dual}}. \tag{2.59}$$

This condition enforce a zero reflection phase at the normalized counterband frequency Ω_{dual}.

Unlike stand-alone filter synthesis, in case of duplexer, the phase evaluated at frequency of the first finite TZ is different from $0°$, and therefore, lumped matching elements are required in order to correctly prepare the annihilation of this TZ. Therefore, the extraction procedure described above has to take into account the external FIR at source node B_S. It is found by evaluation of input admittance at frequency of the first finite TZ by means of

$$jB_S = y_{in}(s)|_{s=j\Omega_1}. \tag{2.60}$$

In case of symmetric network, FIR at load node coincides with the FIR at source node ($B_L = B_S$). In asymmetric topology $B_L \neq B_S$, and B_L is found to be

$$jB_L = y_{out}(s)|_{s=j\Omega_N}. \tag{2.61}$$

Once the source/load FIRs have been extracted, the lowpass-to-bandpass transformation is applied so as to obtain a shunt connected inductor in case of series first resonator and inductor positioned in series for shunt first resonator, as depicted in Figures 2.6 and 2.7. Therefore, bandpass lumped elements are derived as

$$L_{shunt} = -\frac{Z_0}{\omega_0 B_{S/L}}, \tag{2.62a}$$

$$L_{series} = \frac{Z_0}{\omega_0} B_{S/L}, \tag{2.62b}$$

where Z_0 is the reference impedance and ω_0 is passband central frequency. Resulting from (2.62) inductors may have negative values. Thus, sign changing means that instead of inductors, capacitive matching elements have to be implemented so that

$$C = -\frac{1}{\omega_0^2 L}. \tag{2.63}$$

After source/load nodes extraction, the following extraction procedure is exactly the same, as described above. Eventually, two filters Rx and Tx designed separately one by one are connected in duplexer device. Since reflection phase is correctly adjusted, load effect at dual central frequency is canceled. However, a slight alteration may be observed inside the passband because the phase is corrected only at central frequency but not in the whole passband. Additionally, lack of precision of lowpass-to-bandpass transformation provokes a slight passband degradation as well.

Phase correction for networks in lowpass domain is a useful feature which improves transmission and reflection response of duplexers and multiplexers. In lowpass domain, reactive elements at source and load, B_S and B_L, respectively, are considered frequency independent and serve only to prepare the annihilation of the first and the last finite TZs. However, in bandpass domain they introduce additional TZs at the origin and infinity, which are not taken into account in the lowpass synthesis procedure since they are not described mathematically by filtering function. An advanced bandpass synthesis technique introduced in following chapter resolves this drawback and excludes the influence of imprecise lowpass-to-bandpass transformation as well.

2.4 Technological Constraints Accommodation

The synthesis methodology presented above does not take into account any technological or fabrication restriction. However, it is very important to set the input parameters so as to obtain a feasible network before the fabrication procedure. Some constraints are different for SAW and BAW technology and some of them are common such as reliability, performance, and chip size. Besides of high selectivity, low IL level, high out-of-band attenuation, and wide bandwidth, filter designer has to take into account material system, power and temperature influence, electrostatic discharge stability, and nonlinear effects. In this section we discuss some fundamental technological constraints and their relation with synthesis methodology described above for both SAW and BAW resonators.

2.4.1 Electromecanical Coupling Coefficient

Electromecanical coupling coefficient, K, characterizes the efficiency of conversion between electric and acoustic energy and it depends only on the piezoelectric material parameters. AlN is the preferred material for BAW technology since it has a high K, good quality in high-volume production, and thermal conductivity [70]. Additionally, $LiNbO_3$ and $LiTaO_3$ also exhibit high electromechanical coupling coefficient and they are the most commonly used materials for SAW technology.

On the other hand, effective coupling coefficient k_{eff}^2 is a property of resonator, which is related with K but also takes into account finite thickness electrodes made from different materials and fabrication procedures' influence on the whole device. This parameter is of exceptional importance and it is set by relative bandwidth requirement so that the biggest challenge for acoustic filter designer consists of maximization of k_{eff}^2. State-of-the-art coupling coefficient for AlN piezoelectric reaches $6.8 - 7\%$ for FBAR technology and $5.7 - 5.9\%$ for SMR because of wave leakage into Bragg reflector [71, 72]. Unlike K, effective coupling coefficient can be easily measured.

k_{eff}^2 defines the bandwidth of the resonator and it is related with series and parallel resonance frequencies by means of [20]

$$k_{eff}^2 = \frac{\pi}{2} \frac{f_s}{f_p} \cot\left(\frac{\pi}{2} \frac{f_s}{f_p}\right). \tag{2.64}$$

Applying Taylor series approximation, an easier for modeling purposes expression can be derived:

$$k_{eff}^2 = \frac{\pi^2}{4} \left(\frac{f_p - f_s}{f_p}\right) \left(\frac{f_s}{f_p}\right). \tag{2.65}$$

In SAW technology the capacitance ratio r is implemented instead of k_{eff}^2. It is also related

with f_s and f_p so that

$$r = \frac{C_0}{C_a} = \frac{1}{(f_p/f_s)^2 - 1}. \tag{2.66}$$

Therefore, the relationship between k_{eff}^2 and r can be established:

$$k_{eff}^2 = \frac{\pi^2}{8} \left(\frac{1}{r}\right) \left(1 - \frac{1}{r}\right). \tag{2.67}$$

After bandpass filtering prototype obtaining, it is desirable to have uniform values of k_{eff}^2 (r) among all resonators so that to provide the feasibility of fabrication process. Insufficient or too strong coupling requires additional external capacitors and inductors which detune series or parallel resonance frequency, affecting pole-zero distance, and consequently, modify k_{eff}^2 of the resonator. Thus, external capacitor increases and external inductor decreases the effective coupling coefficient [39]. An additional characteristic appears when external inductor is connected in series with shunt resonator to the ground. Since at out-of-band frequencies the acoustic resonator behaves as capacitor, its combination with series inductor creates a secondary resonator and provokes an extra TZ at near-band frequencies, thus augmenting the rejection level, but following transmission pole at higher frequencies deteriorates the attenuation level significantly. Also, it has to be mentioned that the overuse of external elements may lead to bulky device which is unsuitable for mobile applications. Moreover, capacitive and inductive external elements exhibit low quality factor which negatively affects on IL level.

As it has been demonstrated, effective coupling coefficient k_{eff}^2 (r) is defined by f_s and f_p. Since finite TZs coincide with series resonant frequencies in case of shunt resonators and with parallel resonant frequencies in case of resonators positioned in series, then modifying input set of finite TZs' values and RL level, a desirable distribution of k_{eff}^2 can be found.

In lowpass domain the capacitance ratio is related with lowpass elements of dangling resonator model by means of

$$r = \frac{B}{J_R^2} \left(\frac{b}{2} - \alpha\right) - \frac{1}{2} \tag{2.68}$$

for series connected resonator, and

$$r = \frac{B}{J_R^2} \left(\alpha - \frac{b}{2}\right) \tag{2.69}$$

for shunt resonator, where α defines relative bandwidth as $\alpha = \omega_0/(\omega_2 - \omega_1)$. By these relationship, an estimation of r range can be performed in lowpass domain without lowpass-to-bandpass transformation application. However, because of inherent imprecision of this transformation the technological constraints and mask fulfillment has to be evaluated at bandpass domain before the final decision about filtering device has been made.
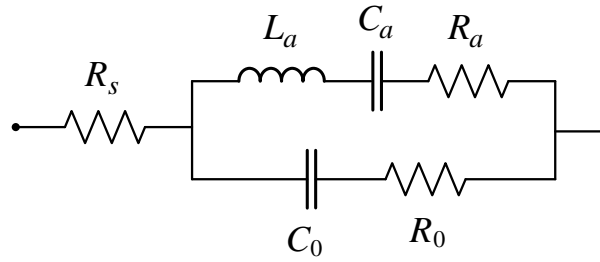
Figure 2.11: Modified BVD equivalent network of real acoustic resonator.

2.4.2 Quality Factor

Another important parameter is quality factor Q. The synthesis procedure for ladder-type acoustic filters presented above deals with ideal lossless network which does not exist in real life. Physical acoustic wave resonator exhibits of electrical and acoustical losses, leaking waves, and other loss mechanisms. Electrical losses are mainly associated with finite resistance of metal electrodes and interconnects. Acoustic losses are appeared because of viscosity and friction between materials, leading to the situation when some of the mechanical energy, propagating in piezoelectric, is converted into heat. Leaking waves are performed by secondary waves propagated in undesirable directions which lead to spurious modes emergence. As it has been explained in Introduction, BAW resonators are characterized by higher Q than SAW resonators since in FBAR and SMR structures the acoustic waves are better confined, leading to standing waves with extremely high Q-factors of several thousand. Conventional SAW resonator exhibit quality factor of around 1000; however, a big advance has been done in this direction, achieving $Q = 4000$ [73].

In order to introduce losses into the resonator, a modified BVD (mBVD) equivalent model depicted in Figure 2.11 was proposed in [49], demonstrating a good agreement with measured data. Here, R_s represents resistance of the metal electrodes, R_a is associated with acoustic losses, and R_0 is responsible of losses in material. Thus, input impedance of such network is found to be

$$Z_{in}(\omega) = R_s + \left[\frac{1}{R_0 + 1/(j\omega C_0)} + \frac{1}{R_a + j(\omega L_a - 1/(\omega C_a))} \right]^{-1}. \tag{2.70}$$

Generally, quality factor is defined by ratio of the total energy in the system to the power lost in half-cycle, and therefore, it depends on frequency. Thus, for acoustic wave resonator we define Q_s for series resonant frequency f_s, and Q_p for parallel resonant frequency f_p so that [20, 74]

$$Q_s = -\frac{1}{2} f_s \left. \frac{\partial \varphi}{\partial f} \right|_{f=f_s} \approx \frac{2\pi f_s L_a}{R_a + R_s}, \tag{2.71a}$$

$$Q_p = \frac{1}{2} f_p \left. \frac{\partial \varphi}{\partial f} \right|_{f=f_p} \approx \frac{2\pi f_p L_a}{R_a + R_0}, \tag{2.71b}$$

where φ is the phase angle of the impedance.

Finite quality factor has to be properly managed in filter's design since not only does it characterize the filter losses, but also determines the steepness of passband and degree of IL edge-rounding. Since quality factor is a measure of the selectivity of a resonant circuit, it is very important for manufacturers to elaborate high-Q resonators for current and future applications.

Lowpass synthesis procedure presented above does not take into account finite quality factor of the resonators. In order to include lossy nature into the synthesis, the poles and zeros of transfer function have to be displaced along the real axis in the complex frequency plane by loss tangent so that the modified complex frequency variable becomes $s \longleftarrow s + \tan \delta$. Therefore, the unloaded quality factor is found to be

$$Q = \frac{1}{\tan \delta}. \tag{2.72}$$

Considering lowpass domain, the lowpass frequency variable is transformed by means of [54]

$$\Omega \longleftarrow \Omega - \frac{j}{Q_{LP}}, \tag{2.73}$$

where Q_{LP} represents lowpass quality factor so that

$$Q_{LP} = Q \frac{\Delta \omega}{\omega_0}. \tag{2.74}$$

This quality factor estimation is a good approximation for synthesis of lossy filters in lowpass domain. However, it has to be taken into account that Q is considered uniform on the whole range of frequencies. A more accurate solution is to calculate elements of mBVD model from Q_s, Q_p, and R_s which are given from chosen technology and fabrication procedures. Therefore, the remaining resistors R_a and R_0 are derived as

$$R_a = \frac{2\pi f_s L_a}{Q_s} - R_s, \tag{2.75a}$$

$$R_0 = \frac{2\pi f_p L_a}{Q_p} - R_a. \tag{2.75b}$$

Capacitive and inductive external elements and inductors at source and load have to be also taken into consideration since their quality factor is relatively small, and therefore, their influence on final response is of high importance.

In course of time, mask specifications have got more stringent. Since finite Q provokes passband edge-rounding, the IL level requirement becomes difficult to fulfill. In this case, a common solution is to widen the filter passband, reducing lower passband edge f_1 and increasing higher passband edge f_2. This adjustment influences on technological parameters and lumped elements of the whole filter, which means that another set of finite TZs and RL level has to be found in order to obtain a uniform effective coupling coefficient k_{eff}^2. Nevertheless, this technique affects on

filter selectivity and isolation and becomes questionable for duplexers' and multiplexers' design, facing future demands. Chapter 5 describes an alternative method for lossy networks synthesis which can resolve the problem of passband edge-rounding in better way.

According to our experience, mBVD model can fail in situations when $Q_s < Q_p$, providing an active network, which is impossible in passive filtering circuit. In this situation an alternative distribution of losses in mBVD has to be applied.

2.4.3   Power Handling

Technological innovations allowed to minimize the form factor of acoustic filters, maintaining their high electrical performance under high power level which can reach +30 dBm in transmitter filters [75]. However, such miniaturization provokes increased level of device power density. It leads to undesired nonlinear effects and self-heating which can affect the transmission and reflection filtering response. Therefore, it is important for designer to take into consideration the power density distribution among the resonators so as to prevent characteristics' deterioration and destruction of device. Generally, BAW resonators endure higher power density, especially SMR since it can conduct more power into the substrate. SAW resonators suffer more from excessive power because it provokes electromigration damage in narrow IDT fingers. Simulation method of SAW resonators for high power performance is described in [76].

Maximum level of power density is determined by technology in terms of maximum transmitted and dissipated power per area. In order to avoid the destruction of resonator when this limit is exceeded, cascading two resonators is applied. As a consequence, the power level is reduced by factor of four; however, the chip size is also increased. In some cases, resonator have to be cascaded more than two times which subsequently increases the total filter size even more.

Self-heating of resonators may be the consequence of an aggressive environment (in terms of temperature) or the presence of a high power signal. The temperature distribution among the resonators can be homogeneous, when the temperature is uniform for every resonator, and heterogeneous, when each resonator is heated differently. This, in turn, leads to uniform and non-uniform frequency shifts in transmission response which negatively affects on selectivity, isolation, and flatness of IL level [77]. Moreover, in heterogeneous distribution scenario the higher passband edge is the most affected. Temperature compensated SAW (TC-SAW) and BAW (TC-BAW) resonators were designed to resolve this problem as it has been outlined in Introduction. A TC-BAW SMR network able to sustain up to 1000° has been reported in [78]. In this thesis we deal with heterogeneous temperature distribution and we manage the power density and occupied area in accordance to resonator's cascading as it is explained in [65].
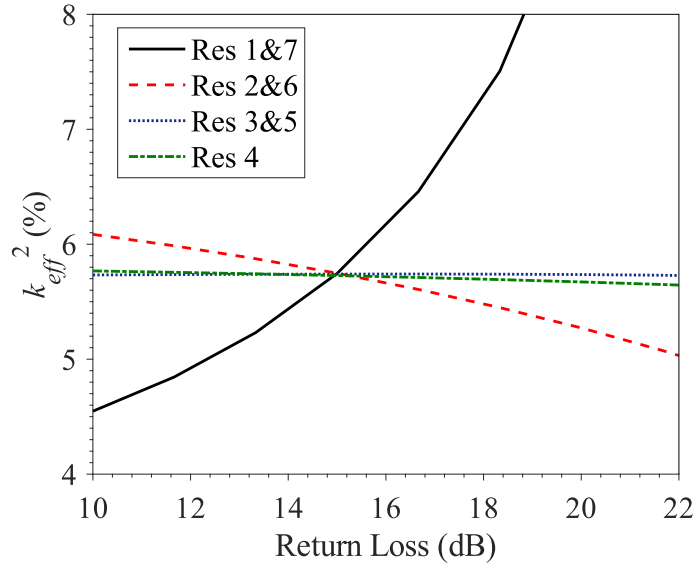
Figure 2.12: Effective coupling coefficient k^2_{eff} dependence on input RL level.

2.5   Numerical Examples

Design of any ladder-type acoustic filter is performed taking into account mask specifications and technological requirements. First step in the design is to define input parameters such as set of finite TZs, RL level, and operating frequency band. These parameters are applied for Chebyshev filtering function obtaining and fully determine the frequency response of the filter.

When finite normalized TZs are established, it is important to maintain the negative sign for shunt resonators and positive values for series connected resonators so as to obtain TZs below and above the passband correctly in accordance with inline topology. Nevertheless, the order of finite TZs is not fixed which means that filters with different elements can be obtained from the same values of TZs and RL, exhibiting the same transmission and reflection response. This feature is useful for accommodation of technological constraints such as the chip size, power handling, and k^2_{eff} (r). Thus, different studies can be done depending on finite TZs' position and RL level value so as to find better filtering solution.

An example of input variables influence on technological parameters is presented in Figure 2.12 where effective coupling coefficient has different values, depending on RL level, while set of finite TZs is maintained unchanged. Here, it can be observed that uniform value of $k^2_{eff} = 5.7\%$ suitable for AlN SMR resonator is achieved when RL=15 dB for given set of normalized finite TZs [1.411j, -1.789j, 1.604j, -1.618j, 1.604j, -1.789j, 1.411j]. Different from 15 dB value of RL will lead to necessity of external elements implementation for resonators 1&7 and 2&6 in order to fulfill the technological constraints. This, in turn, will provoke chip size increase, passband edge-

Table 2.1: Band 1 Transmitter Specifications

Parameter	Freq. Band (MHz)	Value (dB)
Insertion Loss	1920 - 1980	> -2
Isolation	2110 - 2170	< -50
Out-of-Band Rejection	1710 - 1755 (B4-Tx)	< -40
	2400 - 2500 (Wi-Fi)	< -40

rounding because of low quality factor of external capacitors and inductors, and more complex fabrication. Presented example deals with symmetric filtering network which makes technological constraints easier to fulfill since only four different resonators have to be designed. In case of asymmetric filter the complexity of constraints accommodation is increased and external elements inclusion may be inevitable. Thus, RL level has strong influence on acoustic technological requirements and it has to be carefully chosen. However, the inverse relationship between RL and out-of-band rejection level has to be taken into account as well.

Set of finite TZs is also chosen by designer at the beginning of the filter design. As it has been explained before, these TZs are related to resonant frequencies f_s and f_p for shunt and series resonators, respectively. Generally, acoustic technology allows one f_s for all shunt resonators and 2 different f_s among series resonators. This restriction is particularly important in BAW technology where every additional f_s requires another masking step or external element implementation in an already complex fabrication process [20]. Nevertheless, in [79] it has been stated that multiple resonant frequencies can be achieved by fabrication of resonators with multiple thicknesses on the same substrate.

In this section two examples of stand-alone filter and duplexer in Band 1 are performed in order to demonstrate the design methodology suitable for acoustic technology, taking into account aforementioned relationship between input parameters and technological constraints.

Stand-Alone Filter in Band 1

The first example is a ninth-order symmetric stand-alone filter for Band 1 Tx with passband extending from 1.92 to 1.98 GHz and with specifications presented in Table 2.1. Effective coupling coefficient is taken to be $k_{eff}^2 = 6.8\%$. Carrying out the same study on input parameters, a set of finite normalized TZs of [$1.411j$, $-1.779j$, $1.604j$, $-1.608j$, $1.584j$, $-1.608j$, $1.604j$, $-1.779j$, $1.411j$], and RL = 15 dB have been chosen in order to achieve a uniform k_{eff}^2 among all resonators. Thus, no external elements are required for the proposed design.

Resulting BVD reactive elements are presented in Table 2.2. Since it is a stand-alone filter, no reactive elements are needed at input and output port. The magnitude response of S-parameters

Table 2.2: BVD bandpass elements of ninth-order stand-alone transmitter filter in Band 1 Tx.

Parameters	Res 1&9	Res 2&8	Res 3&7	Res 4&6	Res 5
L_a (nH)	56.54	38.01	178.09	35.83	177.88
C_a (pF)	0.1185	0.1866	0.0374	0.1968	0.0374
C_0 (pF)	2.0251	3.1872	0.6373	3.3483	0.6379
k_{eff}^2 (%)	6.8	6.8	6.8	6.8	6.8
f_s (GHz)	1.9449	1.8897	1.9512	1.8952	1.9505

Figure 2.13: Magnitude response of symmetric acoustic bandpass filter in Band 1 Tx at (a) out-of-band and (b) in-band frequencies.
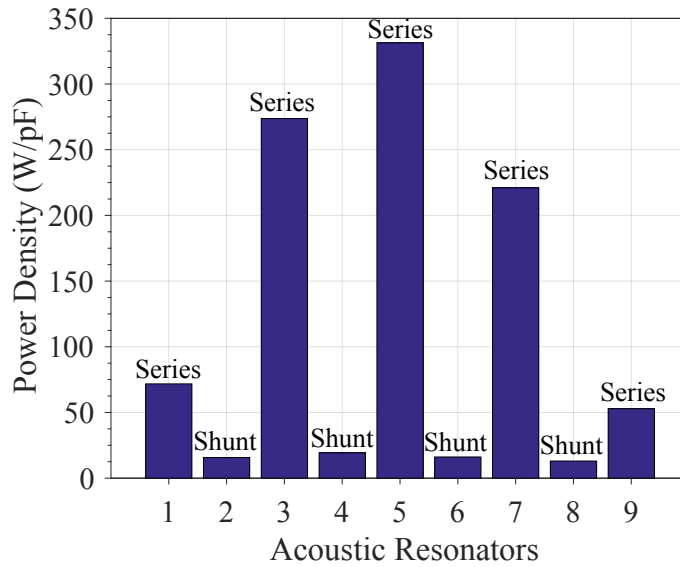
Figure 2.14: Power density distribution among series and shunt connected acoustic resonators evaluated at $f_2 = 1.98$ GHz.

at out-of-band and in-band frequencies is illustrated in Figure 2.13 (a) and (b), respectively. Here, it can be observed that all mask specifications are fulfilled. In order to provide a more realistic filtering network, the quality factor is taken to be $Q = 2000$ for both series and parallel resonant frequencies and fabrication and temperature margins equal 500 ppm. Therefore, to accomplish the in-band IL specification and compensate passband edge-rounding, filter bandwidth has been extended by 4.1 and 6 MHz at the left and the right passband edges, respectively.

The proposed methodology also allows to analyze the power density distribution among resonators illustrated in Figure 2.14. The power density level of each resonator is calculated at the upper passband frequency $f_2 = 1.98$ GHz as it is the most energetically critical point. It can be observed that shunt connected resonators undergo the lowest power level due to their larger values of C_0 or, in other words, due to their bigger size. Meanwhile, series resonators suffer from the highest energy level, especially resonators 3&7 and 5, since they are the smallest resonators in the structure, and therefore, they likely have to be cascaded. Thus, considering input power of 29 dBm, the total capacitance area of designed filter equals to 55 pF.

Duplexer in Band 1

The second example of lowpass synthesis methodology is a duplexer in Band 1. For the design we use the same transmitter filter elaborated in previous example but in this case the input phase has to be accommodated at dual central frequency $f_{dual} = 2.14$ GHz so as to avoid the loading effect at receiver filter passband. Thus, the corrected phase response of S_{11} is illustrated
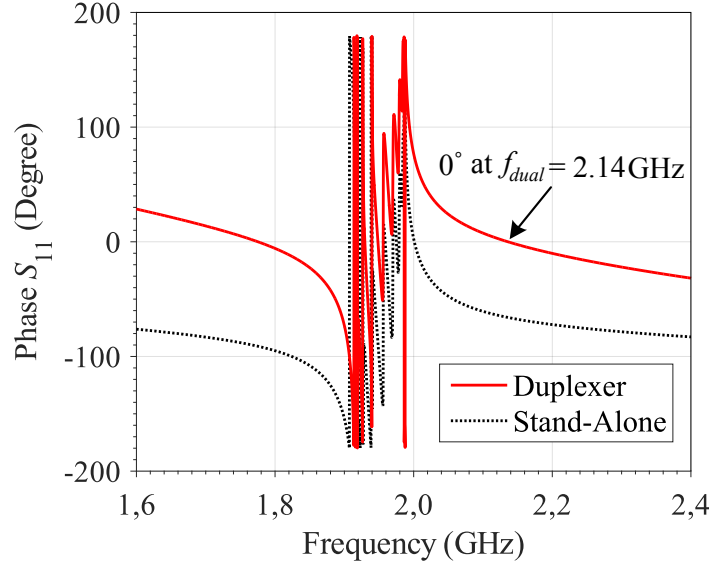
Figure 2.15: S_{11} phase response of the transmitter filter in Band 1.

Table 2.3: BVD bandpass elements of ninth-order transmitter filter in Band 1 Tx as a part of duplexer.

Parameters	Res 1&9	Res 2&8	Res 3&7	Res 4&6	Res 5
L_a (nH)	140.55	22.65	106.13	21.35	106.00
C_a (pF)	0.0463	0.3131	0.0627	0.3303	0.0628
C_0 (pF)	0.7913	5.3482	1.0694	5.6186	1.0704
k_{eff}^2 (%)	6.8	6.8	6.8	6.8	6.8
f_s (GHz)	1.9735	1.8897	1.9512	1.8952	1.9505

$$L_{in} = L_{out} = 4.95 \text{ nH}; \ C_{ext_1} = C_{ext_9} = 0.935 \text{ pF}.$$

in Figure 2.15 where phase modification from $-67°$ to $0°$ has been performed for duplexer design. The BVD elements of updated transmitter filter are shown in Table 2.3 where it can be observed that all reactive elements of the filter are changed. Required in this case shunt connected inductors provokes modification of $k_{eff}^2 = 3.2\%$ of the first and the last resonators, and therefore, series connected external capacitors have to be implemented so as to fulfill the technological requirements, making $k_{eff}^2 = 6.8\%$ for all resonators. Quality factor for inductors and capacitors are considered to be 25 and 100, respectively.

Receiver filter design is performed by the same procedure as described above. A ninth-order symmetric filter with passband extending from 2.11 to 2.17 GHz and specifications presented in Table 2.4 has to be designed, fulfilling technological constraints. For this purpose, a set of normalized finite TZs of [2.171j, -1.973j, 1.784j, -1.788j, 1.777j, -1.788j, 1.784j, -1.973j, 2.171j]

Table 2.4: Band 1 Receiver Specifications

Parameter	Freq. Band (MHz)	Value (dB)
Insertion Loss	2110 - 2170	> -2
Isolation	1920 - 1980	< -50
Out-of-Band Rejection	1710 - 1755 (B4-Tx)	< -40
	2400 - 2500 (Wi-Fi)	< -40

Table 2.5: BVD bandpass elements of ninth-order receiver filter in Band 1 Rx as a part of duplexer.

Parameters	Res 1&9	Res 2&8	Res 3&7	Res 4&6	Res 5
L_a (nH)	107.53	22.92	149.98	22.57	152.77
C_a (pF)	0.0508	0.2569	0.0368	0.2595	0.0362
C_0 (pF)	0.8695	4.3695	0.6310	4.4191	0.6157
k_{eff}^2 (%)	6.8	6.8	6.8	6.8	6.8
f_s (GHz)	2.1533	2.0742	2.1409	2.0800	2.1409

$$L_{in} = L_{out} = 6.57 \text{ nH.}$$

and RL = 18 dB are considered, providing uniform $k_{eff}^2 = 6.8\%$. In this design we have already corrected the input phase so as to adapt the reflection response at dual central frequency of transmitter filter $f_{dual} = 1.95$ GHz. However, since lowpass-to-bandpass transformation lacks of precision at out-of-band frequencies, we have had to adjust the phase value manually in both filters in order to obtain precisely $0°$ at f_{dual}.

Resulting BVD elements of the filter are shown in Table 2.5, including shunt connected inductors at source and load. Magnitude response of S-parameters at out-of-band and in-band frequencies is illustrated in Figure 2.16 (a) and (b), respectively. The same quality factors for resonators $Q = 2000$ and inductors $Q = 25$, and fabrication and temperature margins of 500 ppm are considered. In order to fulfill IL level mask specification, the passband has been enlarged by 3.5 and 5 MHz at the left and the right passband edges, respectively.

Finally, an overall duplexer network has the form presented in Figure 2.17 where both transmitter and receiver filters are connected together. The input inductor at antenna port is calculated as parallel of both L_{in_R} and L_{in_T} so that $L_{in} = 2.82$ nH. Resulting duplexer transmission and reflection response is illustrated in Figure 2.18 where some loading effect can be noticed in RL level since the phase is corrected only at central frequency and not in whole passband. Nevertheless, all specifications of the duplexer remain fulfilled.
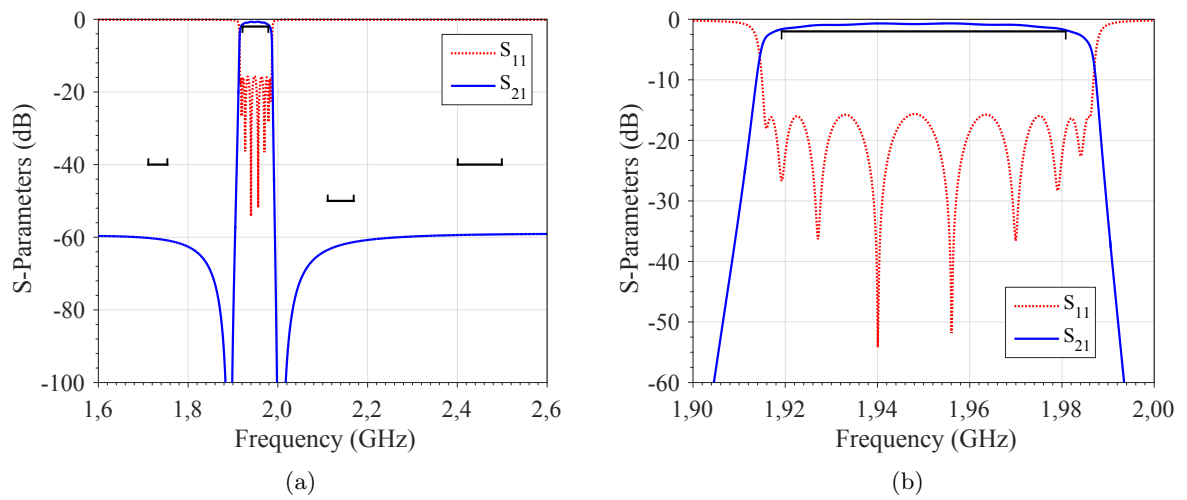
(a)

(b)
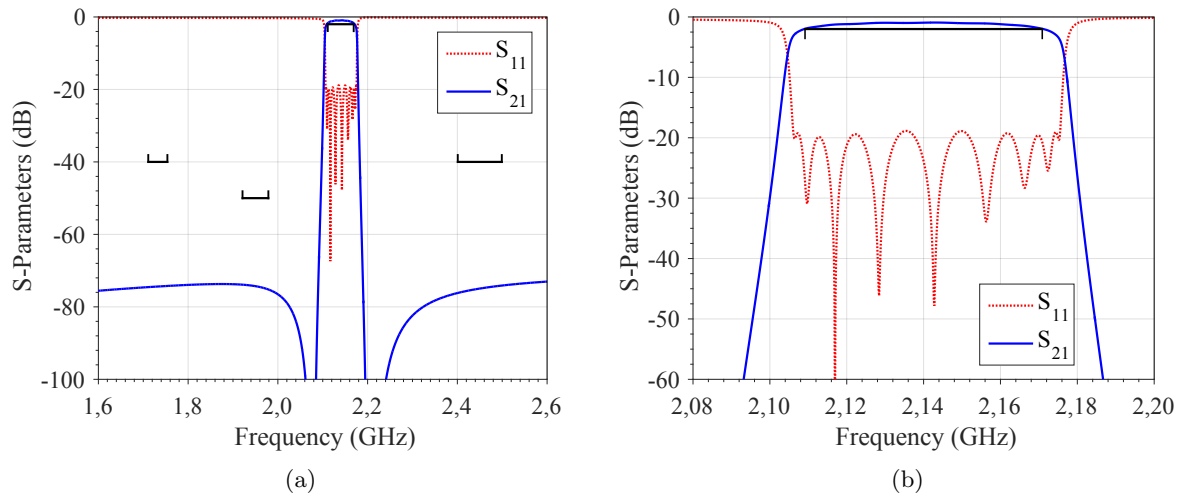
Figure 2.16: Magnitude response of symmetric acoustic bandpass filter in Band 1 Rx at (a) out-of-band and (b) in-band frequencies.
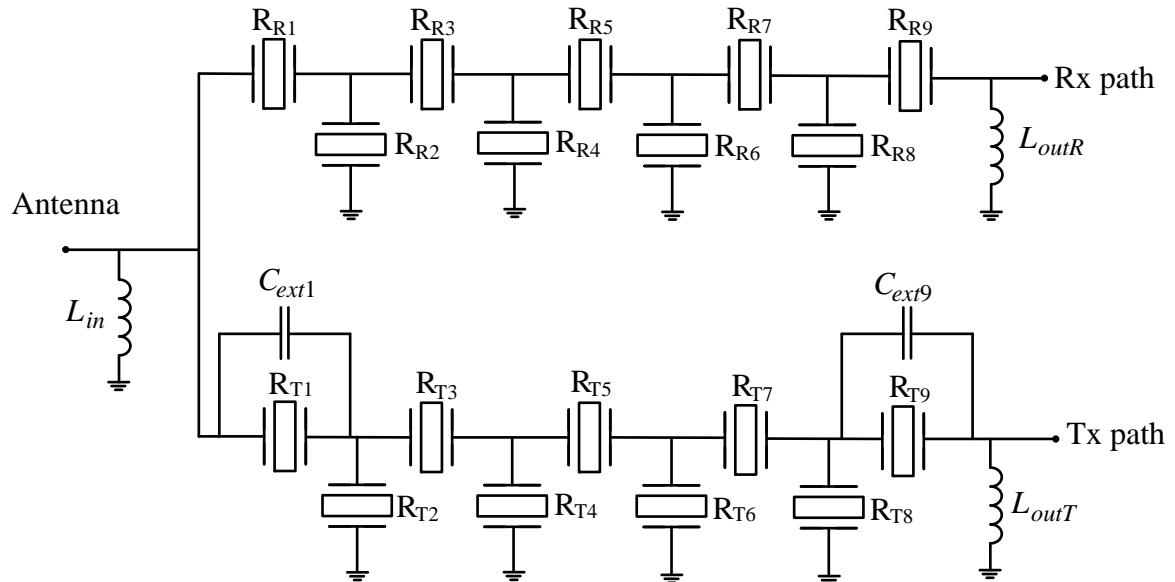
Figure 2.17: Designed duplexer network in Band 1.
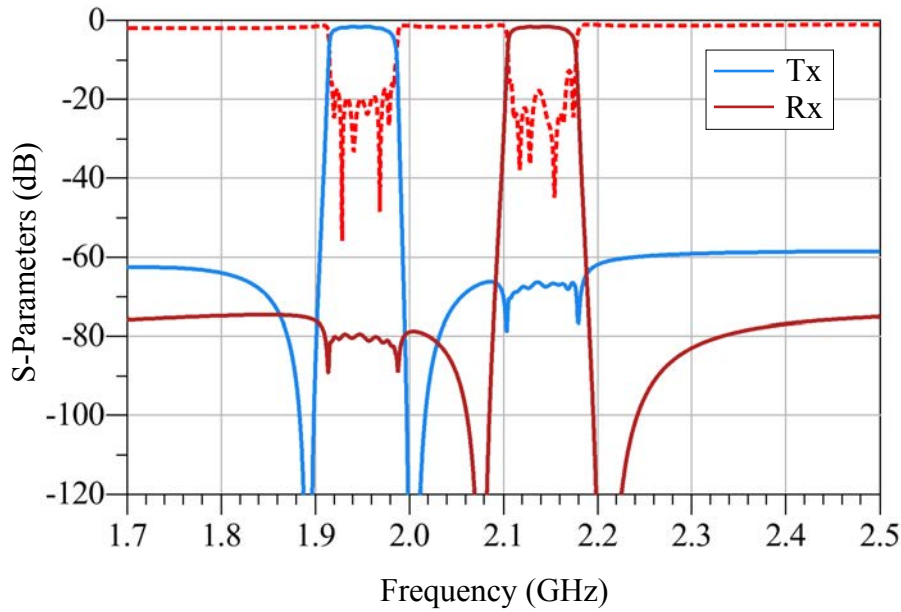
Figure 2.18: Magnitude response of designed duplexer network in Band 1.

2.6   Chapter Summary

In this chapter a detailed procedure of synthesis and design of ladder-type acoustic filters and duplexers has been presented. Dangling resonator model takes part in inline nodal representation of ladder-type topology and provides modularity and flexibility in TZs' assignment, performing fully canonical network. This useful feature allows to obtain frequency response with high selectivity which is particularly important for future demands.

Chebyshev filtering function and characteristic polynomials have been applied in order to describe mathematically the transmission and reflection response of acoustic wave filter. Set of prescribed normalized TZs and RL level are input parameters of the synthesis predetermined by designer. In order to provide a feasible network, important relationships of energy conservation and orthogonality have to be fulfilled. Input admittance is determined from characteristic polynomials which is applied in process of lowpass elements' extraction. Further denormalization finalizes the filter design, providing bandpass BVD acoustic resonators.

Automatic search engine of the input variables permits to obtain the best suited filtering network within the specified ranges of technological constraints. Such network performs as a good initial seed for further optimization procedures such as electromagnetic simulation, package influence, and others. Moreover, different studies can be carried out so as to understand the interdependence of input variables and micro-acoustic technological parameters.

Input phase correction is an additional feature of the methodology which is important for

duplexers' and multiplexers' design. Minimum changes have to be done in stand-alone filter synthesis so as to adapt its phase response. When two filters are connected in duplexer network, no loading effect is produced at counterband central frequency. Unlike phase shifters, appearing in this case inductors at source and load can be implemented in acoustic technology.

Synthesis and Design of Ladder-Type Acoustic Filter in Bandpass Domain

Acoustic filters have been broadly used in mobile telecommunication systems for many years. Throughout this time, they were successfully designed by traditional circuital approach and recently by narrowband lowpass synthesis technique described in Chapter 2; however, both of them have significant limitations. Circuital approach cannot manage a big number of constraints, and optimization process has to be implemented to properly conclude the filter design. Narrowband lowpass synthesis technique overcomes this drawback; however, magnitude and phase estimation at far out-of-band frequencies exhibits lack of precision. Using frequency independent NRN approximation can only give a successful result over a narrow band of frequencies in microwave region. Filter description in lowpass domain neglects poles and zeros at the origin, infinity, and at negative frequencies. Combining it with narrowband lowpass-to-bandpass elements' transformation provides inaccurate magnitude and phase response at out-of-band frequencies in bandpass domain. Therefore, in many cases lowpass approach is not sufficient in order to fulfill technological requirements and mask specifications, which become more complex in course of time.

To overcome these limitations, a direct bandpass methodology for ladder-type acoustic filters has been developed and is explained in this chapter. Different networks with capacitive and inductive matching elements and frequency dependent reactive nodes are carefully analyzed and described by corresponding filtering functions. The methodology concludes with extraction procedure of bandpass elements and accommodation of micro-acoustic technological constraints. An important issue about numerical instabilities, which always occurs in direct bandpass synthesis, is also discussed. Finally, two examples in Band 25 are provided in order to validate the proposed methodology and highlight its differences over traditional lowpass approach described in Chapter 2.

3.1   Basic Principles of Bandpass Methodology for Micro-Acoustic Technology

Lowpass synthesis drawbacks in terms of precision have always been the subject of discussion. Indeed, this fast and simple mathematical tool is the most commonly used in filter's synthesis and the most studied. Introduction of FIR and NRN expanded the field of its application even more. Different solutions to improve the precision of lowpass approach have been proposed by introducing frequency dependent reactive nodes as a separate from resonators elements in [80] or frequency-variant couplings [81]. These approximations represent a more realistic scenario of filter's frequency behavior; however, only narrow or moderate bandwidth filters can be synthesized by them. Moreover, inline nodal representation consisted of all dangling resonators is considered neither. Frequency-variant couplings cannot be implemented in acoustic technology since they do not physically exist and serve just to serialize shunt connected resonator.

The direct bandpass methodology presented in this chapter takes into account special characteristics of micro-acoustic technology in terms of topology and frequency response. Here, all reactive nodes (except matching elements at source and load) are linked with resonant nodes and no frequency-variant couplings are considered. This leads to a predetermined number of TZs at the origin and infinity which cannot be modified. Moreover, two passbands at positive and negative frequencies are taken into account, thus fully describing the frequency behavior of filtering network.

In order to obtain reactive elements responsible of TZs at the origin and infinity, partial and complete extraction procedure is applied. When partial extraction is implemented, the degree of reactance function does not change. Reactive capacitive and inductive elements, which prepare the extraction of following finite TZs, are obtained by this operation. At the same time, all of them operate on one TZ at the origin and one TZ at infinity. Number of these TZs does not depend on number of partially extracted reactive elements. Complete extraction is applied for elements which do not take part in resonator equivalent circuit nor prepare the extraction of following finite TZs. Each element extracted by this manner acts separately and introduce its own TZ at the origin or infinity. Number of such TZs depends on the number of completely extracted reactive elements. As a result, the degree of reactance function does reduce during the extraction.

In this work we consider two basic ladder-type networks started either with series or shunt connected resonators. Adding two options of matching elements at source and load, i.e., capacitive or inductive reactive nodes, four different solutions of bandpass filtering network are proposed. Each solution provides different number of TZs at the origin, and therefore, it is described by different filtering function.
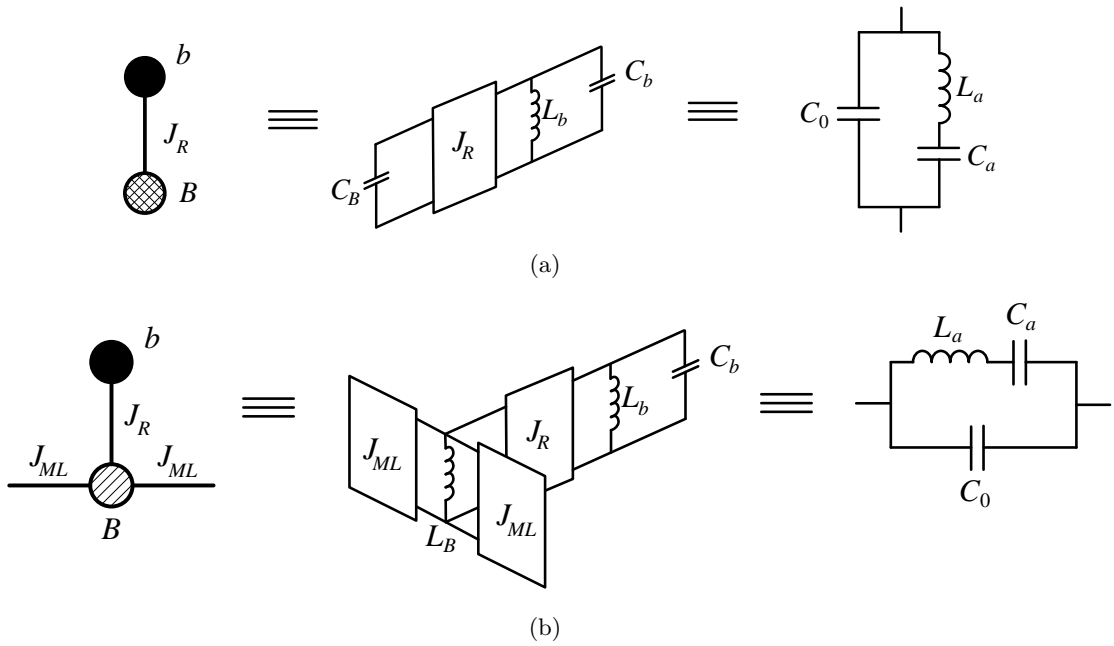
Figure 3.1: Bandpass equivalent circuit of dangling resonator connected in (a) shunt and (b) series.

Hereafter, the detailed bandpass synthesis and design process of four possible networks is explained, taking into account the specificity of micro-acoustic technology, particular features of acoustic resonator representation, and fabrication constraints.

3.2 Filter Topology Definition

As it has been outlined in Chapter 2, the most commonly used topology for acoustic wave filters in high-frequency applications is inline configuration [20]. Similarly to lowpass approach, in bandpass domain it is also a fully canonical network, finite TZs of which are independently controlled by dangling resonators. Figure 3.1 shows dangling model of shunt and series resonators in bandpass approach. Here, instead of FIR, reactive frequency dependent nodes are implemented: capacitive reactive node for shunt resonator depicted in Figure 3.1 (a), and inductive reactive node for series resonator illustrated in Figure 3.1 (b). Resonant node corresponds to the motional acoustic branch in electrical equivalent circuit, and reactive node represents static capacitance path. These frequency dependent nodes introduce additional TZs at the origin or infinity, and taking them into account increases accuracy of transmission and reflection response. The nature of reactive nodes is important in order to obtain finite TZs below and above the passband correctly. Inductive reactive node of series resonator is transformed to the capacitive one due to admittance side inverters. These inverters are considered ideal because their function is just to

serialize the shunt resonator, and therefore, no inverters are physically implemented.

Once the bandpass model of dangling resonator has been defined, the inline topology of the filter can be described. It consists of several cascaded dangling resonators alternating series and shunt position. Depending on nature of reactive nodes at source and load there are two options of feasible networks which are outlined below.

3.2.1   Networks with Capacitive Matching Elements

Two possible networks with capacitive reactive nodes at source and load can be obtained starting either with series or shunt resonator. Both inline configurations, with corresponding ladder-type topologies, are presented in Figure 3.2. Alternating capacitive and inductive nodes B_i of the shunt or series resonators are important for the finite TZ removal of the following series or shunt resonator, respectively, which is similar to sign alternation of NRNs in lowpass methodology. As well as in lowpass approach, where NRN of one resonator prepares the annihilation of the next TZ above or below the passband, in bandpass methodology not only do capacitive and inductive reactive nodes prepare the following finite TZ removal, but they also introduce TZs at the origin and infinity. Being part of the equivalent dangling resonator circuit presented in Figure 3.1, these reactive nodes can only be obtained by partial extraction, and therefore, capacitive nodes of all shunt connected resonators from networks depicted in Figure 3.2 operate on one TZ at infinity, and inductive reactive nodes of all series connected resonators introduce one TZ at the origin. Thus, without source and load reactive elements consideration, any ladder-type Nth-order filter topology starting either with series or shunt resonator and regardless of the filter's order exhibits one TZ at the origin, one TZ at infinity and $2 \times N$ finite TZs at positive and negative passbands.

As it has been explained, the following finite TZ removal is carried out by capacitive or inductive reactive node of previous resonator. Therefore, following this rule, finite TZs of the first and the last resonators need to be prepared by source and load reactive nodes. Thus, in case of series first/last resonator the source/load node must be capacitive, and in equivalent circuit presented in Figure 3.2 (a) it is performed by shunt connected capacitor. And in case of shunt first/last resonator the source/load node must be inductive, but taking into account two side inverters it is converted into capacitive which is then realized by series connected capacitor. This case is demonstrated in Figure 3.2 (b). Since these capacitors serve to prepare the following finite TZ annihilation, they are also obtained by partial extraction, and therefore, they contribute to the existing TZs at the origin and infinity, thus not increasing their multiplicity. Finally, networks with capacitive matching elements are characterized by presence of one TZ at the origin, one TZ at infinity, and $2 \times N$ finite TZs at both passbands.

The explanation written above for ladder-type acoustic filters can be summarized in following

(a)

(b)
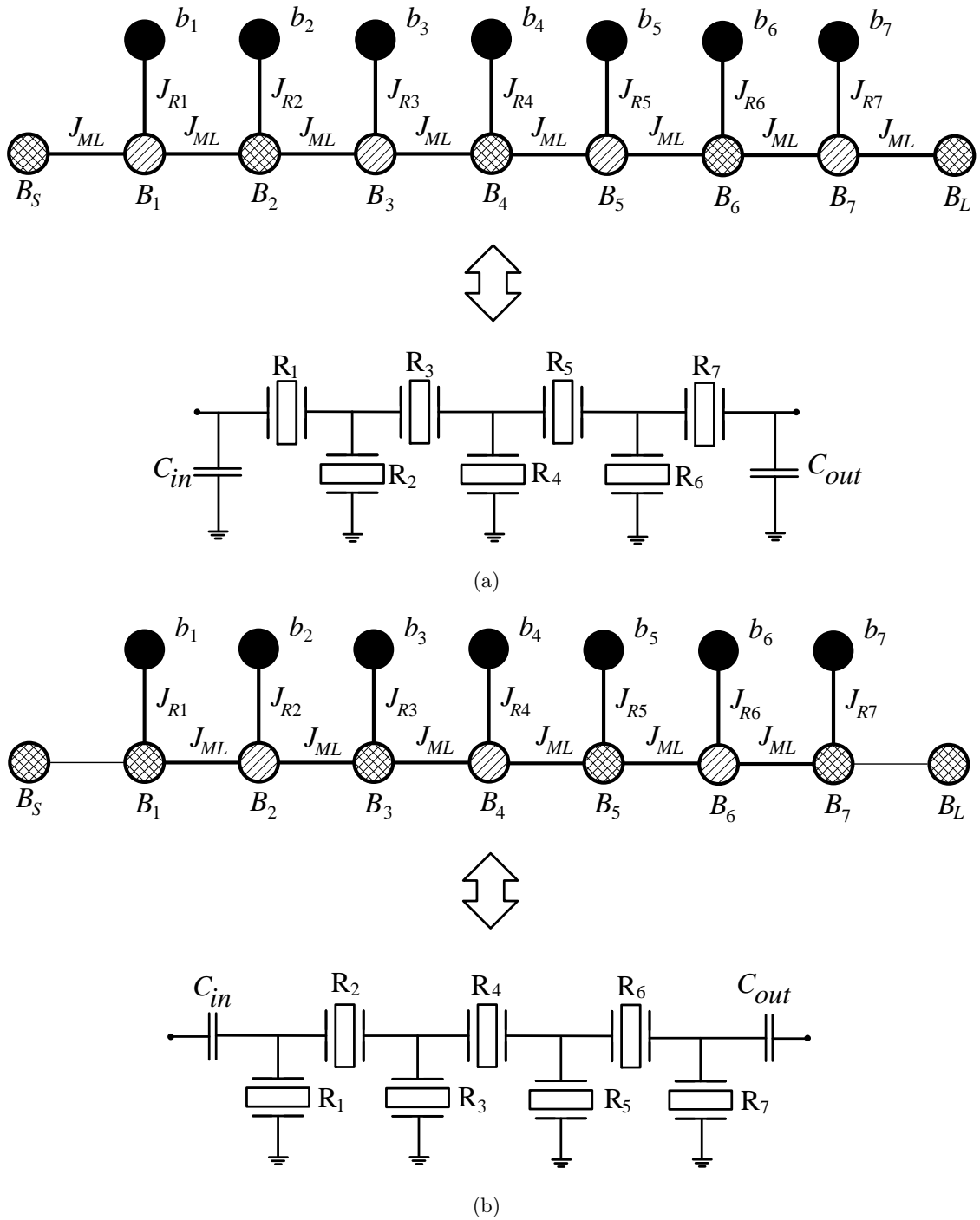
Figure 3.2: Networks with capacitive matching elements starting with (a) series and (b) shunt resonator. Series resonators are shown with inductive nodes and shunt connected resonators are depicted with capacitive nodes.

rules:

1. Regarding reactive nodes of dangling resonators:

    - Partial extraction of TZ at infinity performed by capacitive reactive node prepares the annihilation of following finite TZ at $s_i = \pm j\omega_i$ above the passband.

    - Partial extraction of TZ at the origin performed by inductive reactive node prepares the annihilation of following finite TZ at $s_i = \pm j\omega_i$ below the passband.

    - Partial extraction of inductive and capacitive reactive nodes of all resonators contribute to one TZ at the origin and one TZ at infinity, respectively.

2. Regarding reactive nodes at source and load:

    - Partial extraction of shunt connected capacitor is needed in order to prepare the annihilation of first/last finite TZ at $s_i = \pm j\omega_i$ ($i = 1, N$) above the passband performed by series resonator.

    - Partial extraction of series connected capacitor is needed in order to prepare the annihilation of first/last finite TZ at $s_i = \pm j\omega_i$ ($i = 1, N$) below the passband performed by shunt resonator.

    - Partial extraction of capacitive reactive nodes at source and load contributes to the existing TZs at the origin and infinity.

3.2.2   Networks with Inductive Matching Elements

Apart from capacitive matching elements, acoustic ladder-type filters can be realized with inductive reactive nodes at source and load. The choice of elements' nature depends on practical realization and technological requirements. Networks under consideration are presented in Figure 3.3, where Figure 3.3 (a) illustrates the case of series first resonator and Figure 3.3 (b) shows the case of shunt first resonator. As it has been demonstrated above, the capacitors C_{in} and C_{out} are necessary in order to correctly prepare the extraction of the first and the last finite TZs. Therefore, the only way to have inductive matching elements at source and load is to introduce shunt connected inductors before and after the whole scheme. Each of them is obtained by complete extraction, and therefore, introduces additional TZ at the origin (two TZs at zero frequency from both L_{in} and L_{out}). Taking into consideration the rules mentioned above, it can be noticed that both networks depicted in Figure 3.3 have three TZs at the origin, one TZ at infinity, and $2 \times N$ finite TZs at both passbands. Since the number of TZs is changed, depending on nature of matching elements, two filtering functions described each case are required.

It may seem that presence of four reactive elements of different nature at source and load can complicate the practical realization of the network. If the case of four reactive elements
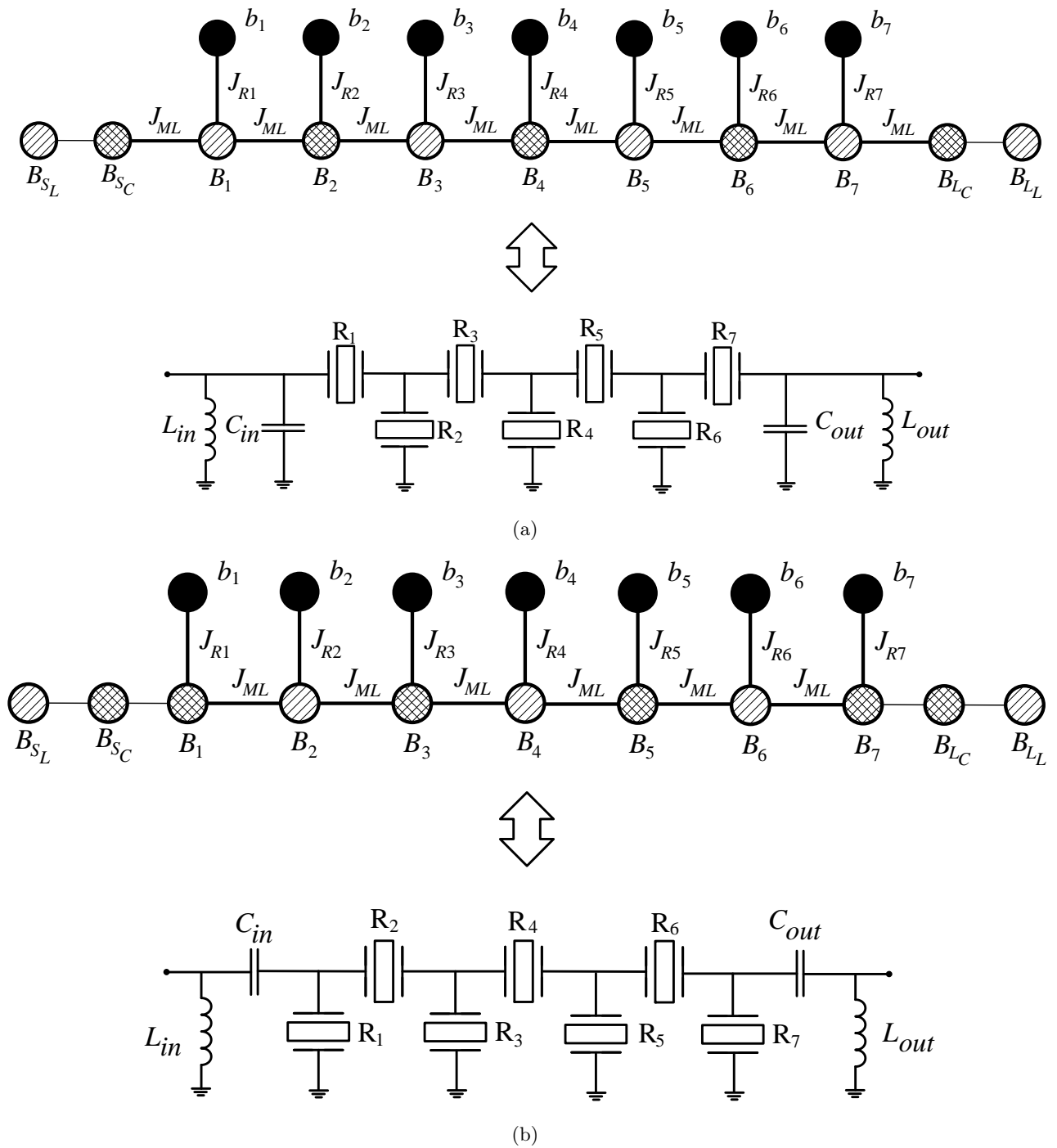
Figure 3.3: Networks with inductive matching elements starting with (a) series and (b) shunt resonator.
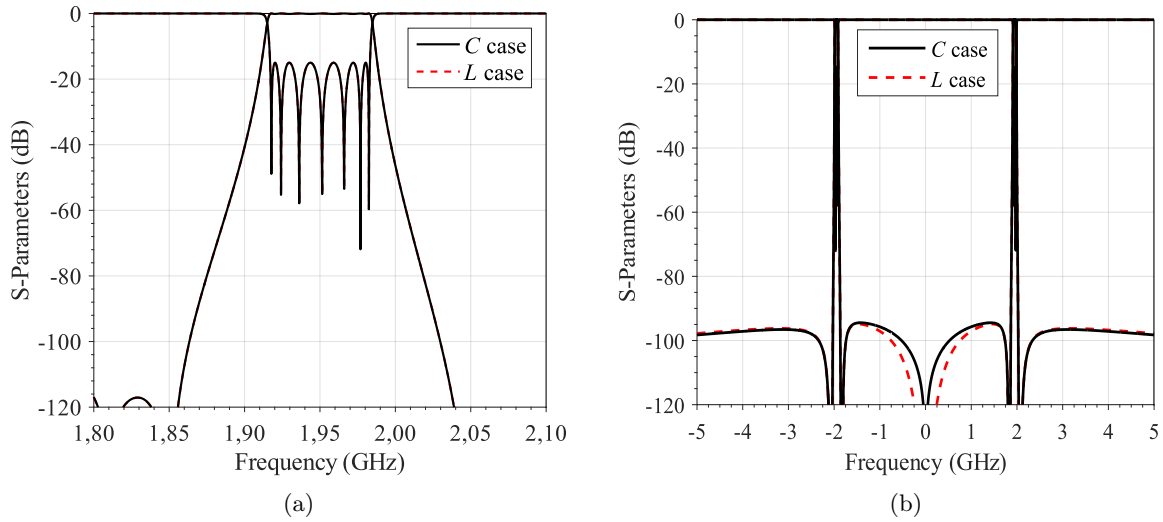
Figure 3.4: Filters' transmission and reflection parameters for networks with capacitive and inductive matching elements at (a) in-band and (b) out-of-band frequencies.

is undesirable, phase modification technique described in Chapter 4 can be used. Input phase correction can make the capacitors C_{in} and C_{out} to be neglected, and therefore, only shunt connected inductors will remain. Adding optimization process can also lead to the networks with only shunt connected inductors at input and output. Then, the most important thing that has to be taken into account is the accordance between number of TZs realized by filtering function and by optimized network.

3.3   Definition of Bandpass Filtering Function

In Chapter 2 Chebyshev filtering function $C_N(\Omega)$, which completely describes the fully-canonical ladder-type network in lowpass domain, has been presented. There, only normalized finite TZs of dangling resonators are taken into account, whereas poles and zeros far away from the passband, specifically at zero frequency are neglected, since central frequency of the filter is located at the origin. Therefore, lowpass response of Nth-order filter described by lowpass filtering function is characterized by presence of N finite TZs and N RZs inside the passband.

In order to define new filtering functions for ladder-type configuration with two types of matching elements, we are going to analyze the features of transmission and reflection parameters of the networks depicted in Figures 3.2 and 3.3. Figure 3.4 illustrates behavior of S-parameters of seventh-order filter started with series resonator and with different matching elements. It can be noticed that both responses are identical at in-band frequencies depicted in Figure 3.4 (a), the only difference is in near zero fly-back levels which is due to different number of TZs at the

origin which is illustrated in Figure 3.4 (b). Observing the response at in-band and out-of-band frequencies, the following requirements for bandpass filtering functions can be stated:

1. A dual-passband response at positive $[\omega_1, \omega_2]$ and negative $[-\omega_2, -\omega_1]$ passbands has to be considered.
2. An Nth-order filter is characterized by presence of N finite TZs with reference to one passband.
3. An Nth-order filter is characterized by presence of N RZs with reference to one passband.
4. For networks with capacitive matching elements one TZ at the origin and one TZ at infinity have to be taken into account which do not introduce additional RZs over the whole range of frequencies.
5. For networks with inductive matching elements three TZs at the origin and one TZ at infinity have to be taken into account which do not introduce additional RZs over the whole range of frequencies.

Therefore, new filtering functions have to be able to accommodate these requirements in order to achieve feasible network in bandpass domain. Hereafter, two filtering functions are derived, suitable for networks with capacitive and inductive reactive nodes at source and load. The procedure is identical for both networks started with series or shunt connected resonator.

3.3.1 Bandpass Filtering Function for Networks with Capacitive Matching Elements

Taking into account the requirements outlined before, a new filtering function for topologies with capacitive matching elements is found to be [82]:

$$K(\omega) = \cosh\left[\cosh^{-1}\left(T_0\left(\omega\right)\right) + \sum_{n=1}^{N} \cosh^{-1}\left(X_n\left(\omega\right)\right)\right], \tag{3.1}$$

Function $X_n(\omega)$ is the bandpass equivalent of the function $x_n(\Omega)$ in lowpass domain, and it introduces finite TZs and RZs at both positive and negative passbands. In addition, $X_n(\omega)$ has to satisfy a number of requirements:

1. At $\omega = \omega_n$, where ω_n is a finite TZ at both positive and negative frequencies, $X_n(\omega) = \pm\infty$.
2. At the passband edges of both positive and negative bands, $X_n(\pm\omega_1) = -X_n(\pm\omega_2) = -1$.
3. Between $\omega = \pm\omega_1$ and $\omega = \pm\omega_2$, i.e., both positive and negative passband frequency range, $1 \geq X_n(\omega) \geq -1$.

Considering these specification, the function $X_n(\omega)$ is found to be

$$X_n(\omega) = \frac{T_1(\omega) - 1/T_1(\omega_n)}{1 - T_1(\omega)/T_1(\omega_n)}, \tag{3.2}$$
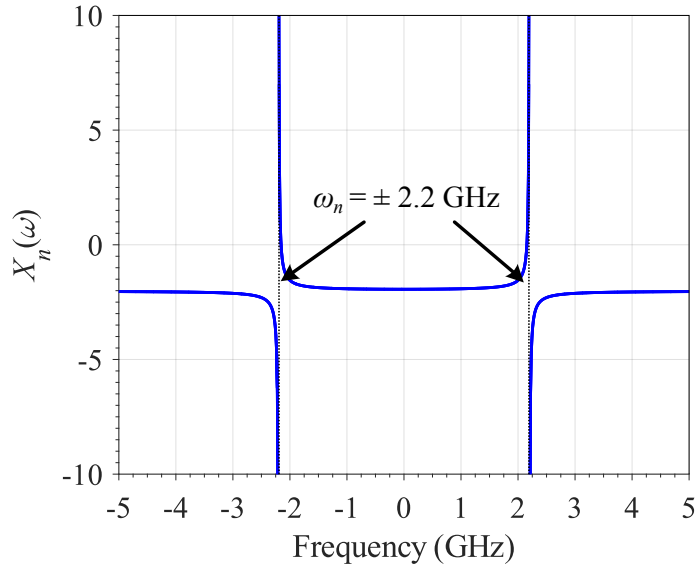
Figure 3.5: Graphical representation of function $X_n(\omega)$ with prescribed TZ at $\omega_n = 2.2$ GHz and passband extending from $f_1 = 2.11$ GHz to $f_2 = 2.17$ GHz.

where $T_1(\omega)$ is derived as

$$T_1(\omega) = \frac{2\omega^2 - \left(\omega_1^2 + \omega_2^2\right)}{\omega_2^2 - \omega_1^2}. \tag{3.3}$$

Figure 3.5 shows frequency behavior of $X_n(\omega)$ considering $\omega_n = 2.2$ GHz and passband extending from 2.11 to 2.17 GHz. Here, it can be noticed that all conditions imposed on $X_n(\omega)$ are fulfilled.

Another function $T_0(\omega)$ from (3.1) is responsible for introduction of TZ at the origin, but no RZ over the whole range of frequencies. $T_0(\omega)$ has following properties:

1. $T_0(\omega = 0) = \pm\infty$ to introduce a TZ in the origin.
2. At the passband edges of both positive and negative bands, $T_0(\pm\omega_1) = T_0(\pm\omega_2) = \pm 1$.

Thus, the function $T_0(\omega)$ is derived to be

$$T_0(\omega) = \frac{T_2(\omega)}{\omega}, \qquad T_2(\omega) = \frac{\omega^2 + \omega_1\omega_2}{\omega_2 - \omega_1}. \tag{3.4}$$

The term $T_0(\omega)$ from (3.4) was obtained by mixing two different solutions proposed in [82] by Amari et al. for bandpass transversal filters of arbitrary bandwidth where TZs at infinity are performed by resonators; and in [83] by Zhang et al. for dual-wideband bandpass filters with source-load coupling. A comparison between three functions $T_0(\omega)$ is illustrated in Figure 3.6. There, it can be noticed that the term derived by Amari et al. crosses zero at a frequency inside the passband, and therefore, introduces an additional undesirable RZ. Nevertheless, it has a good
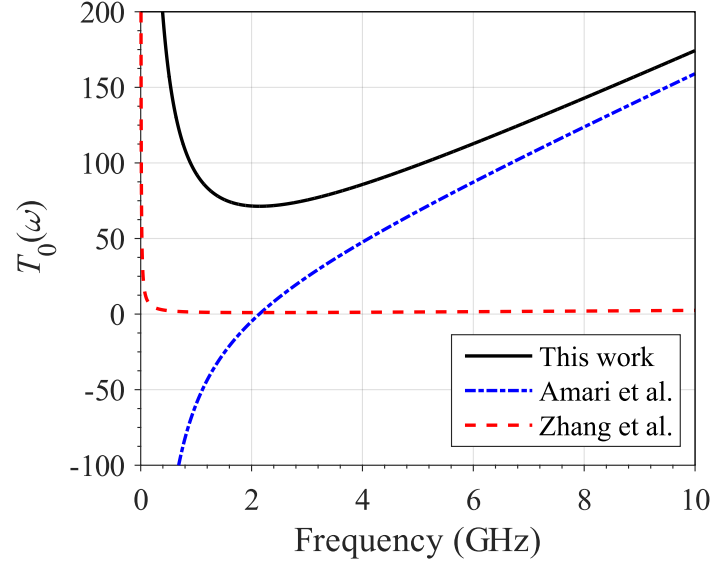
Figure 3.6: Comparison of the functions $T_0(\omega)$ proposed by Amari et al., Zhang et al., and the one introduced in this work suitable for a ladder-type acoustic filter with passband extending from $f_1 = 2.11$ GHz to $f_2 = 2.17$ GHz.

attenuation at out-of-band frequencies. The function proposed by Zhang et al. does not cross zero but its attenuation is flat at higher frequencies. The term proposed in this work (3.4) combine both needed features, i.e., step slope at out-of-band frequencies and no additional RZ. The slope maintains its steepness over the whole range of frequencies; thus, the term $T_0(\omega = \infty) = \infty$. This means that TZ at infinity is intrinsically introduced by $T_0(\omega)$. Therefore, $T_0(\omega)$ derived by (3.4) is appropriate for synthesis of ladder-type acoustic filters in bandpass domain and permits to realize partial extraction of series or shunt connected capacitors at source and load, and capacitive and inductive reactive nodes of dangling resonators.

3.3.2 Bandpass Filtering Function for Networks with Inductive Matching Elements

As it has been explained in Section 3.2.2, filters with shunt connected inductors at source and load exhibit three TZs at zero frequency, one TZ at infinity, and $2 \times N$ finite TZs at both positive and negative passbands. Therefore, the filtering function from (3.1) has to be updated including another term which introduces two TZs at the origin more, and which permits to realize complete extraction of shunt connected inductors. Thus, resulting filtering function in this case is found to be

$$K(\omega) = \cosh \left[\cosh^{-1}\left(T_0\left(\omega\right)\right) + \cosh^{-1}\left(T_0'\left(\omega\right)\right) + \sum_{n=1}^{N} \cosh^{-1}\left(X_n\left(\omega\right)\right) \right]. \qquad (3.5)$$
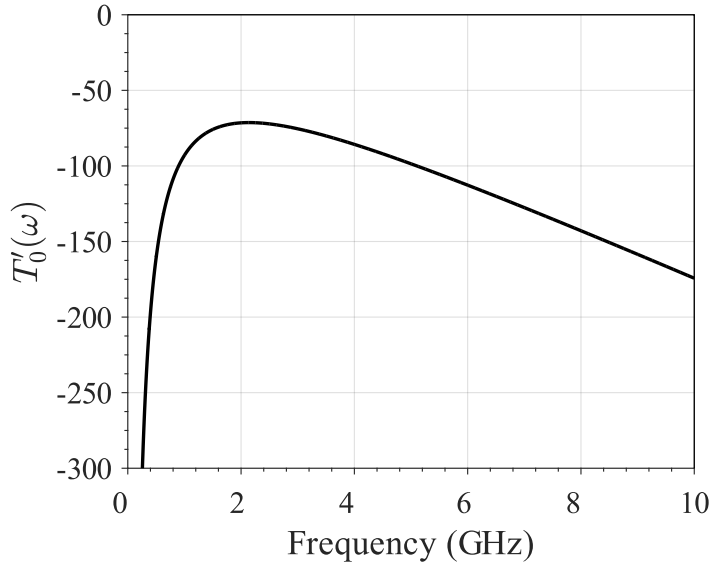
Figure 3.7: Function $T_0'(\omega)$ for ladder-type acoustic filter with inductive matching elements. The passband extends from $f_1 = 2.11$ GHz to $f_2 = 2.17$ GHz.

Functions $X_n(\omega)$ and $T_0(\omega)$ are derived as in previous case of capacitive matching elements by (3.2) and (3.4).

The new term $T_0'(\omega)$ able to accommodate two TZs at zero frequency so that $T_0'(\omega^2 = 0) = \pm\infty$, is represented as

$$T_0'(\omega) = \frac{T_2'(\omega)}{\omega^2}, \qquad T_2'(\omega) = \frac{-\omega^3 - \omega_1\omega_2\omega}{\omega_2 - \omega_1}. \tag{3.6}$$

Figure 3.7 shows the behavior of function $T_0'(\omega)$. It can be noticed that high attenuation level and no additional undesirable RZs appears in this case either. The term $T_0'(\omega)$ also introduces one TZ at infinity as $T_0(\omega)$, but since it is obtained by partial extraction its multiplicity does not increase, i.e., one TZ at infinity is preserved.

Thus, two filtering functions have been introduced in order to synthesize networks with capacitive and inductive matching elements. In the process of filtering function obtaining every additional TZ has to be reflected in new added term and then be properly extracted by reactive elements. Therefore, an agreement between mathematical description and physical realization of the network must be maintained. Only reactive matching elements at source and load can be extracted by elaborated in this section filtering functions for ladder-type acoustic filters. This means, that if ground inductors or cross-couplings (couplings between nonsequential resonators) have to be implemented in the network, they have to be correctly described by mathematical term in filtering function. As a result, depending on complexity of the final filter topology, the filtering function elaboration can be difficult to realize, which makes the methodology hard to

generalize.

3.4   Definition of Characteristic Polynomials

The filtering system is completely described by its characteristic polynomials $P(\omega)$, $F(\omega)$, and $E(\omega)$, since transmission and filtering functions are derived as

$$H(\omega) = \frac{E(\omega)}{P(\omega)} \tag{3.7}$$

and

$$K(\omega) = \frac{F(\omega)}{P(\omega)}. \tag{3.8}$$

As well as in lowpass synthesis approach, in order to obtain a physically realizable network bandpass characteristic polynomials have to fulfill the following requirements:

1. Coefficients of $P(\omega)$, $F(\omega)$, and $E(\omega)$ must be real.
2. $P(\omega)$ and $F(\omega)$ are either pure even or pure odd.
3. $E(\omega)$ must be a Hurwitz polynomial, i.e., its singularities must be located at the left side of the complex plane.
4. Degree of $P(\omega)$ must be lower or equal to that of $F(\omega)$.

Further derivation of polynomials $P(\omega)$, $F(\omega)$, and $E(\omega)$ is performed by similar method as for lowpass synthesis described in [54].

Capacitive Matching Elements Case

In order to establish accordance between equations (3.1) and (3.8), the filtering function has been rewritten by introduction (3.2) and (3.4) into (3.1). Then, after several mathematical steps the alternative expression for $K(\omega)$ results to be

$$K(\omega) = \frac{1}{2} \frac{(c_0 + d_0) \prod_{n=1}^{N} (c_n + d_n) + (c_0 - d_0) \prod_{n=1}^{N} (c_n - d_n)}{\omega \prod_{n=1}^{N} (1 - s_n T_1(\omega))}. \tag{3.9}$$

And functions c_0, d_0, c_n, d_n, and s_n are derived as follows

$$c_0 = T_2(\omega), \tag{3.10a}$$

$$d_0 = \sqrt{T_2^2(\omega) - \omega^2}, \tag{3.10b}$$

$$c_n = s_n T_1(\omega), \tag{3.10c}$$

$$d_n = \sqrt{1 - s_n^2}\sqrt{T_1^2(\omega) - 1}, \tag{3.10d}$$

$$s_n = 1/T_1(\omega_n). \tag{3.10e}$$

By simple inspection it can be noticed that denominator of $K(\omega)$ in (3.9) contains zeros of polynomial $P(\omega)$, i.e., all set of TZs at both passbands, including that at zero frequency. Since TZs are prescribed at the beginning of the synthesis, the polynomial $P(\omega)$ can be directly obtained.

At the same time, zeros of $F(\omega)$, i.e., all set of RZs are comprised in the numerator of $K(\omega)$ in (3.9). Therefore, in order to compute coefficients of $F(\omega)$ a recursive technique, where solution of the nth step is built up from the results of the $(n-1)$th step, is elaborated, following the same strategy as described in [54]. Thus, the numerator of $K(\omega)$ can be rearranged into two polynomials $U(\omega)$ and $V(\omega)$ so that

$$U_N(\omega) = u_{2N}\omega^{2N} + u_{2N-1}\omega^{2N-1} + \ldots + u_1\omega + u_0, \tag{3.11a}$$

$$V_N(\omega) = \omega'\left(v_{2N}\omega^{2N} + v_{2N-1}\omega^{2N-1} + \ldots + v_1\omega + v_0\right), \tag{3.11b}$$

where ω' is the transformed variable and it is found to be

$$\omega' = \sqrt{T_1^2(\omega) - 1}. \tag{3.12}$$

The iteration routine starts with the term which introduces one TZ at zero frequency. Thus, initial polynomials $U_0(\omega)$ and $V_0(\omega)$ are found to be

$$U_0(\omega) = c_0 = T_2(\omega) = \frac{\omega^2 + \omega_1\omega_2}{\omega_2 - \omega_1}, \tag{3.13a}$$

$$V_0(\omega) = d_0 = \sqrt{T_2^2(\omega) - \omega^2} = \omega'\left(\frac{\omega_1 - \omega_2}{2}\right). \tag{3.13b}$$

Then, the cycle is repeated N times in order to introduce the term describing finite TZs. Therefore, the polynomials $U_i(\omega)$ and $V_i(\omega)$ are updated at each iteration by following expressions:

$$U_i(\omega) = U_{i-1}(\omega)\left(T_1(\omega) - s_i\right) + \omega'\sqrt{1 - s_i^2}V_{i-1}(\omega), \tag{3.14a}$$

$$V_i(\omega) = \omega'\sqrt{1 - s_i^2}U_{i-1}(\omega) + V_{i-1}(\omega)\left(T_1(\omega) - s_i\right). \tag{3.14b}$$

Here, s_i is calculated for positive set of TZs, since TZs at negative passbands are inherently included in function $T_1(\omega)$ in (3.3) and do not have to be considered apart. Last polynomial U_N with real coefficients represents $F(\omega)$ and its roots are set of all RZs.

Knowing both $P(\omega)$ and $F(\omega)$, Hurwitz polynomial $E(\omega)$ is calculated according to Feldtkeller equation which is found to be

$$|H(\omega)|^2 = 1 + |K(\omega)|^2, \tag{3.15}$$

and therefore,

$$|E(\omega)|^2 = |F(\omega)|^2 + |P(\omega)|^2. \tag{3.16}$$

Finally, when all characteristic polynomials of the filtering network are known, real normalizing constants ε and ε_R can be defined. Since number of finite TZs $n_{fz} > N$ in bandpass ladder-type configuration, which means that it is no fully canonical network, parameter $\varepsilon_R = 1$. Therefore, the constant ε is derived as

$$\varepsilon = \frac{1}{\sqrt{1 - 10^{-RL/10}}} \left| \frac{P(\omega)}{E(\omega)} \right|_{\omega=\omega_1}, \tag{3.17}$$

where ω_1 is the frequency of left edge of positive passband.

Inductive Matching Elements Case

Applying the same mathematical procedures, the rational form of filtering function from (3.5), which accommodates two TZs at the origin more, is obtained and has the following expression:

$$K(\omega) = \frac{1}{2} \frac{(c_0 + d_0)(c'_0 + d'_0) \prod_{n=1}^{N} (c_n + d_n) + (c_0 - d_0)(c'_0 - d'_0) \prod_{n=1}^{N} (c_n - d_n)}{\omega^3 \prod_{n=1}^{N} (1 - s_n T_1(\omega))}, \tag{3.18}$$

where functions c_0, d_0, c_n, d_n, and s_n are calculated by the same way as in previous case of capacitive matching elements using (3.10), and terms c'_0 and d'_0 are obtained as

$$c'_0 = T'_2(\omega), \tag{3.19a}$$

$$d'_0 = \sqrt{T'^2_2(\omega) - \omega^4}. \tag{3.19b}$$

As it can be noticed, the roots of denominator of $K(\omega)$ now contain three TZs at the origin which take part in polynomial $P(\omega)$ calculation.

Polynomial $F(\omega)$ is derived by recursive technique proposed above, but an additional step has to be included after obtaining $U_0(\omega)$ and $V_0(\omega)$ by (3.13). New polynomials $U'_0(\omega)$ and $V'_0(\omega)$, which introduce two TZs at the origin more, have to be taken into account and they are found to be

$$U'_0(\omega) = U_0(\omega)T'_2(\omega) + \omega' V_0(\omega) \left(\frac{\omega(\omega_1 - \omega_2)}{2} \right), \tag{3.20a}$$

$$V'_0(\omega) = V_0(\omega)T'_2(\omega) + \omega' U_0(\omega) \left(\frac{\omega(\omega_1 - \omega_2)}{2} \right). \tag{3.20b}$$

Then, the cycle is repeated N times for finite TZs introduction by expressions (3.14). Resulting polynomial $U_N(\omega)$ represents $F(\omega)$. Remaining polynomial $E(\omega)$ and normalizing constant ε are found according to (3.16) and (3.17).

Characteristic polynomials $P(\omega)$, $F(\omega)$, and $E(\omega)$ for networks with different matching elements at source and load have been obtained by methodology similar to that for lowpass synthesis approach. Here, the same situation as with filtering functions can be noticed, i.e., the recursive technique for polynomial $F(\omega)$ derivation is not general, but depends on topology. Therefore,
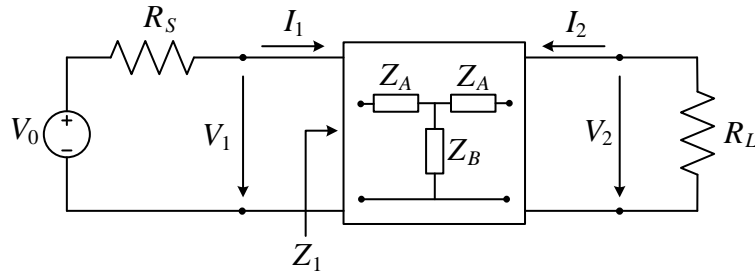
Figure 3.8: Impedance equivalent network with its operating conditions for filters started with series resonator.

each new TZ introduced by additionally coupled reactive elements has to be described by new polynomials $U_0^n(\omega)$ and $V_0^n(\omega)$ and be implemented in overall recursive routine. This means that as well as filtering function, iterative procedure cannot be generalized either.

3.5   Bandpass Ladder-Type Network Realization

After defining bandpass filtering functions and characteristic polynomials which mathematically describe transmission and reflection behavior of networks with capacitive and inductive matching elements, we proceed to their circuital realization. In this section open- and short-circuit reactance functions are introduced which then are applied in extraction procedure of inline nodal representation elements. Further, the extracted elements are denormalized and inline topology is transformed into ladder-type configuration based on BVD resonators.

3.5.1   Open- and Short-Circuit Reactance Functions

Derived in Section 3.4 $H(\omega)$ and $K(\omega)$ expressed as ratio of two polynomials are applied to determine impedance function for networks with series first resonator, and admittance function for topologies with first resonator connected in shunt.

Equivalent circuit with its typical operating conditions for series first resonator case is presented in Figure 3.8, where R_S is internal resistance of voltage source and R_L is load resistance. Z-equivalent circuit inside the quadripole describes the filter with the first and the last resonators positioned in series. Therefore, according to the Kirchhoff's law the following expressions can be written:

$$V_1 = Z_{11}I_1 + Z_{12}I_2, \tag{3.21a}$$

$$V_2 = Z_{21}I_1 + Z_{22}I_2. \tag{3.21b}$$

Also, according to the network in Figure 3.8, the voltages V_1 and V_2 can be expressed as

$$V_1 = V_0 - I_1 R_S, \tag{3.22a}$$

$$V_2 = -I_2 R_L. \tag{3.22b}$$

Substituting V_1 and V_2 from (3.21) into (3.22), currents I_1 and I_2 are found to be

$$I_1 = V_0 \frac{Z_{22} + R_L}{(Z_{11} + R_S)(Z_{22} + R_L) - Z_{12}^2}, \tag{3.23a}$$

$$I_2 = -V_0 \frac{Z_{12}}{(Z_{11} + R_S)(Z_{22} + R_L) - Z_{12}^2}, \tag{3.23b}$$

since generally for passive network $Z_{12} = Z_{21}$. It is known that transmission function can be represented as [84]

$$H(\omega) = \frac{1}{2}\sqrt{\frac{R_L}{R_S}}\frac{V_0}{V_2} = \frac{1}{2}\sqrt{\frac{R_L}{R_S}}\frac{V_0}{-I_2 R_L}. \tag{3.24}$$

Therefore, applying expressions for currents I_1 and I_2 from (3.23), the equation (3.24) can be rewritten as

$$H(\omega) = \frac{(Z_{11} + R_S)(Z_{22} + R_L) - Z_{12}^2}{2Z_{12}\sqrt{R_S R_L}}. \tag{3.25}$$

The input impedance parameter Z_1 is obtained as

$$Z_1 = \frac{V_1}{I_1} = \frac{V_0 - I_1 R_S}{I_1} = \frac{V_0}{I_1} - R_S, \tag{3.26}$$

and applying expression (3.23) for current I_1, it becomes

$$Z_1 = \frac{(Z_{11} + R_S)(Z_{22} + R_L) - Z_{12}^2}{Z_{22} + R_L} - R_S = Z_{11} - \frac{Z_{12}^2}{Z_{22} + R_L}. \tag{3.27}$$

From [54] the filtering function is defined as

$$K(\omega) = H(\omega)\rho(\omega), \tag{3.28}$$

where the reflection coefficient $\rho(\omega)$ is found to be

$$\rho(\omega) = \frac{Z_1 - R_S}{Z_1 + R_S} = \frac{(Z_{11} - R_S)(Z_{22} + R_L) - Z_{12}^2}{(Z_{11} + R_S)(Z_{22} + R_L) - Z_{12}^2}. \tag{3.29}$$

Therefore, taking into account (3.29), $K(\omega)$ can be expressed as

$$K(\omega) = \frac{(Z_{11} - R_S)(Z_{22} + R_L) - Z_{12}^2}{2Z_{12}\sqrt{R_S R_L}}. \tag{3.30}$$

According to Foster's theorem [85], $Z(\omega)$ is always an odd function. This means that polynomials Z_{11}, Z_{22}, and Z_{12} are also odd. Therefore, transmission function $H(\omega)$ from (3.25) and filtering
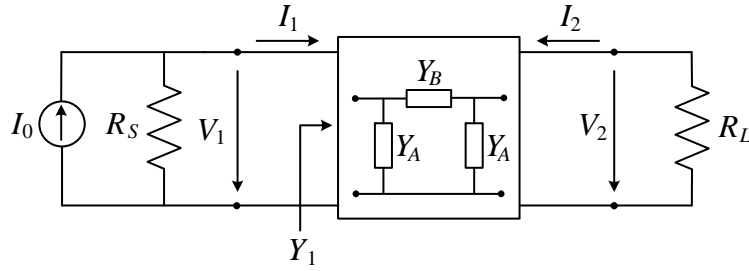
Figure 3.9: Admittance equivalent network with its operating conditions for filters started with shunt resonator.

function $K(\omega)$ from (3.30) can be divided into their even and odd parts:

$$H_e(\omega) = \frac{Z_{11}R_L + Z_{22}R_S}{2Z_{12}\sqrt{R_S R_L}} \,, \qquad H_o(\omega) = \frac{Z_{11}Z_{22} - Z_{12}^2 + R_S R_L}{2Z_{12}\sqrt{R_S R_L}}, \tag{3.31a}$$

$$K_e(\omega) = \frac{Z_{11}R_L - Z_{22}R_S}{2Z_{12}\sqrt{R_S R_L}} \,, \qquad K_o(\omega) = \frac{Z_{11}Z_{22} - Z_{12}^2 - R_S R_L}{2Z_{12}\sqrt{R_S R_L}}. \tag{3.31b}$$

With addition and subtraction application:

$$H_e + K_e = \sqrt{\frac{R_L}{R_S}} \frac{Z_{11}}{Z_{12}}, \tag{3.32a}$$

$$H_e - K_e = \sqrt{\frac{R_S}{R_L}} \frac{Z_{22}}{Z_{12}}, \tag{3.32b}$$

$$H_o + K_o = \frac{Z_{11}Z_{22} - Z_{12}^2}{Z_{12}\sqrt{R_S R_L}}, \tag{3.32c}$$

$$H_o - K_o = \frac{\sqrt{R_S R_L}}{Z_{12}}. \tag{3.32d}$$

And resolving (3.32) for input and output impedance parameters Z_{11} and Z_{22}:

$$Z_{11} = R_S \frac{H_e + K_e}{H_o - K_o}, \tag{3.33a}$$

$$Z_{22} = R_L \frac{H_e - K_e}{H_o - K_o}. \tag{3.33b}$$

The same analysis for admittance parameters can be realized for networks with the first and the last resonators positioned in shunt. This type of networks is described by admittance equivalent circuit presented in Figure 3.9 and its equations:

$$I_1 = Y_{11}V_1 + Y_{12}V_2, \tag{3.34a}$$

$$I_2 = Y_{21}V_1 + Y_{22}V_2. \tag{3.34b}$$

Table 3.1: Input/output open- and short-circuit reactance parameters for Z- and Y-equivalent circuits, respectively [84].

	Z-Equivalent Circuit		Y-Equivalent Circuit	
	P even	P odd	P even	P odd
X_{1o}, X_{1s}	$R_S \dfrac{E_e + F_e}{E_o - F_o}$	$R_S \dfrac{E_o + F_o}{E_e - F_e}$	$\dfrac{1}{R_S} \dfrac{E_o - F_o}{E_e + F_e}$	$\dfrac{1}{R_S} \dfrac{E_e - F_e}{E_o + F_o}$
X_{2o}, X_{2s}	$R_L \dfrac{E_e - F_e}{E_o - F_o}$	$R_L \dfrac{E_o - F_o}{E_e - F_e}$	$\dfrac{1}{R_L} \dfrac{E_o - F_o}{E_e - F_e}$	$\dfrac{1}{R_L} \dfrac{E_e - F_e}{E_o - F_o}$

After similar mathematical derivations short-circuit input and output parameters Y_{11} and Y_{22} are found to be

$$Y_{11} = \frac{1}{R_S} \frac{H_o - K_o}{H_e + K_e}, \tag{3.35a}$$

$$Y_{22} = \frac{1}{R_L} \frac{H_o - K_o}{H_e - K_e}. \tag{3.35b}$$

Taking into consideration that characteristic polynomials $F(\omega)$ and $E(\omega)$ can be subdivided into their even and odd parts, the expressions (3.7) and (3.8) can be rewritten as

$$H(\omega) = \frac{E_e + E_o}{P}, \tag{3.36a}$$

$$K(\omega) = \frac{F_e + F_o}{P}, \tag{3.36b}$$

where polynomial $F(\omega)$ is either even or odd function, and therefore, either $F_e(\omega) = 0$ or $F_o(\omega) = 0$. Since polynomial $P(\omega)$ is also either an even or odd function [84], the impedance and admittance parameters can be divided in two parts for each equivalent circuit. Table 3.1 represents input and output open- and short-circuit reactance functions for both networks. Obtained reactance parameters and set of zeros of $P(\omega)$ completely define the filtering network. Therefore, circuit elements values can be realized by partial or complete removal of residues at these poles.

3.5.2   Elements Extraction Procedure

Once impedance and admittance functions have been defined, network elements can be realized by extraction procedure. Extraction routine consists of two operations: partial and complete removal of TZs. The former is used to prepare the following finite TZ introduced by resonator and does not reduce degree of reactance function. In ladder-type topology only TZs at the origin and infinity can be realized by partial extraction. Complete removal does reduce degree of

(a)   (b)
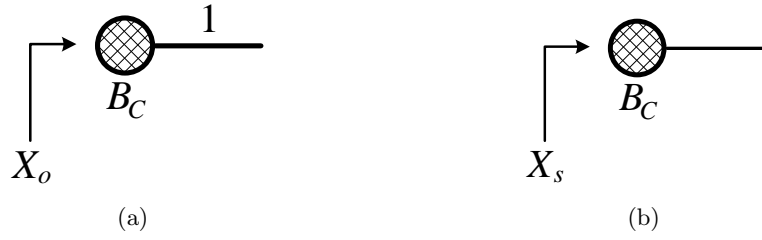
Figure 3.10: Capacitive reactive nodes to be extracted positioned in (a) shunt and (b) series.

reactance function since it operates on finite TZs of the resonators or reactive elements (in case of inductive matching elements) which do not take part in following finite TZ preparation. Below, the extraction of basic blocks from the input port of inline nodal representation is presented. The procedure from the output port is the same.

Capacitive Reactive Node

Capacitive reactive nodes for two networks started either with series or shunt connected resonator are shown in Figure 3.10, where Figure 3.10 (a) represents shunt connected capacitor and Figure 3.10 (b) illustrates series connected capacitor. Therefore, in order to extract the capacitive node from the Figure 3.10 (a) impedance function is used:

$$B_C = \left. \frac{X_o(s)}{s} \right|_{s=j\omega_1}, \tag{3.37a}$$

$$z_2(s) = X_o(s) - s \cdot B_C. \tag{3.37b}$$

The capacitor is evaluated at the first finite TZ, since it prepares its complete extraction, and then partially extracted. Also, it contributes in TZ at infinity. Then, considering inverter $J_{ML} = 1$, we obtain $y_3(s) = 1/z_2(s)$.

In case of series connected capacitor for networks with shunt first resonator depicted in Figure 3.10 (b) admittance function is applied:

$$B_C = \left. \frac{1}{X_s(s) \cdot s} \right|_{s=j\omega_1}, \tag{3.38a}$$

$$y_2(s) = X_s(s) - \frac{1}{s \cdot B_C}. \tag{3.38b}$$

Here, the capacitor is also evaluated at the first finite TZ, but in this case it contributes in TZ at the origin. Although there is no inverter between source node and shunt resonator, we have to change the nature of reactance function by $z_3(s) = 1/y_2(s)$ in order to complete the extraction of the whole network.
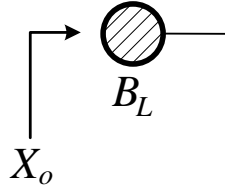
Figure 3.11: Shunt inductive reactive node to be extracted.

Inductive Reactive Node

Shunt connected inductor operates in one TZ at the origin and it does not prepare further annihilation of the first finite TZ. Therefore, it is obtained by complete extraction which is the same for both networks. Its nodal representation is shown in Figure 3.11. Therefore, using impedance reactance function:

$$B_L = \left. \frac{X_o(s)}{s} \right|_{s=0}, \tag{3.39a}$$

$$z_2(s) = X_o(s) - \frac{1}{s \cdot B_L}. \tag{3.39b}$$

Then, the following capacitive node is extracted by (3.37) or (3.38). However, for shunt first resonator network a previous step of reactance function nature changing must be applied. Since connection and introduced TZ value of the capacitors are different, they cannot be extracted by the same reactance function. This is why changing of its nature is required.

Series Connected Resonator

Series resonator under consideration and its equivalent circuit is shown in Figure 3.12 where inverters $J_{ML} = J_R = 1$. Here, resonant node b_i represented by pair of shunt connected L_{b_i} and C_{b_i} introduces finite TZs above the passband at positive and negative frequencies, and these TZs have to be completely extracted. Thus, after previous matching elements extraction described above, the capacitor C_{b_i}, which contains both TZs, is found to be

$$C_{b_i} = \left. \frac{s}{y_k(s) \cdot (s^2 + \omega_i^2)} \right|_{s=j\omega_i}, \tag{3.40a}$$

$$y_{k+1}(s) = y_k(s) - \frac{s/C_{b_i}}{s^2 + \omega_i^2}, \tag{3.40b}$$

where ω_i $(i = 1, 2, ..., N)$ is finite TZ at positive passband, $k = 3$ for networks with capacitive matching elements, and $k = 4$ for topologies including shunt connected inductors at source and load.
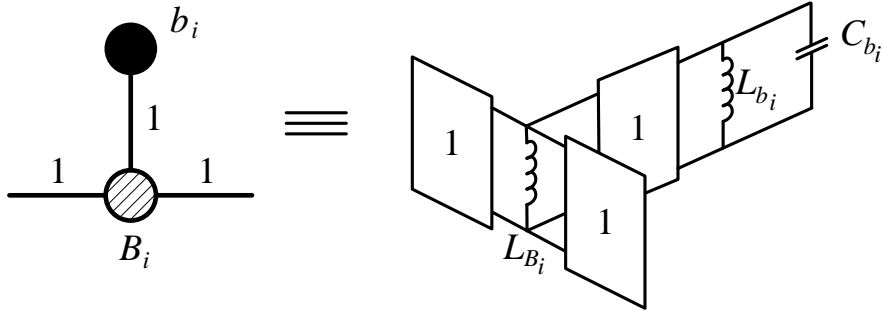
Figure 3.12: Series connected resonator to be extracted.
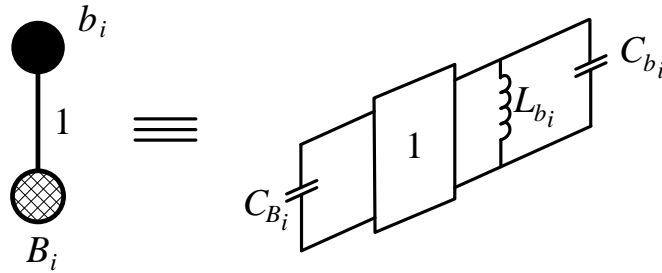
Figure 3.13: Shunt connected resonator to be extracted.

Applying expression for resonant frequency, inductor L_{b_i} is derived as

$$L_{b_i} = \frac{1}{\omega_i^2 C_{b_i}}. \tag{3.41}$$

Reactive node B_i, which is realized by shunt connected inductor L_{B_i}, prepares the annihilation of following finite TZ ω_{i+1} below the passband of the next shunt connected resonator, and it also contributes in TZ at the origin. Therefore, it has to be partially extracted:

$$L_{B_i} = \left. \frac{1}{s \cdot y_{k+1}(s)} \right|_{s=j\omega_{i+1}}, \tag{3.42a}$$

$$y_{k+2}(s) = y_{k+1}(s) - \frac{1}{sL_{B_i}}. \tag{3.42b}$$

Finally, the unit inverter makes $z_{k+3}(s) = 1/y_{k+2}(s)$, and the elements extraction procedure of following shunt connected resonator can be fulfilled.

Shunt Connected Resonator

Figure 3.13 represents shunt connected resonator and its equivalent circuit. As well as in case of series resonator, pair of shunt connected L_{b_i} and C_{b_i} introduces finite TZs below the passband

at positive and negative frequencies. Here, the inductor L_{b_i} is obtained by complete removal of these two TZs by following expression:

$$L_{b_i} = \left. \frac{s}{z_k(s) \cdot (s^2 + \omega_i^2)} \right|_{s=j\omega_i}, \tag{3.43a}$$

$$z_{k+1}(s) = z_k(s) - \frac{s/L_{b_i}}{s^2 + \omega_i^2}, \tag{3.43b}$$

where $k = 3$ for networks with capacitive reactive nodes, and $k = 5$ for inductive reactive nodes at source and load. Capacitor C_{b_i} is found to be

$$C_{b_i} = \frac{1}{\omega_i^2 L_{b_i}}. \tag{3.44}$$

The same way, shunt connected capacitor C_{B_i} prepares the annihilation of following finite TZ ω_{i+1} above the passband of the next series connected resonator, and it contributes in TZ at infinity as well. Therefore, partial extraction has to be applied:

$$C_{B_i} = \left. \frac{z_{k+1}(s)}{s} \right|_{s=j\omega_{i+1}}, \tag{3.45a}$$

$$z_{k+2}(s) = z_{k+1}(s) - sC_{B_i}. \tag{3.45b}$$

Then, the following unit inverter of series resonator provides $y_{k+3}(s) = 1/z_{k+2}(s)$, and extraction of the following series connected resonator can be realized.

In order to increase accuracy, the extraction routine has to be realized from both input and output port. Presented circuital extraction of bandpass elements leads to feasible positive capacitors and inductors of the network. The procedure is similar to that from lowpass approach, although it does not result in negative values proper to series resonators in lowpass domain which also requires a sign alternation of inverters $J_{ML} = \pm 1$. Instead of sign changing, in direct bandpass synthesis there is an alternation between reactance functions and nature of extracted elements. This is the reason of all positive values of inverters $J_{ML} = 1$ in bandpass approach.

3.5.3 Normalization

It is known that in bandpass domain typical values of circuit capacitors and inductors of acoustic filters are about pF and nH, respectively, and operating frequency is about few GHz. Derivation of filtering function and characteristic polynomials may have additional computational problems if denormalized values are considered, and their derivation becomes more difficult with the filter's order increase.

To overcome this problem the variables of the synthesis procedure are normalized. Thus, two reference values are applied: resistance R_c which can be taken as internal resistance of

voltage or current source R_S; and frequency ω_n which can be equal to $\omega_c = 2\pi 10^9$ rad/s or $\omega_c = \omega_0 = \sqrt{\omega_1 \omega_2}$, i.e., to be set as central frequency. Running synthesis routine with normalized values provides accuracy and accelerates the computation.

Thus, after normalized circuital elements obtaining, l, c, normalized frequencies ω_n, and unit admittance J_n can then be denormalized by following expressions:

$$J = \frac{J_n}{R_c}, \tag{3.46a}$$

$$\omega = \omega_c \omega_n \text{ [rad/s]}, \tag{3.46b}$$

$$L = \frac{R_c}{\omega_c} l \text{ [H]}, \tag{3.46c}$$

$$C = \frac{1}{R_c \omega_c} c \text{ [F]}. \tag{3.46d}$$

Reactive elements obtained by (3.46) still represent the inline nodal configuration. In order to obtain a ladder-type network, the mathematical transformation using chain matrix can be straightforwardly applied.

3.6 Numerical Instabilities

The proposed methodology is sensitive for accumulative round-off errors and numerical instabilities. Indeed, as both negative and positive passbands are considered, the degree of characteristic polynomials is very high (up to 23 for ninth order filter with three TZs at the origin). Moreover, polynomials coefficients of lower degrees may reach values of tens of millions, especially in case of series first resonator network. This situation makes the recursive technique fail for networks' order higher than 5, and also it leads to impossibility to synthesize filters with relative bandwidth less than 4%. Return loss level and nearness of finite TZs to the passband are also constrained. In multiplexer module design position of finite TZs is important in order to fulfill mask specifications and achieve needed rejection in other frequency bands.

The reactance functions from parameter extraction procedure, where they are converted to partial fraction expansion representation, may be ill-conditioned as well. This means that small changes in input parameters can result in large variation in impedance and admittance functions, so the network elements cannot be extracted even if the extraction is performed from both the input and output port simultaneously. Thus, both procedures of polynomials synthesis and elements extraction depend a lot on input parameters, such as filter's order, return loss level, relative bandwidth and nearness of finite TZs to the passband.

Throughout the elaboration of the methodology we could improve computational accuracy

by organizing and sorting of zeros of characteristic polynomials $P(\omega)$, $F(\omega)$, and $E(\omega)$. This solution permitted us to synthesize filters with order seven and nine but only a wide passband could be applied.

As a major part of standard LTE bands cannot be designed by this methodology if there are aforementioned limitations in input parameters, the Multiprecision Computing Toolbox (MCT) for MATLAB from Advanpix [86] was incorporated into design process. It allowed to overcome the problems mentioned above by passing from double to quadruple precision (compliant with IEEE 754-2008 standard). Here, the algorithms are converted to precision-independent C++ code with various vector optimizations and parallel multicore execution. An addition advantage is that toolbox is fast and easy to implement. By this way, filters of order up to 11, return loss level up to 25 dB, relative bandwidth down to 0.5%, and any set of finite TZs can be properly designed.

Other mathematical solutions such as frequency variable replacement [82] or polynomials' definition by their roots rather than by their coefficients [87] can improve the initial situation. However, for our purpose the MCT is the best solution.

3.7 Accommodation of Micro-Acoustic Technological Constraints

Presented methodology realizes ladder-type networks directly in bandpass domain which increases accuracy in transmission and reflection response. However, obtained filter has to fulfill micro-acoustic technological constraints as well which have to be taken into account in design procedure before the fabrication process. As it has been explained in Chapter 2, SAW and BAW filters are characterized by low insertion loss level, high rejection at out-of-band frequencies, power durability, and minimization capability. Quality factor Q of resonators, presence of reactive elements, and operating temperature influence on insertion loss level and passband edge-rounding. High rejection and selectivity depend on position of finite TZs and multiplicity of TZs at zero frequency and infinity. Power dissipation affects to resonators cascading, and therefore, to occupied area. Effective coupling coefficient k_{eff}^2 or r defines set of TZs and RL level, and also determine the presence of external elements. All these technological parameters have to be taken into consideration in order to obtain a feasible filtering network.

For this purpose, the programming code of mathematical synthesis procedures was complemented by additional computations of technological parameters in order to fulfill micro-acoustic constraints and mask specifications. Since finite TZs are defined in bandpass domain, the needed selectivity and rejection can be easily set from the beginning of the synthesis. However, together with RL level they influence on k_{eff}^2 (r). Therefore, a filter design is always a trade-off be-

Table 3.2: Band 25 Receiver Specifications

Parameter	Freq. Band (MHz)	Value (dB)
Insertion Loss	1930 - 1995	> -2.5
Isolation	1850 - 1915	< -50
Out-of-Band Rejection	1710 - 1755 (B4-Tx)	< -45
	2110 - 2155 (B4-Rx)	< -45
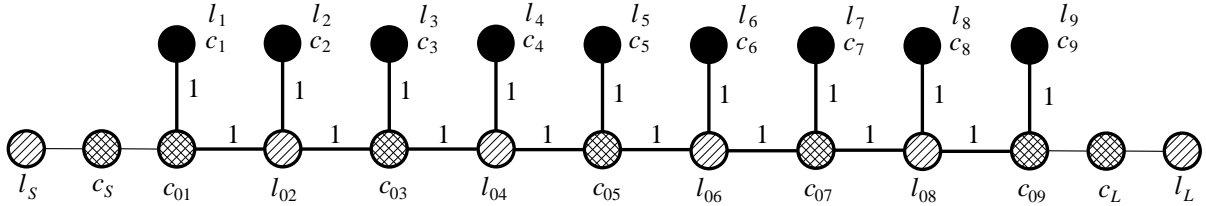
Figure 3.14: Receiver symmetric ladder-type filter to realize in Band 25 Rx.

tween different technological parameters. In next section two examples are realized in order to demonstrate the possibilities of proposed methodology.

3.8   Numerical Examples

In this section two ladder-type acoustic filtering networks are elaborated. Process of direct bandpass synthesis and design of ladder-type acoustic filters is demonstrated by first example. Then, the second filter demonstrates advantages and disadvantages of two types of synthesis: direct bandpass methodology described in this chapter and lowpass synthesis approach from Chapter 2.

3.8.1   Ladder-Type Filter Realization with Inductive Matching Elements

In this example we consider a receiver ninth-order symmetric bandpass filter started with shunt resonator in Band 25 Rx with passband extending from 1.930 to 1.995 GHz (relative bandwidth 3.3%). Transmission and reflection responses have to fulfill mask specifications presented in Table 3.2. An AlN piezoelectric crystal with effective coupling coefficient k_{eff}^2 of 6.8% is considered in this example. Therefore, set of TZs and RL level have to be chosen in order to achieve the declared value of k_{eff}^2. Applying the same study of RL influence on k_{eff}^2, RL level has been taken to be 17 dB and set of TZs includes 3 TZs at zero frequency and finite TZs prescribed at 1.9160, 2.0270, 1.9044, 2.0185, 1.9060, 2.0185, 1.9044, 2.0270, and 1.9160 GHz. Inline configuration of the network is presented in Figure 3.14. MCT is used in synthesis process in order to increase the computational accuracy.

The first step of the synthesis is reference values defining. Here, we establish $R_c = R_S = 50$ Ohm and $\omega_c = 2\pi 10^9$ rad/s. Therefore, the normalized set of all TZs becomes $\omega_n = [\pm 1.9160, \pm 2.0270, \pm 1.9044, \pm 2.0185, \pm 1.9060, \pm 2.0185, \pm 1.9044, \pm 2.0270, \pm 1.9160, 0, 0, 0]$.

Then, characteristic polynomials $P(s)$, $F(s)$, and $E(s)$ for $s = j\omega$ are calculated. Set of defined TZs characterizes the polynomial $P(s)$. $F(s)$ is obtained by recursive technique, operating with polynomials $U(\omega)$ and $V(\omega)$, and $E(s)$ is derived by Feldtkeller equation. The resulting polynomials' coefficients are presented in Table 3.3. It can be noticed that all polynomials' coefficients are real; moreover, $P(s)$ is purely odd and $F(s)$ is purely even. In addition, among the roots of polynomial $F(s)$ $\omega_r = [\pm 1.9880j, \pm 0.5016j, \pm 1.9987, \pm 1.9948, \pm 1.9857, \pm 1.9703, \pm 1.9519, \pm 1.9374, \pm 1.9289, \pm 1.9248, \pm 1.9231]$ appear two pairs of purely imaginary roots which do not create any additional RZ over the whole range of frequencies. These purely imaginary roots characterize inductive and capacitive matching elements at source and load making possible their extraction. As both polynomials $P(s)$ and $F(s)$ contains only purely real and purely imaginary roots, the condition of orthogonality is always fulfilled, and therefore, the multiplication $jP(s)$ is not required in direct bandpass synthesis technique. Moreover, such multiplication gives complex coefficients of $P(s)$ which can only be possible when FIR elements are presented in the network. Since polynomial $E(s)$ is obtained from polynomial $F(s)$, its roots also contain two pairs of purely imaginary roots among the complex ones.

Once characteristic polynomials have been obtained, we proceed to reactance function definition and extraction procedure. Since the first reactive element is shunt connected inductor, impedance parameters are used. Considering that polynomial $P(s)$ is odd (18 finite TZs at both positive and negative passband plus 3 TZs at the origin result in 21 TZs totally), X_{1o} is found to be

$$
X_{1o} = \frac{E_o + F_o}{E_e - F_e} =
$$

$$
= \frac{5s^{21} + 182s^{19} + 2890s^{17} + 27014s^{15} + 164092s^{13} + 675381s^{11} + ...}{13s^{20} + 448s^{18} + 6842s^{16} + 60909s^{14} + 348516s^{12} + 1329253s^{10} + ...}
$$

$$
\frac{1901783s^9 + 3601837s^7 + 4361751s^5 + 3016512s^3 + 886955s}{3379399s^8 + 5522350s^6 + 5263367s^4 + 2229253s^2},
$$

where $F_o = 0$ since $F(s)$ is purely even. The extraction procedure starts with the first element, i.e., shunt connected inductor which introduces one TZ at zero frequency. It is derived as

$$
l_S = \left. \frac{X_{1o}}{s} \right|_{s=0} = 2.5134.
$$

Table 3.3: Coefficients of characteristic polynomials $P(s)$, $F(s)$, and $E(s)$.

Degree	Coefficient of $P(s)$	Coefficient of $F(s)$	Coefficient of $E(s)$
22		1.0	1.0
21	1.0		5.11
20		30.28	43.34
19	34.59		181.78
18		384.55	832.85
17	531.68		2 890.33
16		2 536.99	9 379.24
15	4 764.65		27 014.34
14		7 810.97	68 720.42
13	27 437.44		164 091.56
12		−5 447.14	343 069.01
11	105 289.43		675 381.49
10		−144 644.38	1 184 609.06
9	269 249.68		1 901 783.82
8		−576 948.52	2 802 450.73
7	442 446.89		3 601 837.37
6		−1 150 519.86	4 371 830.38
5	423 941.32		4 361 751.42
4		−1 142 549.12	4 120 817.44
3	180 463.97		3 016 512.39
2		−331 042.56	1 898 210.52
1			886 955.52
0		176 447.01	176 447.01

$\varepsilon_R = 1$; $\varepsilon = 62.64$.

Then, the remaining impedance parameter is updated to be

$$z_2 = X_{1o} - \frac{1}{s \cdot l_S} =$$

$$= \frac{0.39s^{20} + 13.5s^{18} + 207.8s^{16} + 1861.1s^{14} + 10715.1s^{12} + 41120.2s^{10} + \ldots}{s^{19} + 34.3s^{17} + 524.2s^{15} + 4666.5s^{13} + 26701.3s^{11} + 101839.7s^9 + \ldots}.$$

$$\frac{105184.6s^8 + 172939.1s^6 + 165836.7s^4 + 70666.7s^2}{258910.1s^7 + 423090.6s^5 + 403248.7s^3 + 170792.5s}.$$

It can be noticed that both the numerator and denominator of impedance function z_2 have been decreased by one degree, as expected. Then, we change the nature of reactance function to admittance function by $y_3 = 1/z_2$.

Next step is extraction of series connected capacitor which prepares the annihilation of the first finite TZ at 1.9160 below the passband and also contributes in second TZ at zero frequency, different from that of shunt connected inductor. The capacitor is found to be

$$c_S = \left. \frac{1}{y_3 \cdot s} \right|_{s=1.9160j} = 216.9341,$$

and the admittance parameter becomes

$$y_4 = y_3 - \frac{1}{s \cdot c_S} =$$

$$= \frac{2.5s^{19} + 87.5s^{17} + 1336.7s^{15} + 11899.3s^{13} + 68085.8s^{11} + 259678.7s^9 + \ldots}{s^{20} + 34.6s^{18} + 530.8s^{16} + 4754.5s^{14} + 27373.0s^{12} + 105046.8s^{10} + \ldots}.$$

$$\frac{660180.9s^7 + 1078803.8s^5 + 1028198.8s^3 + 435479.6s}{268707.8s^8 + 441795.7s^6 + 423651.5s^4 + 180527.4s^2},$$

and applying nature changing we obtain $z_5 = 1/y_4$.

After partial extraction the order of numerators and denominators of z_2 and z_5 is the same, as expected. In case of partial contribution in TZs at the origin and infinity the degree of reactance function will be decreased after extraction of all elements which operate on these TZs.

Now we proceed to complete annihilation of the finite TZs at $s = \pm j\omega_1 = \pm 1.9160$ introduced by first shunt resonator:

$$l_1 = \left. \frac{s}{z_5 \left(s^2 + 1.9160^2\right)} \right|_{s^2=(j1.9160)^2} = 29.2475, \qquad c_1 = \frac{1}{\omega_1^2 l_1} = 0.0093.$$

Then, the impedance function has to be updated as follows:

$$z_6 = z_5 - \frac{s/l_1}{s^2 + \omega_1^2} =$$

$$= \frac{0.4s^{18} + 12.1s^{16} + 162.8s^{14} + 1252.9s^{12} + 6026.9s^{10} + 18551.8s^8 + \ldots}{s^{17} + 30.7s^{15} + 411.6s^{13} + 3155.4s^{11} + 15116.3s^9 + 46339.9s^7 + \ldots}.$$

$$\frac{35684.2s^6 + 39214.9s^4 + 18850.8s^2}{88772.3s^5 + 97161.7s^3 + 46518.3s}.$$

It can be observed that both numerator and denominator of z_6 have been reduced by two degrees compared with z_5 since two finite TZs have been removed. Next step is partial extraction of capacitive reactive node of shunt resonator which prepares the complete removal of the second finite TZ at 2.0270 above the passband introduced by series connected resonator and contributes in TZ at infinity. The capacitor is derived as

$$c_{01} = \left.\frac{z_6}{s}\right|_{s=2.0270j} = 0.1643,$$

and impedance function becomes

$$z_7 = z_6 - s \cdot c_{01} =$$

$$= \frac{0.2s^{18} + 7.0s^{16} + 95.1s^{14} + 734.6s^{12} + 3543.9s^{10} + 10939.6s^8 + ...}{s^{17} + 30.7s^{15} + 411.6s^{13} + 3155.4s^{11} + 15116.3s^9 + 46339.9s^7 + ...}.$$

$$\frac{21101.8s^6 + 23254.4s^4 + 11209.3s^2}{88772.3s^5 + 97161.7s^3 + 46518.3s}.$$

And again, the degrees of numerator and denominator of z_7 are maintained because of feature of partial removal.

Extraction of the second series connected resonator starts with unit inverter, which makes $y_8 = 1/z_7$. Annihilation of the second finite TZs at $s = \pm j\omega_2 = \pm 2.0270$ above the passband is derived as

$$c_2 = \left.\frac{s}{y_8\left(s^2 + 2.0270^2\right)}\right|_{s^2=(j2.0270)^2} = 5.0860, \qquad l_2 = \frac{1}{\omega_2^2 c_2} = 0.0479,$$

and the remaining admittance function is found to be

$$y_9 = y_8 - \frac{s/c_2}{s^2 + \omega_2^2} =$$

$$= \frac{4.2s^{15} + 112.1s^{13} + 1285.0s^{11} + 8181.0s^9 + 31245.2s^7 + 71587.2s^5 91105.0s^3 + 49682.0s}{s^{16} + 26.8s^{14} + 307.5s^{12} + 1960.2s^{10} + 7497.1s^8 + 17201.4s^6 + 21922.3s^4 + 11971.7s^2}.$$

The same as before, the numerator and denominator of y_9 have been decreased by two degrees comparing with y_7 because of two finite TZs complete removal. Then, the inductive reactive node, which prepares the full extraction of the third finite TZ at 1.9044 below the passband and contributes in second TZ at the origin (the same TZ from c_S), is realized by means of

$$l_{02} = \left.\frac{1}{y_9 \cdot s}\right|_{s=1.9044j} = 0.2909.$$

Updated admittance function becomes

$$y_{10} = y_9 - \frac{1}{s \cdot l_{02}} =$$

$$= \frac{0.8s^{15} + 20.0s^{13} + 227.9s^{11} + 1441.8s^9 + 5469.8s^7 + 12448.0s^5 + 15735.1s^3 + 8522.6s}{s^{16} + 26.8s^{14} + 307.5s^{12} + 1960.2s^{10} + 7497.1s^8 + 17201.4s^6 + 21922.3s^4 + 11971.7s^2}.$$
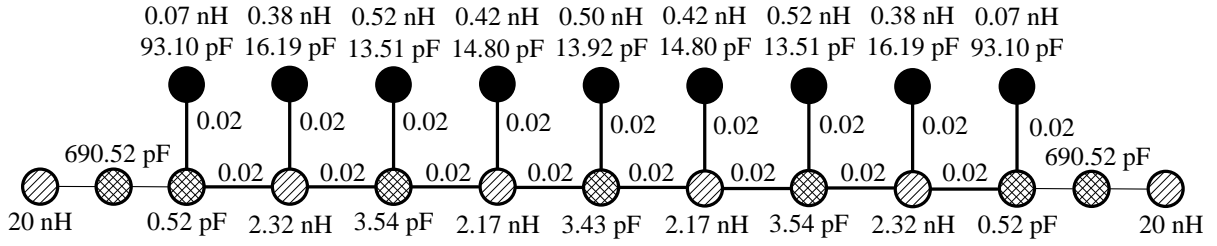
Figure 3.15: Inline representation of receiver symmetric ladder-type filter in Band 25 Rx.

Table 3.4: BVD bandpass elements of ninth-order receiver filter in Band 25 Rx.

Parameters	Res 1&9	Res 2&8	Res 3&7	Res 4&6	Res 5
L_a (nH)	232.74	130.13	33.79	136.74	34.81
C_a (pF)	0.0296	0.0501	0.2067	0.0481	0.2003
C_0 (pF)	0.5229	0.8758	3.5403	0.8202	3.4326
k_{eff}^2 (%)	6.8	6.8	6.8	6.8	6.8
f_s (GHz)	1.9160	1.9714	1.9044	1.9618	1.9060

$$C_{in} = C_{out} = 690.5 \text{ pF}; \; L_{in} = L_{out} = 20.0 \text{ nH}.$$

It can be observed that degrees of y_{10} and y_9 are the same, since the inductor has been performed by partial extraction. Finally, the unit inverter provides $z_{11} = 1/y_{10}$.

Then, the extraction procedure is performed by the same way for the third, forth, and fifth resonator. After this, the extraction starts again from the output port of the network in order to increase the computational accuracy, using secondary impedance parameter:

$$X_{2o} = \frac{E_o - F_o}{E_e - F_e} = X_{1o},$$

since $F_o = 0$. As the network is symmetric, the extraction process is the same and results in identical circuital elements.

It is interesting to notice that where there was elements' sign changing in lowpass pole extraction technique, there is a nature switching of them in bandpass approach. Extracted series connected capacitors c_S and c_L, and all inductive nodes of series resonators contribute in one TZ at the origin, whereas all capacitive nodes of shunt resonator contribute in one TZ at infinity. Each of shunt connected inductors introduces one TZ at zero frequency more, thus increasing the number of TZs at dc to three.

The resulting inline topology with denormalized extracted elements is presented in Figure 3.15. After applying of mathematical transformation by means of chain matrix the BVD resonators have been realized. The final network elements with effective coupling coefficient and
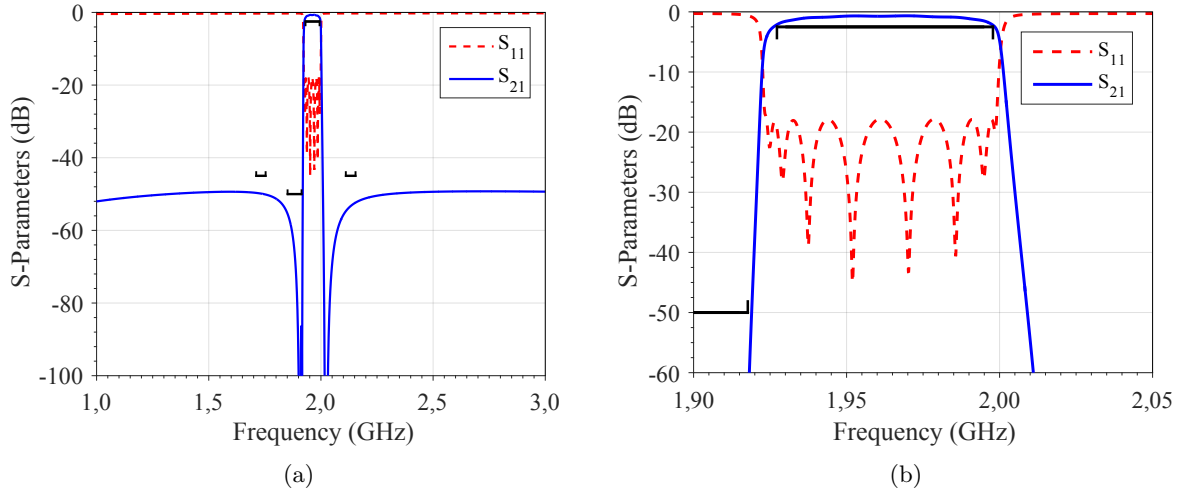
Figure 3.16: Magnitude response of symmetric acoustic bandpass filter in Band 25 Rx at (a) out-of-band and (b) in-band frequencies.

resonant frequencies of each resonator are presented in Table 3.4, and filter response is shown in Figure 3.16. Since input/output capacitors have a very large value, they can be neglected without any impact on final result because the third TZ at the origin will be maintained by inductive reactive nodes of series resonators. Shunt connected inductors at source and load also have a large value; however, as they introduce additional TZs at zero frequency, they cannot be neglected. Otherwise, disagreement between mathematical description by filtering function and practical realization of the network will be observed.

For the design a resonators' quality factor $Q = 2000$ typical for AW technology has been taken at both series and parallel resonance frequencies and $Q = 25$ for shunt connected inductors L_{in} and L_{out}. Fabrication tolerance and temperature margin coefficient is taken to be 1600 ppm in this example. Observing Figure 3.16 (a) it can be noticed that a good rejection has been achieved at frequencies of Band 25 Tx and Band 4. In order to fulfill insertion loss mask specification, the bandwidth of the filter has been enlarged by 4 MHz and 1 MHz at the left and the right passband edge frequencies, respectively. The resulting passband response is shown in Figure 3.16 (b).

Minimization capability and power durability are important aspects which have to be taken into account as well. Since presented in Table 3.4 k_{eff}^2 is identical for every resonator, no additional external element is required for its adjustment which positively influences on filter size reduction. However, final area depends not only on existence of external elements, but also on power density of each resonator. In Figure 3.17 an energetic behavior of every resonator is performed considering input power of 29 dBm. The power density is calculated at the upper passband frequency $f_2 = 1.995$ GHz, as it is the most energetically critical point. It can be seen
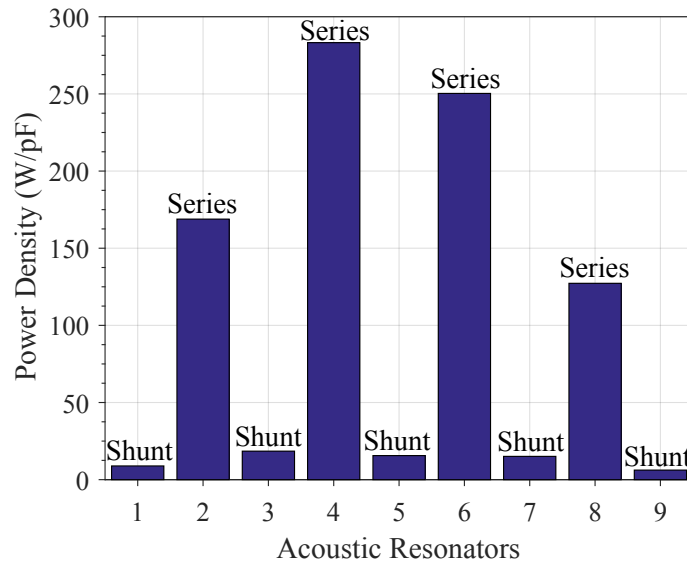
Figure 3.17: Power density distribution among shunt and series connected resonators evaluated at $f_2 = 1.995$ GHz.

that series connected resonators, especially the fourth and the sixth, are exposed to the highest energy level. This happens because of their small value of static capacitance C_0. The less C_0, the smaller is the resonator, and the more energy it undergoes. Therefore, in order to ensure a long lifetime of the filter, series resonators have to be cascaded, thus increasing the area size. Finally, the total capacitance area of designed filter equals to 54 pF.

The proposed filter design contains five different resonant frequencies, making their fabrication a challenging task for BAW technology. Frequencies of resonators 3&7 and 5 are very similar, so the total number of f_s can be reduced by one. Taking into account further processes of electromagnetic simulation and package optimization, number of f_s can become three since resonant frequencies of resonators 2&8 and 4&6 are close to each other.

In order to demonstrate the difference between capacitive and inductive matching elements, i.e., between one and three TZs at the origin, another filter with the same input parameters and specifications is synthesized following the same procedure, as the one described above. A comparison between both networks is presented in Figure 3.18. Both filters fulfill mask specifications; however, the network with inductive matching elements has an additional rejection at left side far away from the passband illustrated in Figure 3.18 (a) which can be useful for some applications. An identical in-band response can be observed in Figure 3.18 (b). It has to be taken into consideration that since input/output elements have been changed, the first and the last resonators may require an external elements in order to achieve uniform values of k_{eff}^2.
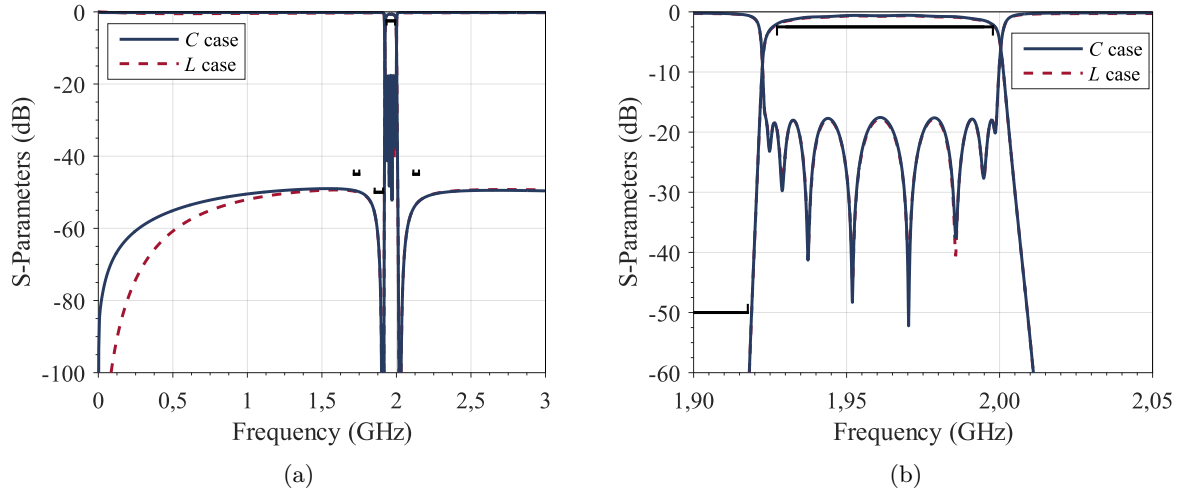
Figure 3.18: Magnitude response comparison between filters with capacitive and inductive matching elements designed for Band 25 Rx at (a) out-of-band and (b) in-band frequencies.

Table 3.5: Band 25 Transmitter Specifications

Parameter	Freq. Band (MHz)	Value (dB)
Insertion Loss	1850 - 1915	> -2.3
Isolation	1930 - 1995	< -50
Out-of-Band Rejection	1710 - 1755 (B4-Tx)	< -45
	2110 - 2155 (B4-Rx)	< -45

3.8.2 Comparison of Ladder-Type Filter Realization by Lowpass and Bandpass Methodologies

In order to evaluate advantages and disadvantages of the direct bandpass methodology over lowpass synthesis approach explained in Chapter 2, a ninth-order symmetric bandpass filter in Band 25 Tx with passband extending from 1.850 to 1.915 GHz (relative bandwidth 3.45%) is designed by both techniques. In this case, capacitive matching elements are applied, thus providing one TZ at the origin. Mask specifications that designed filter has to fulfill are shown in Table 3.5. The comparison procedure follows a diagram presented in Figure 3.19.

Firstly, the network has been synthesized using direct bandpass methodology applying the same procedure, as in previous example. Set of TZs contains one TZ at the origin and finite TZs prescribed at 1.9308, 1.8253, 1.9378, 1.8305, 1.9370, 1.8305, 1.9378, 1.8253, and 1.9308 GHz. RL level equals 12 dB. Filter starts with series connected resonators, and therefore, capacitors positioned in shunt are realized. Obtained after synthesis BVD elements are presented in Table 3.6. Here, instead of k_{eff}^2 we operate with capacitance ratio coefficient r which characterizes
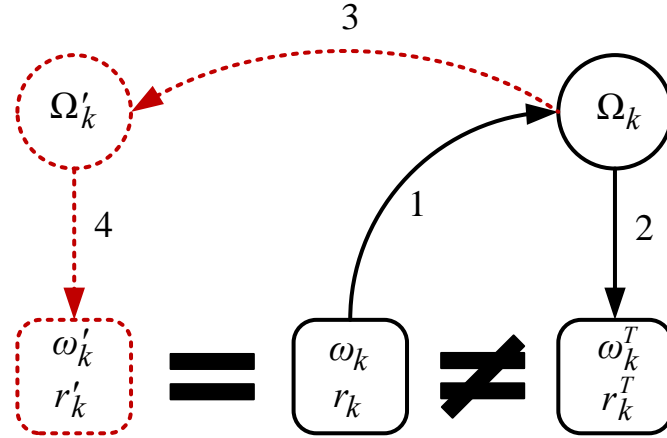
Figure 3.19: Illustrative diagram describing comparison procedure.

Table 3.6: BVD bandpass elements of ninth-order transmitter filter in Band 25 Tx obtained by direct bandpass methodology.

Parameters	Res 1&9	Res 2&8	Res 3&7	Res 4&6	Res 5
L_a (nH)	54.60	41.24	171.13	40.18	169.75
C_a (pF)	0.1317	0.1843	0.0417	0.1881	0.0421
C_0 (pF)	2.2666	3.1412	0.7190	3.2527	0.7266
r	17.2151	17.0407	17.2402	17.2880	17.2690
f_s (GHz)	1.8771	1.8253	1.8839	1.8305	1.8832

$$C_{in} = C_{out} = 0.2062 \text{ pF}.$$

SAW resonators. Since all of them have almost identical value of r, no external elements are needed in this case.

In order to synthesize the network by lowpass approach, TZs defined in bandpass domain have to be transformed by mapping formula

$$\Omega_k = j \frac{\omega_0}{\omega_2 - \omega_1} \left[\frac{\omega_k}{\omega_0} - \frac{\omega_0}{\omega_k} \right], \tag{3.47}$$

where $\omega_0 = \sqrt{(\omega_1 \omega_2)}$ is the bandpass center frequency, ω_2 and ω_1 are the upper and lower band-edge frequencies, respectively, and ω_k are bandpass TZs. This transformation process is illustrated by arrow 1 in diagram from Figure 3.19. Therefore, TZs in lowpass domain are obtained to be $\Omega_k =$[1.4760j, –1.7787j, 1.6856j, –1.6138j, 1.6617j, –1.6138j, 1.6856j, –1.7787j, 1.4760j]. Then, synthesis is performed in lowpass domain with further lowpass-to-bandpass elements' transformation, following the methodology explained in Chapter 2. This process corresponds to arrow 2 in diagram from Figure 3.19. Resulted BVD elements, capacitance ratio, and resonant frequencies of obtained network are shown in Table 3.7. Comparing this result with the one

Table 3.7: BVD bandpass elements of ninth-order transmitter filter in Band 25 Tx obtained by lowpass synthesis methodology with further lowpass-to-bandpass transformation.

Parameters	Res 1&9	Res 2&8	Res 3&7	Res 4&6	Res 5
L_a^T (nH)	95.16	36.84	189.93	36.92	189.73
C_a^T (pF)	0.0749	0.2069	0.0376	0.2053	0.0377
C_0^T (pF)	1.3772	3.3397	0.5835	3.4200	0.5871
r^T	18.3786	16.1388	15.5110	16.6576	15.5835
f_s^T (GHz)	1.8847	1.8228	1.8829	1.8280	1.8824

from Table 3.6, it can be noticed that insufficient accuracy of lowpass-to-bandpass transformation provokes alteration in all parameters, including capacitance ratio r and resonant frequencies f_s, which is shown by sign of inequality in diagram from Figure 3.19. This means that additional external elements are needed for all resonators which influences on fabrication complexity and occupied filter area. Moreover, in lowpass approach no reactive elements at source and load are required for stand-alone filters.

Comparison of S-parameters' magnitude at in-band and out-of-band frequencies is presented in Figure 3.20 (a) and (b), respectively. Because of narrowband feature of lowpass-to-bandpass transformation, a TZs' movement from the passband to further frequencies can be clearly seen in Figure 3.20 (a). RZs inside the passband slightly change their position as well. Different TZs influence on fly-back levels at out-of-band frequencies shown in Figure 3.20 (b). Although in this example both filters fulfill mask specifications, a situation can be found when unexpected TZs' position leads to mask's breach. Since no TZ at the origin is possible to synthesize in lowpass approach, the dashed transmission trace from Figure 3.20 (b) will never achieve zero frequency.

S_{11} phase evaluation using both methodologies is presented in Figure 3.21. Since network resulted from lowpass synthesis is different from the one obtained by direct bandpass approach, an in-band phase traces from Figure 3.21 (a) do not match, even though they are very similar. The out-of-band phase difference illustrated in Figure 3.21 (b) is due to inaccurate narrowband lowpass-to-bandpass transformation. Direct bandpass approach provide precise phase value at any frequency which is crucial for multiplexer module design where up to six filters have to be combined in the same package, and therefore, lack of phase precision cannot be accepted. Optimization process can improve this drawback in lowpass approach; however, it can be a time-consuming process. Phase correction technique for direct bandpass synthesis is presented in Chapter 4.

Since inaccuracy of lowpass-to-bandpass transformation is its inherent feature, the final result is evaluated at bandpass domain because exact position of TZs cannot be straightforwardly predicted at lowpass frequencies. Therefore, we can make TZs of both filters from the example match by degradation of finite TZs at lowpass domain. This operation corresponds to arrow 3 in
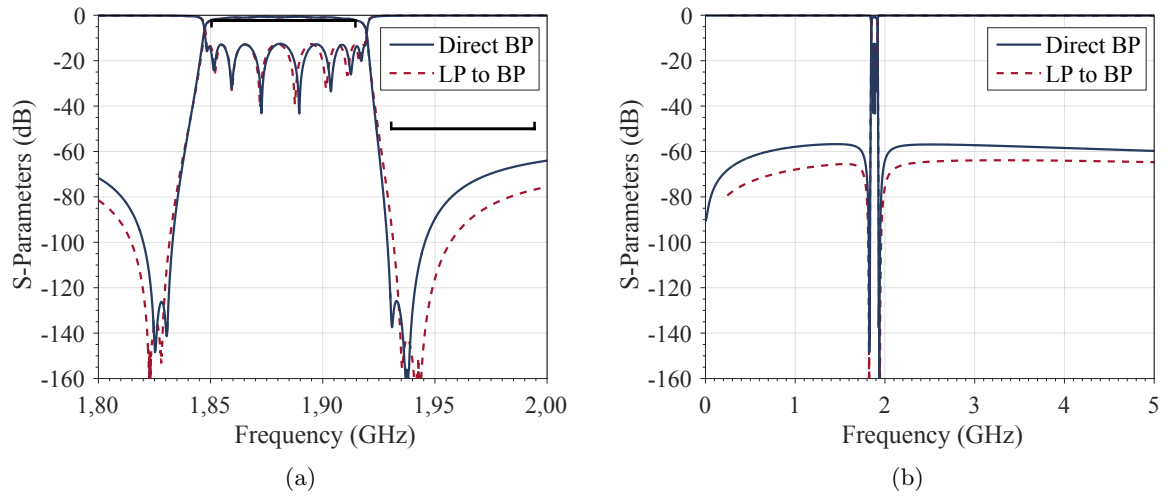
Figure 3.20: Magnitude response comparison between filters synthesized by direct bandpass methodology and lowpass approach with further lowpass-to-bandpass transformation at (a) in-band and (b) out-of-band frequencies.

Figure 3.21: S_{11} phase response comparison between filters synthesized by direct bandpass methodology and lowpass approach with further lowpass-to-bandpass transformation at (a) in-band and (b) out-of-band frequencies.

Table 3.8: BVD bandpass elements of ninth-order transmitter filter in Band 25 Tx obtained by lowpass synthesis methodology from degraded finite TZs.

Parameters	Res 1&9	Res 2&8	Res 3&7	Res 4&6	Res 5
L'_a (nH)	79.02	41.32	178.59	39.99	176.81
C'_a (pF)	0.0902	0.1840	0.0400	0.1890	0.0404
C'_0 (pF)	1.8226	3.1350	0.6882	3.2566	0.6968
r'	20.1970	17.0416	17.2208	17.2282	17.2472
f'_s (GHz)	1.8847	1.8255	1.8839	1.8304	1.8832
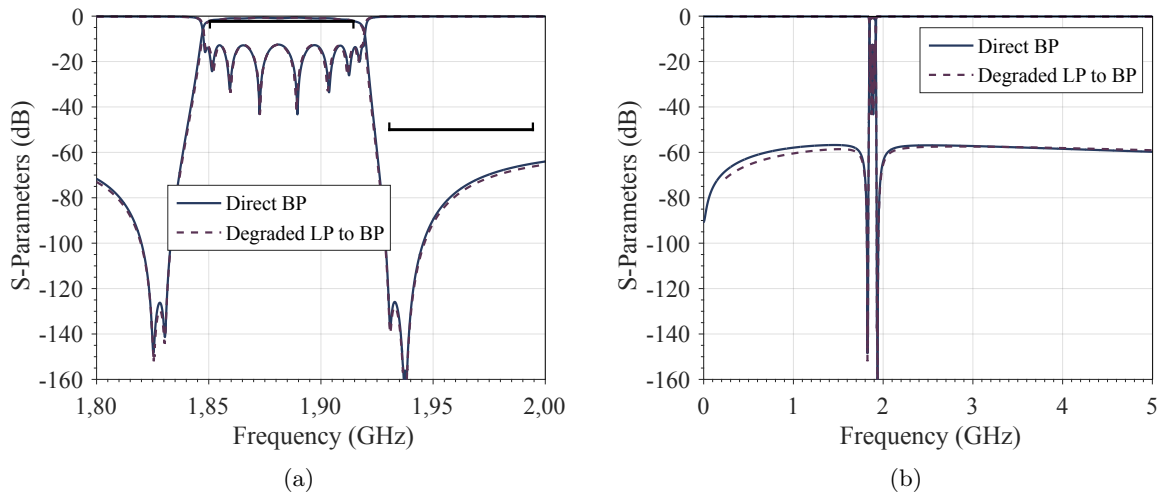
Figure 3.22: Magnitude response comparison between filters synthesized by direct bandpass methodology and lowpass approach from degraded TZs at (a) in-band and (b) out-of-band frequencies.

Figure 3.19. Thus, new TZs are found to be $\Omega'_k =$ [1.3460j, –1.6967j, 1.5456j, –1.5418j, 1.5217j, –1.5418j, 1.5456j, –1.6967j, 1.3460j]. Parameters of new filter resulted from lowpass synthesis are presented in Table 3.8. Comparing this result with the one from Table 3.6 it can be noticed that all resonators, except the first and the last ones, have almost identical values of reactive elements, capacitance ratio, and resonant frequency. In diagram from Figure 3.19 it is illustrated by arrow 4 and sign of equality. Since lowpass synthesis methodology does not accommodate reactive elements at source and load for stand-alone filters, the total identity between two filters cannot be achieved. This is why the first and the last resonators differ from the original ones. From here two options are possible: the former is to equalize parameter r, degrading more TZs of the first and the last resonators or applying phase modification, and the latter is to match TZs of the first and the last resonators. In this example we have chosen the last one which has led to different r' values.

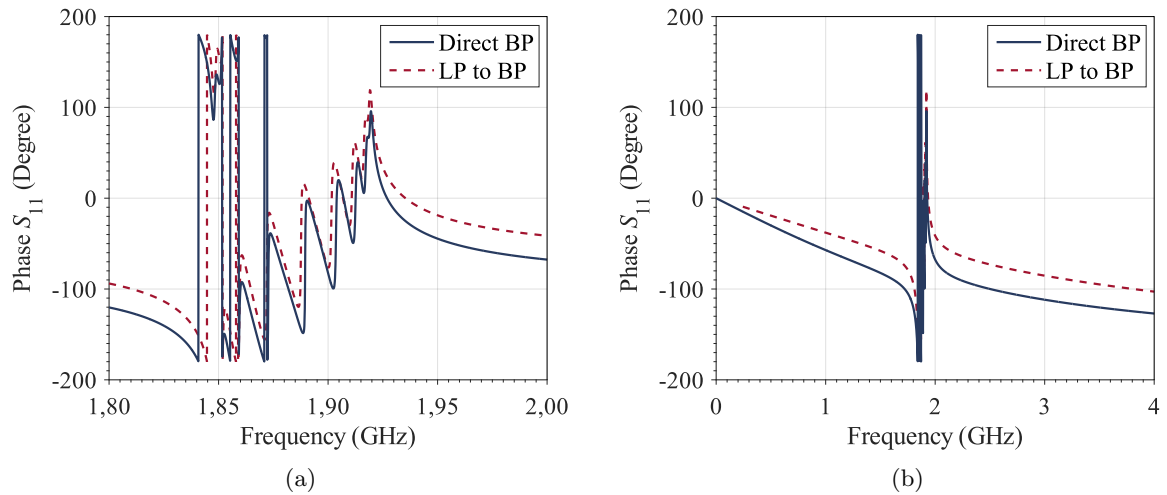A comparison between S-parameters magnitude of two networks at in-band and out-of-band
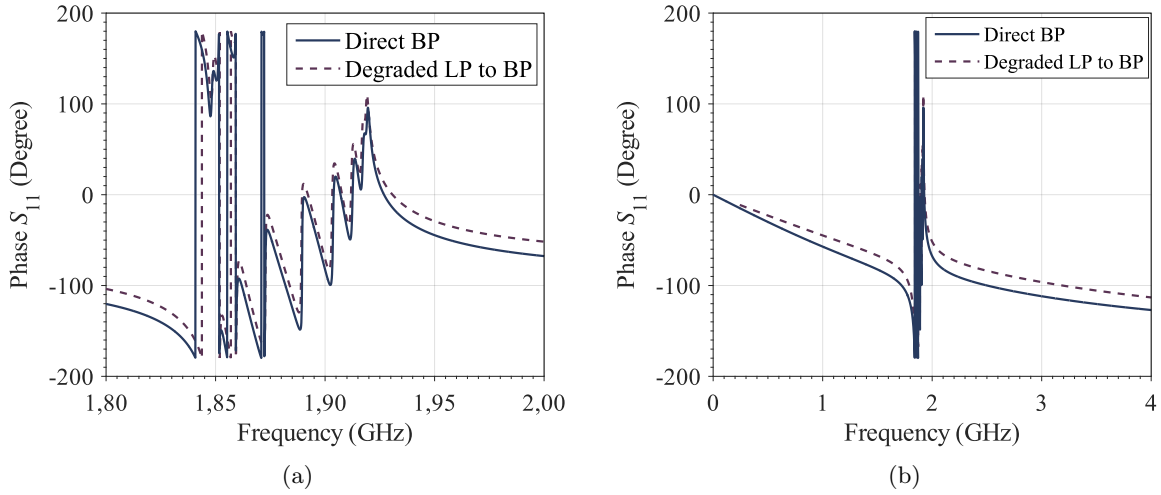
Figure 3.23: S_{11} phase response comparison between filters synthesized by direct bandpass methodology and lowpass approach from degraded TZs at (a) in-band and (b) out-of-band frequencies.

frequencies are shown in Figure 3.22 (a) and (b), respectively. Figure 3.22 (a) illustrates a good agreement between two networks, both RZs and TZs match in this case which, in turn, has led to fly-back levels adjustment presented in Figure 3.22 (b) as well. The fly-back small mismatching at the left side from passband is due to different values of C_0 of the first and the last resonators which define a S_{21} trace slope near zero frequency.

S_{11} phase response of two networks presented in Figure 3.23 is similar to that from Figure 3.21, although the gap between two traces is smaller. The phase difference at out-of-band frequencies is maintained, since lowpass-to-bandpass transformation is a narrowband approximation.

In this section differences between two lowpass and bandpass methodologies have been demonstrated. Lowpass synthesis is faster and does not have computational problems since TZs of only one passband are considered. However, the lowpass-to-bandpass transformation exhibits lack of precision which means that evaluation of technological parameters and mask specifications has to be done in bandpass domain, considering the transformation error. Direct bandpass methodology takes into account TZs at the origin and infinity, and at both passbands, and gives total precision at any frequency which is important for duplexers' and multiplexers' design. Bandpass approach is more complex and numerically more instable. Therefore, additional solutions like MCT have to be implemented in the synthesis routine. Finally, a network which fulfills mask specifications and technological constraints can be designed by both lowpass and bandpass techniques, taking into account their inherent advantages and disadvantages.

3.9   Chapter Summary

Direct bandpass methodology for ladder-type acoustic filters has been presented in this chapter, taking into account synthesis procedure and technological constraints accommodation. It has been demonstrated that networks started either with series or shunt resonators and any type of matching elements can be realized by this technique.

Mathematical description by means of filtering function and physical realization of the network have to be in agreement. In this chapter filters with cross-couplings and ground inductors have not been considered since every additional TZ introduced by them has to be included in filtering function and recursive technique, and then be correctly extracted. A future work can be done in this direction; however, it can be a challenging task to include and manage all possible network configurations and it should be done first in lowpass synthesis approach.

Bandpass methodology consists of set of different complex procedures which negatively influence on computational accuracy. Various solutions were tested, and in the end, a MCT was implemented in synthesis routine. It made possible to synthesize filters operating in standard LTE bands and fulfilling mask specifications with high degree, narrow bandwidth, and TZs positioned close to passband.

The main advantage of direct bandpass methodology, comparing with lowpass synthesis approach, is that here no narrowband elements' transformation is used. Evaluation of S-parameters phase and magnitude is accurate at any frequency which is particularly important for multiplexers' design. Frequency dependent reactive nodes have been applied which introduce additional TZs at the origin and infinity, and represent a more realistic scenario of bandpass network. Finally, two examples of receiver and transmitter bandpass filters in Band 25 have been elaborated in order to show the possibilities and functionalities of the method, comparing with classical lowpass approach.

Bandpass Phase Correction Methodology for Ladder-Type Acoustic Filters

In Chapter 3 direct bandpass methodology suitable for synthesis and design of ladder-type acoustic filters has been described, taking into account micro-acoustic technological constraints and mask specifications. It has been demonstrated in Chapter 2 that phase matching is an essential element in duplexer and multiplexer module design. By multiplying characteristic polynomial $F(s)$ by complex phase term, the external source/load element can be accommodated, thus providing required phase in the common port of the device. In stand-alone filters phase matching can lead to modification or even exclusion of source/load reactive nodes whether it is indicated by proper network realization.

However, since direct bandpass synthesis technique operates with purely real input parameters, and consequently, with purely real coefficients of both characteristic polynomials and reactive open/short functions, the operation of complex phase term multiplication cannot be straightforwardly implemented because it leads to complex network elements which are impossible to realize. Thus, the feasible network cannot be performed.

In our best of knowledge, no solution to this problem has been found until now. In this chapter a novel technique able to accommodate a new phase correction term in direct bandpass synthesis is outlined. Filtering functions for capacitive and inductive matching elements cases are updated in order to provide a desirable phase evaluated at certain finite frequency. Then, some methodological and technological limitations are described which have to be taken into consideration in the design process. Finally, throughout the chapter some examples are realized in order to demonstrate the possibilities of proposed methodology.
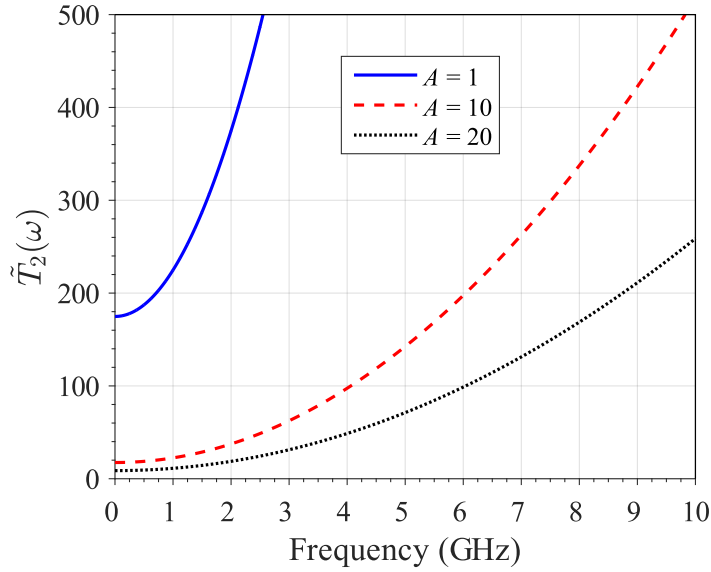
Figure 4.1: Coefficient A influence on function $\tilde{T}_2(\omega)$ for network with capacitive matching elements.

4.1 Filtering Function Updating

As it has been outlined in Chapter 3, network with capacitive matching elements is characterized by presence of function $X_n(\omega)$, which realizes finite TZs and RZs of both positive and negative passbands from dangling resonators, and also by function $T_0(\omega)$ which accommodates TZ at the origin. For the network with inductive matching elements there is an additional term $T_0'(\omega)$ which includes two TZs at zero frequency more. Since the values of input/output reactive elements are defined by $T_0(\omega)$ and $T_0'(\omega)$, precisely these functions have to be updated according to needed phase correction. Below, each type of networks is considered separately.

4.1.1 Capacitive Matching Elements Case

Bandpass filtering function for network with capacitive matching elements derived in previous chapter is defined as

$$K(\omega) = \cosh\left[\cosh^{-1}\left(T_0\left(\omega\right)\right) + \sum_{n=1}^{N}\cosh^{-1}\left(X_n\left(\omega\right)\right)\right], \qquad (4.1)$$

where $T_0(\omega)$ is found to be

$$T_0(\omega) = \frac{T_2\left(\omega\right)}{\omega}, \qquad T_2(\omega) = \frac{\omega^2 + \omega_1\omega_2}{\omega_2 - \omega_1}. \qquad (4.2)$$

To introduce a phase correction into the function $T_0(\omega)$, a new coefficient A related to a
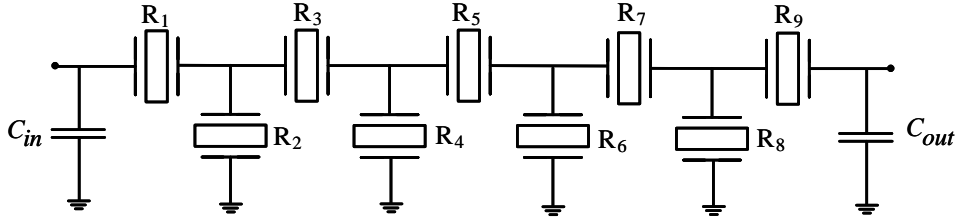
Figure 4.2: Realization of ninth-order ladder-type bandpass network with capacitive matching elements.

certain phase is added to the denominator of $T_2(\omega)$; therefore, the updated functions are found to be

$$\tilde{T}_0(\omega) = \frac{\tilde{T}_2(\omega)}{\omega}, \qquad \tilde{T}_2(\omega) = \frac{\omega^2 + \omega_1 \omega_2}{A \cdot (\omega_2 - \omega_1)}. \tag{4.3}$$

The influence of coefficient A over function $\tilde{T}_2(\omega)$ can be observed in Figure 4.1. Unlike lowpass phase modification, in bandpass approach apart from network phase value variation, the out-of-band attenuation level is changed as well which is explained hereafter. This new feature of $\tilde{T}_2(\omega)$ influences directly on the filter characteristic polynomial $F(s)$ (for $s = j\omega$) since it is obtained by recursive technique where $\tilde{T}_0(\omega)$ takes place. From Chapter 3 it is known that for Nth order filter $2 \times N$ roots of polynomial $F(s)$ are purely real and can be seen inside both negative and positive passbands, and other two roots are purely imaginary. This pair of purely imaginary roots corresponds to TZ at the origin and does not create a RZ over the whole frequency range. According to the value of new added coefficient A, only this pair of purely imaginary roots is modified, whereas the rest of the roots is maintained. Consequently, the pair of purely imaginary roots of characteristic polynomial $E(s)$ is modified as well. As a result, the in-band filter response is preserved without any change, whereas out-of-band fly-backs are modified in agreement with new values of purely imaginary pairs of roots from polynomials $F(s)$ and $E(s)$ which, respectively, are updated in agreement with new phase.

In order to illustrate the explanation described above, we present an example of a ninth-order symmetric stand-alone bandpass filter for Band 42 presented in Figure 4.2 with a passband extending from 3.4 to 3.6 GHz. The network starts with series connected resonator, and therefore, shunt connected capacitors at source and load are introduced. In Table 4.1 different values of phase φ evaluated at frequency of the first finite TZ (3.63 GHz) are presented. The first row describes the network without phase modification, i.e., it is synthesized using (4.2). Corresponding pairs of purely imaginary roots of polynomials $F(s)$ and $E(s)$ are presented as well. Purely real roots are not shown there since they are preserved almost at the same frequencies. Coefficient A is changed in agreement with phase modification value $\Delta\varphi$, and consequently, it leads to correction of input/output capacitive matching elements realization, even changing their sign. Negative capacitors resulted after 70° phase application are impossible to implement, and

Table 4.1: Phase influence on the network with capacitive matching elements.

φ, degrees	$\Delta\varphi$, degrees	$F(s)$ roots	$E(s)$ roots	A	In/Out C, pF
−11.87	0	3.60i −3.60i	−3.60i −3.60i	1	0.091
−50	−38.13	1.75i −1.75i	−1.75i −1.75i	−21.02	0.409
0	11.87	4.43i −4.43i	−4.44i −4.43i	8.14	0
70	81.87	48.27i −48.27i	−48.39i −48.14i	34.63	−0.614*

*Cannot be realized in real network.

therefore, the phase value has to be carefully chosen for each particular network. Moreover, the elimination of source/load reactive elements can be achieved with a certain value of phase (0° in this case) which is useful for stand-alone filter networks.

S_{11} phase modification for positive passband is shown in Smith Chart in Figure 4.3. The lobes of the phase response change their position in agreement with applied phase. In Figure 4.4 the magnitude response of the filter at in-band and out-of-band frequencies is shown. In Figure 4.4 (a) it can be observed that in-band response is maintained since the purely real roots of polynomials $F(s)$ are preserved at the same frequencies. However, Figure 4.4 (b) demonstrates that the out-of-band fly-backs are varied significantly because of different values of purely imaginary pair of roots. This is the main difference from phase correction in lowpass synthesis approach where source/load reactive nodes are considered frequency independent, and therefore, no additional pair of roots of polynomial $F(s)$ appears in the synthesis procedure. And since the phase term is applied directly on open/short reactance function, the roots of polynomial $F(s)$ do not change. As a result, these two lowpass characteristic features make no out-of-band variation in filter response. Nevertheless, the modification of fly-backs in bandpass synthesis approach can be considered as an additional advantage since different levels of rejection, and consequently, mask specification fulfillment can be achieved.

4.1.2 Inductive Matching Elements Case

Networks with shunt connected inductors exhibit presence of two TZs at the origin more since these inductors are obtained by complete extraction. As a result, networks with inductive matching elements at source and load are characterized by other filtering function derived as

$$K(\omega) = \cosh\left[\cosh^{-1}\left(T_0\left(\omega\right)\right) + \cosh^{-1}\left(T_0'\left(\omega\right)\right) + \sum_{n=1}^{N} \cosh^{-1}\left(X_n\left(\omega\right)\right)\right], \tag{4.4}$$
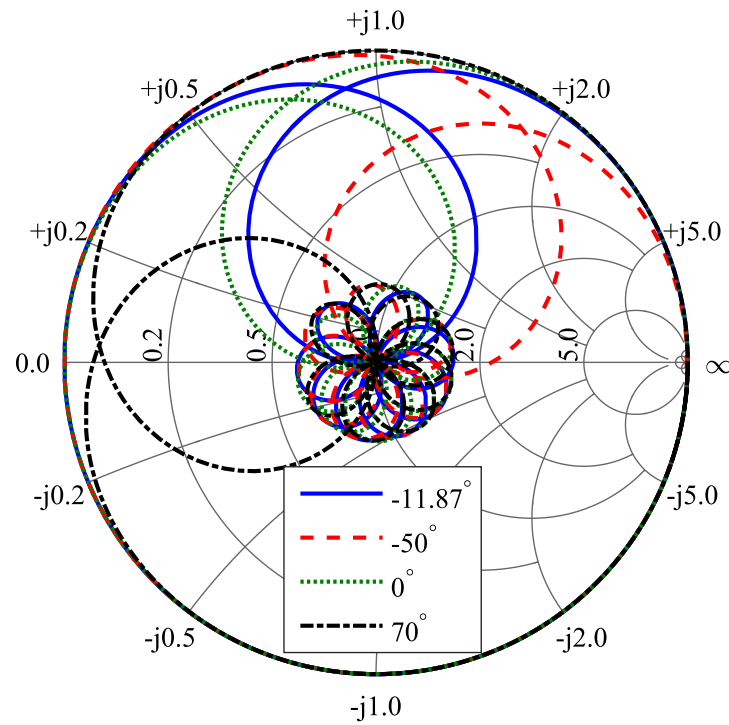
Figure 4.3: S_{11} phase modification for network with capacitive matching elements considering only positive passband.
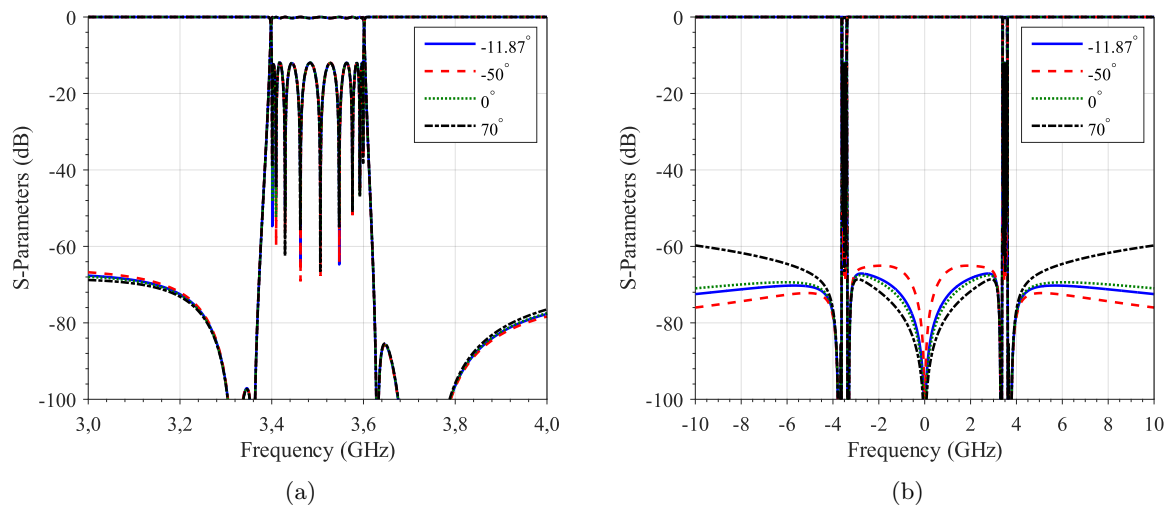
Figure 4.4: Phase correction term influence on S-parameters of network with capacitive matching elements at (a) in-band and (b) out-of-band frequencies.
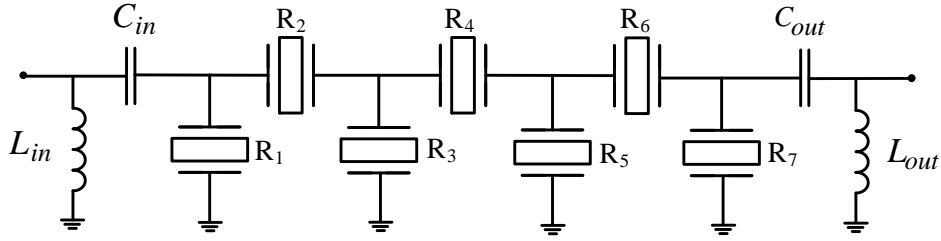
Figure 4.5: Realization of seventh-order ladder-type network with inductive matching elements.

Table 4.2: Phase influence on the network with inductive matching elements. Coefficient A modification.

φ, degrees	$\Delta\varphi$, degrees	A	In/Out C, pF	In/Out L, nH
−69.11	0	1	2.703	21.057
0	69.11	69.17	1.105	12.409
−100	−30.89	−19.72	4.992	64.433

where $T_0(\omega)$ introduces one TZ at the origin and it is defined by (4.2), and $T_0'(\omega)$ is responsible for another two TZs at zero frequency and it is found to be

$$T_0'(\omega) = \frac{T_2'(\omega)}{\omega^2}, \qquad T_2'(\omega) = \frac{-\omega^3 - \omega_1\omega_2\omega}{\omega_2 - \omega_1}. \tag{4.5}$$

Since in this case two functions define input/output reactive elements' value, three options are possible to introduce a phase correction term: using coefficient A in $\tilde{T}_2(\omega)$, using coefficient B in $\tilde{T}_2'(\omega)$ or combining both of them. Below, each case is considered separately.

Case 1. Phase Introduction by Coefficient A

In order to control the phase value, the function $\tilde{T}_0(\omega)$ from (4.3) is implemented. Changing coefficient A, not only do series/shunt connected capacitors vary, but also shunt connected inductors. The resulting situation is similar to that with capacitive reactive nodes at source and load described above. To demonstrate the functionality we propose an example of seventh-order filter in Band 1 Rx with passband extended from 2.11 to 2.17 GHz depicted in Figure 4.5. This time the filter is considered to be a receiver path of a duplexer, and therefore, the phase is evaluated at dual central frequency (1.95 GHz) of transmitter path so as to know how to balance the common port of the device. Different values of phase and corresponding capacitors and inductors are presented in Table 4.2. The purely imaginary roots of polynomials $F(s)$ and $E(s)$ are changed by the similar way as in previous case, so they are not listed here. The first row describes the network without any phase modification. The common case of 0° phase needed for duplexer design is shown in the second row. The filter response is illustrated in Figure 4.6. Here,
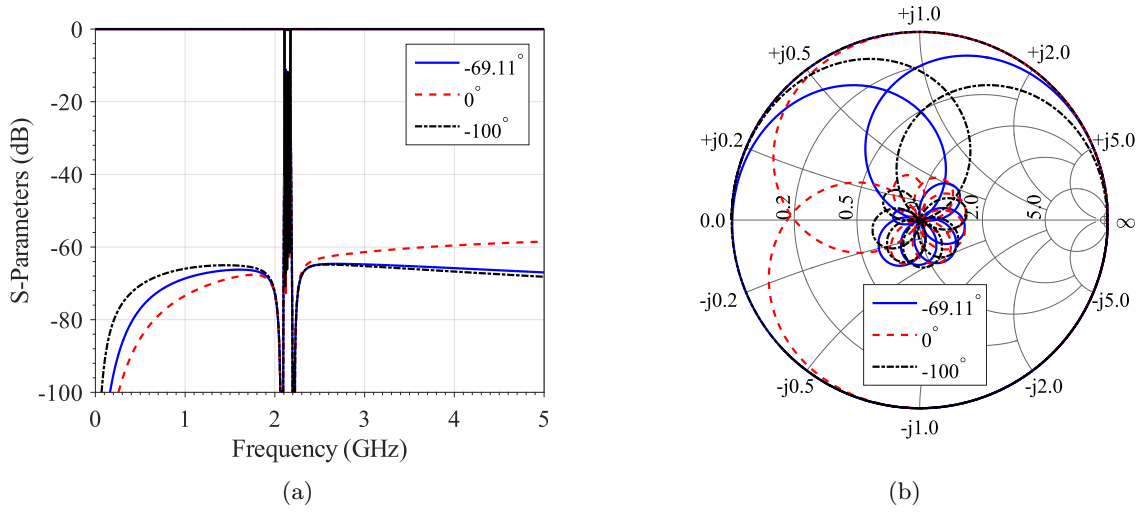
Figure 4.6: Phase correction term influence on the S-parameters of network with inductive matching elements by coefficient A modification: (a) magnitude response (b) S_{11} phase response.

only positive passband is represented. The same effect of rejection level variation at out-of-band frequencies can be observed in Figure 4.6 (a). Smith Chart in Figure 4.6 (b) demonstrates the lobes rotation of S_{11} phase, depending on phase correction value.

Case 2. Phase Introduction by Coefficient B

The phase term can be introduced into the function $T_2'(\omega)$ as well as into the function $T_2(\omega)$ from the previous case because both of them determine source/load reactive nodes values. The updated function from (4.5), which introduces two TZs in the origin by shunt connected inductors at source and load, is derived as

$$\tilde{T}_0'(\omega) = \frac{\tilde{T}_2'(\omega)}{\omega^2}, \qquad \tilde{T}_2'(\omega) = \frac{-\omega^3 - \omega_1\omega_2\omega}{B \cdot (\omega_2 - \omega_1)}. \tag{4.6}$$

At the same time, it is considered that $A = 1$. The influence of coefficient B on the function $\tilde{T}_2'(\omega)$ can be observed in Figure 4.7. It can be noticed that different rejection level at out-of-band frequencies can be achieved with coefficient B modification only as well. Since the behavior of the traces is steeper than in case of capacitive matching elements from Figure 4.1, the influence from coefficient B on the function $\tilde{T}_2'(\omega)$, and consequently, on the source/load inductors is stronger.

The same network illustrated in Figure 4.5 is used to implement the phase correction. The same values of phase evaluated at dual central frequency are chosen and presented in Table 4.3. Comparing the capacitive and inductive matching elements values with those from Table 4.2, it can be noticed that capacitors are preserved almost the same, whereas the inductors are
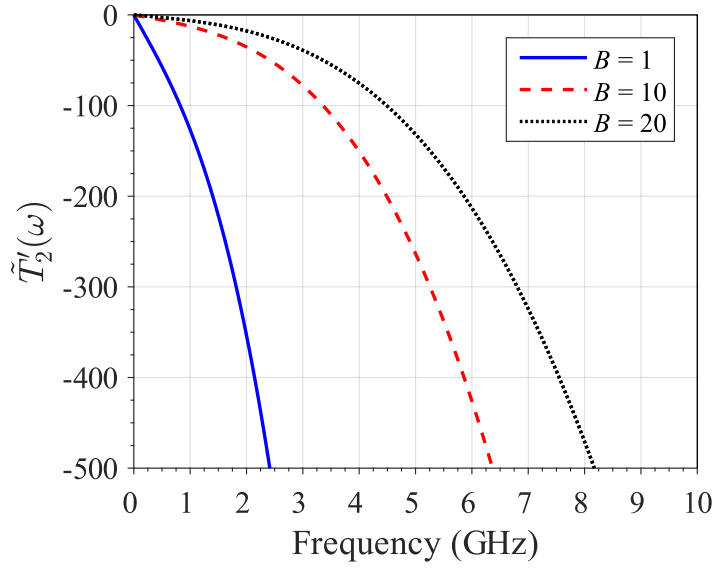
Figure 4.7: $\tilde{T}'_2(\omega)$ modification depending on different values of B.

Table 4.3: Phase influence on the network with inductive matching elements. Coefficient B modification.

| φ, degrees	$\Delta\varphi$, degrees	B	In/Out C, pF	In/Out L, nH
–69.11	0	1	2.703	21.057
0	69.11	–161.33	1.258	9.710
–100	–30.89	29.65	4.834	2586.321
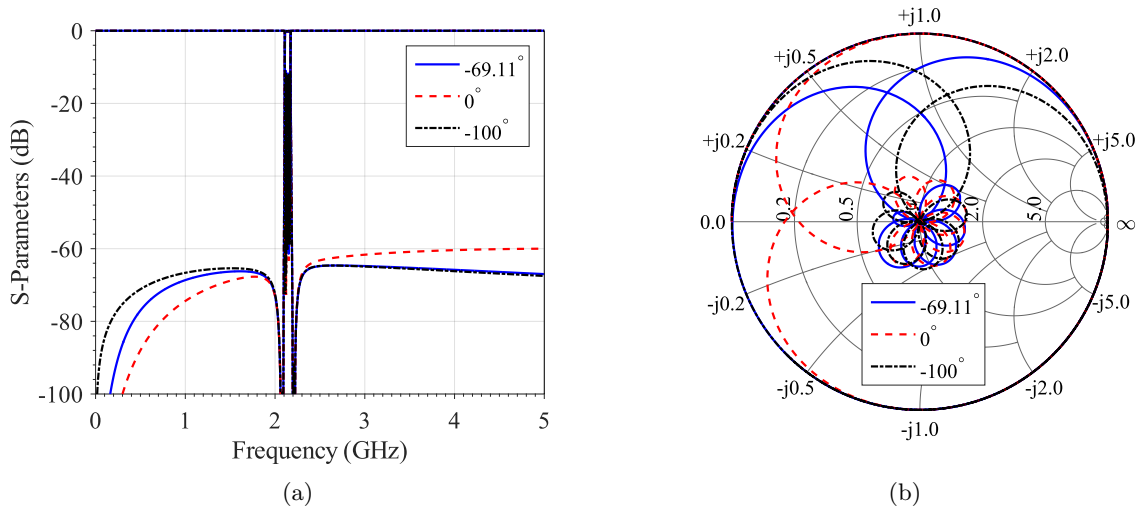
Figure 4.8: Phase correction term influence on the S-parameters of network with inductive matching elements by coefficient B modification: (a) magnitude response (b) S_{11} phase response.

changed significantly since the function $\tilde{T}_2'(\omega)$ is modified only. The response of the network is depicted in Figure 4.8. The magnitude response of S-parameters presented in Figure 4.8 (a) is comparable with the response from Figure 4.6 (a); however, as inductors differ notably, the out-of-band rejection levels near zero frequency are slightly varied. S_{11} phase response is shown in Figure 4.8 (b) and it is very similar to that from Figure 4.6 (b).

Case 3. Phase Introduction by Coefficients A and B

This time both of the functions with corresponding coefficients from (4.3) and (4.6) are used in process of phase modification. The same network in Band 1 Rx depicted in Figure 4.5 is implemented in order to observe the elements modification because of different network phase. After applying both A and B coefficients, the input/output inductive and capacitive nodes are also changed, corresponding to the Table 4.4. The magnitude response of the network is illustrated in Figure 4.9 (a), and S_{11} phase response is presented in Figure 4.9 (b).

Comparing three different methods of phase correction for network with inductive matching elements, it can be noticed that the trace of $0°$ of the third $A\&B$ case has higher level of rejection at the origin and at infinity, comparing with other two cases. This happens because both of the functions $\tilde{T}_0(\omega)$ and $\tilde{T}_0'(\omega)$ are applied, and therefore, the filtering function from (4.4) has a higher rejection at out-of-band frequencies. Since at $-100°$ phase the coefficient B slightly differs from 1, this effect of high rejection cannot be properly observed. A comparison between three cases described above for $0°$ phase is presented in Figure 4.10. In Figure 4.10 (a) a high attenuation level of S_{21} of the third case can be observed. This feature is useful for duplexers' and multiplexers' design where high level of rejection is needed at counterpart frequency bands. In Figure 4.10 (b) different behavior of S_{11} phase response at out-of-band frequencies for $A\&B$ case can be noticed; however, three of the cases fulfill the requirement of $0°$ phase evaluated at dual central frequency. This is the reason of changed lobe position on Smith Chart for $A\&B$ case in Figure 4.9 (b), comparing with the first two cases.

The main advantage of phase correction for networks with inductive matching elements is that there are three possible options to introduce needed phase: by coefficient A, by coefficient B, and by both of them. Each option provides different values of inductive and capacitive matching elements which influence on filter magnitude and phase response. This multiple choice gives the possibility to design a network with needed specifications.

Networks with capacitive matching elements have only one option to introduce phase correction by coefficient A. Nevertheless, it also makes possible to adjust phase to $0°$ at counterpart frequency bands and eliminate input/output reactive elements as well.

Table 4.4: Phase influence on the network with inductive matching elements. Coefficients A and B modification.

| φ, degrees	$\Delta\varphi$, degrees	A	B	In/Out C, pF	In/Out L, nH
−69.11	0	1	1	2.703	21.057
0	69.11	44.61	39.79	2.547	3.454
−100	−30.89	−17.16	1.25	4.948	88.595
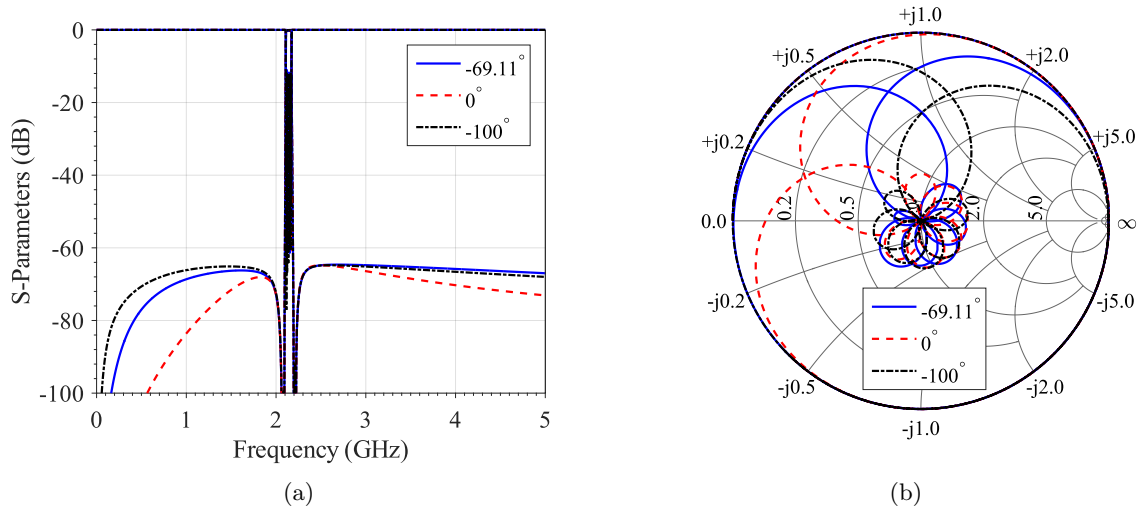
Figure 4.9: Phase correction term influence on the S-parameters of network with inductive matching elements by coefficients A and B modification: (a) magnitude response (b) S_{11} phase response.
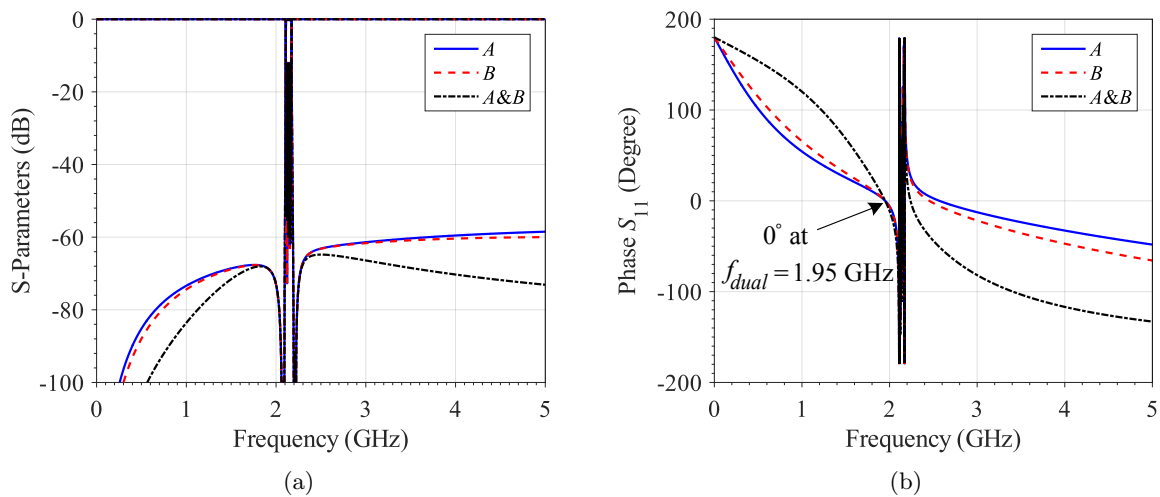
Figure 4.10: Comparison of three networks with 0° phase evaluated at dual central frequency, using coefficients A, B, and $A\&B$: (a) magnitude response (b) S_{11} phase response.

4.2   Relation between Phase and Coefficients A and B

In previous section the coefficients A and B, which lead to modification of the S_{11} phase, have been introduced. However, a direct relation between phase evaluated at certain frequency and corresponding coefficients has not been presented. In this part we explain how to link these parameters.

In Chapter 2 the explanation of phase introduction and evaluation in lowpass domain has been outlined. By simple multiplication of characteristic polynomial $F(s)$ by complex phase term $e^{j\theta_{11}}$, the phase value can be applied after the polynomials synthesis procedure. However, in bandpass domain this method cannot be used, as it leads to complex reactive elements of the network which are impossible to implement. By this reason, phase coefficients A and B are introduced directly in the polynomials synthesis routine. Since the modification is done from the beginning of the synthesis procedure, the rest of the direct bandpass methodology is assured to be converged as long as the filter characteristic polynomials $F(s)$, $P(s)$, and $E(s)$ are correctly obtained.

Whereas the introduction of the phase is realized from the polynomials synthesis, i.e., inside the recursive technique, the evaluation of introduced phase value is carried out only after the polynomials obtaining by expression

$$\varphi = \arctan \left. \frac{F(s)}{\varepsilon_R E(s)} \right|_{s=s_{ph}}, \tag{4.7}$$

where s_{ph} is the frequency at which the phase is evaluated. Generally, it is a frequency of the first finite TZ in case of stand-alone filter or central frequency of the duplexer dual passband.

Since the functions $\tilde{T}_0(\omega)$ and $\tilde{T}_0'(\omega)$ form part of the recursive technique at very beginning of the synthesis and appear in different summands at every iteration, it can be a challenging task to establish the mathematical relation between coefficients A or B and the needed phase. The situation of applying both of the coefficients is even more complex, as it leads to the equation with two variables.

To resolve this problem the MATLAB nonlinear programming solver *fminsearch* compatible with MCT was introduced into the polynomials synthesis routine. This solver works with real parameters and finds minimum of unconstrained multivariable function, and therefore, it is totally suitable for our purpose. By this way, a unique A or B values are found, corresponding to the desired phase established at the beginning of the synthesis. For the case of $A\&B$ coefficients combination various solutions can be found, depending on initial input vector $[A_0 \ B_0]$. This ability can be useful for needed source/load reactive elements modification, leaving the desired phase value intact.

4.3   Limitations of the Phase Correction Methodology

Presented methodology works well with ladder-type acoustic filters, taking into account different types of matching elements at source and load. However, there are some limitations which can be divided in two parts. The former part represents intrinsic limitations of the synthesis procedures after applying a certain phase value. The latter part is related with feasibility of acoustic wave technology. Both types of limitations are outlined in detail below.

4.3.1   Intrinsic Limitations

It has been explained before that purely imaginary roots of characteristic polynomial $F(s)$ are the object of the main changes when phase correction is applied by coefficients A and/or B. Unlike the lowpass synthesis approach, not any value of phase can be introduced into the direct bandpass methodology. Certain phase value may lead to the situation when purely imaginary roots are converted to the real ones, and therefore, an additional undesirable RZ at out-of-band frequencies appears. To demonstrate this effect the same example of stand-alone filter in Band 42 from capacitive matching elements case depicted in Figure 4.2 is considered. As it can be seen in the Table 4.1, there is only one corrected negative phase value presented for this network, i.e., –50°. Now, we decrease the phase value until –120°. As a result, the needed coefficient A becomes –2330.5, the pair of purely imaginary roots of polynomial $F(s)$ turns to be purely real of ± 3.36, and the pair of purely imaginary roots of polynomial $E(s)$ becomes complex. The resulting response of the filter is presented in Figure 4.11 where an additional RZ and transmission pole on the left out-of-band side can be clearly seen.

The same situation occurs for network with shunt first resonator and series connected capacitors. However, unlike the topology with series first resonator and shunt capacitors, it exhibits additional RZ and transmission pole at the right side at far out-of-band frequency. This situation is illustrated in Figure 4.12.

According to our experience, for the networks with capacitive nodes at source and load the initial phase can be corrected into the range of around $\pm 90°$ without undesirable RZ appearance. This means that if duplexer module design is considered and absolute value of filter initial phase evaluated at dual central frequency is more than 90°, then corrected phase cannot achieve needed 0° to balance the input port. In this case, initial input parameters of the filter such as set of finite TZs and return loss level have to be changed. Another option is to add a pair of shunt connected inductors at source and load, converting the network into the one with inductive matching elements.

Since in networks with inductive matching elements phase correction can be performed by both A and B coefficients, the range of phase modification increases until around $\pm 130°$ thanks

Figure 4.11: Appearance of undesirable RZ and transmission pole at out-of-band frequency when inapplicable phase value is considered for network with series first resonator and shunt connected capacitors at source and load.
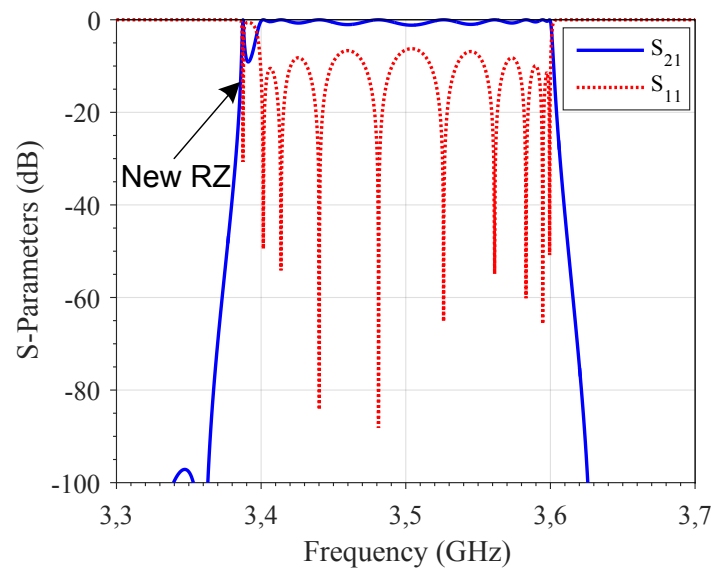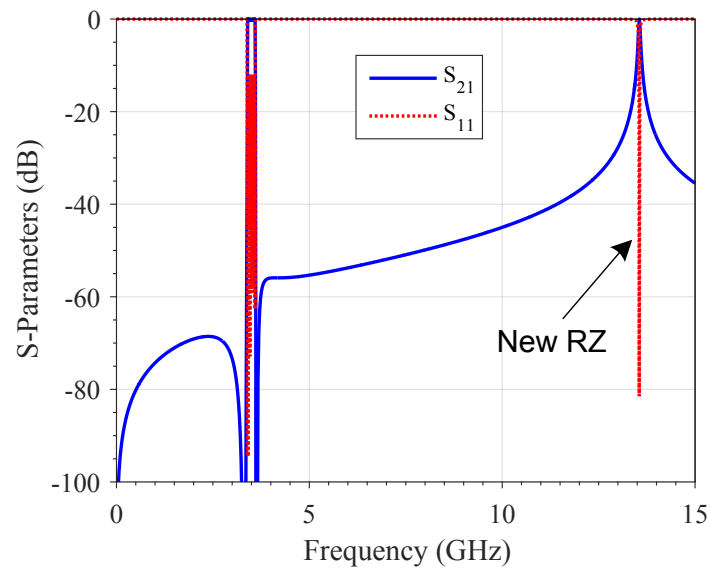

Figure 4.12: Appearance of undesirable RZ and transmission pole at out-of-band frequency when inapplicable phase value is considered for network with shunt first resonator and series connected capacitors.

to possibility of setting different initial input vector $[A_0 \ B_0]$. This option makes the duplexer design requirement easier to fulfill and also provides the response with higher rejection level at out-of-band frequencies.

4.3.2   Technological Limitations

From point of view of technological feasibility, as it has been explained in Chapter 2 and Chapter 3, acoustic filters are constrained by electroacoustic conversion parameter r or k_{eff}^2. Uniform values of k_{eff}^2 (r) are desirable in order to optimize the fabrication process in agreement with material system and to reduce the number of external reactive elements.

Applying phase correction in lowpass synthesis approach, significant modification of k_{eff}^2 (r) of the first and the last resonators can be observed since both series resonant frequency f_s and parallel resonant frequency f_p of these resonators are modified. Moreover, a slight variation in all reactive elements of the network such as L_a, C_a, C_0, and reactive nodes at source and load can be noticed as well.

In bandpass synthesis methodology all reactive elements are also modified, but the situation about f_s and f_p is slightly different. If network started with series resonator is considered, the series resonant frequency of the first and the last resonators and parallel resonant frequency of the second and penultimate resonators are changed. In case of shunt first resonator, the parallel resonant frequency of the first and the last resonators and series resonant frequency of the second and penultimate resonators are varied. Therefore, parameter k_{eff}^2 of the first two and the last two resonators are modified when phase correction in bandpass methodology is applied. Depending on phase value, the effective coupling coefficient may vary significantly, and therefore, the values of external elements for these resonators may be so large that it would be incompatible with micro-acoustic technology. Moreover, the situation of negative source/load reactive elements, which are impossible to realize, can also be obtained at certain value of phase. Thus, the trade-off between phase correction and feasibility of the network has to be taken into account at the design process in a similar way, as it has been described in Chapter 2. However, a situation of parameter k_{eff}^2 (r) adjustment for the first two and the last two resonators can also be found as a result of phase modification.

4.4   Numerical Example

In order to demonstrate the functionality of proposed phase correction methodology in direct bandpass synthesis, a duplexer in Band 1 is designed, using MCT. A receiver filter is taken from the case of phase introduction by coefficients A and B so as to provide an additional rejection at out-of-band frequencies. It is a seventh-order network depicted in Figure 4.5 with RL level of

Table 4.5: BVD bandpass elements of seventh-order receiver filter in Band 1 Rx.

Parameters	Res 1&7	Res 2&6	Res 3&5	Res 4
L_a (nH)	24.09	84.76	6.1075	93.33
C_a (pF)	0.2407	0.0650	0.9679	0.0593
C_0 (pF)	4.5874	1.2360	13.9277	0.7720

$C_{in} = C_{out} = 2.547$ pF; $L_{in} = L_{out} = 3.454$ nH.

Table 4.6: BVD bandpass elements of seventh-order transmitter filter in Band 1 Tx.

Parameters	Res 1&7	Res 2&6	Res 3&5	Res 4
L_a (nH)	154.04	29.82	264.78	8.4481
C_a (pF)	0.0433	0.2378	0.0252	0.8761
C_0 (pF)	0.3128	4.1796	0.2351	7.8670

$C_{in} = C_{out} = 1.102$ pF; $L_{in} = L_{out} = 4.608$ nH.

15 dB, prescribed TZs at 2.09, 2.20, 2.07, 2.22, 2.07, 2.20, and 2.09 GHz, and with three TZs at the origin. In order to achieve a 0° phase at dual central frequency (1.95 GHz), coefficients $A = 44.61$ and $B = 39.79$ have been applied according to Table 4.4. Reactive BVD elements' values of the network are presented in Table 4.5. Since in this example we only show the capability of phase correction methodology, we do not take into account technological constraints and mask specifications; therefore, effective coupling coefficient and resonant frequencies of the resonators are not presented.

Now, remaining transmitter filter of the duplexer has to be designed. Chosen seventh-order network starts with series resonator and accommodates shunt connected inductors and capacitors at source and load, thus providing three TZs at the origin. Passband of the filter extents from 1.92 to 1.98 GHz, RL level equals to 18 dB, prescribed TZs are positioned at 2.08, 1.89, 2.05, 1.85, 2.05, 1.89, and 2.08 GHz. After synthesis procedure, initial phase value evaluated at dual central frequency (2.14 GHz) has been found to be –53.015°, and input/output reactive elements result in $C_{in} = C_{out} = 0.959$ pF and $L_{in} = L_{out} = 19.852$ nH. Then, phase correction methodology has been applied by introducing both coefficients A&B for higher rejection level at out-of-band frequencies. Therefore, by $A = 69.80$ and $B = 11.39$ a 0° phase at counterpart frequency has been provided. Resulting values of network reactive elements are presented in Table 4.6. In this design technological constraints are not taken into consideration either.

The out-of-band magnitude of S-parameters and S_{11} phase with and without phase correction application can be seen in Figure 4.13 (a) and (b), respectively. In Figure 4.13 (a) it can be noticed that an additional rejection level has been provided by including both A and B
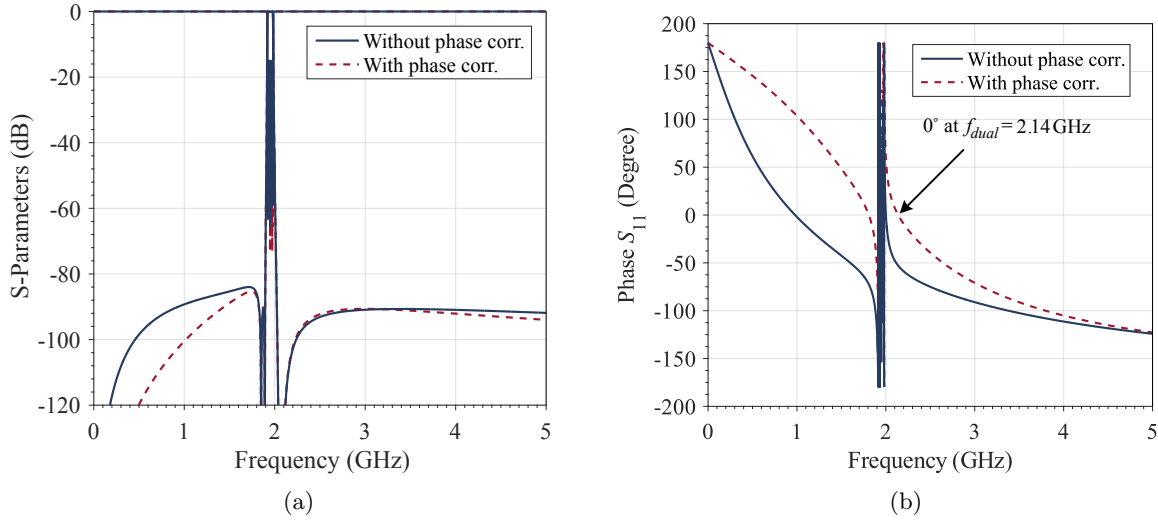
Figure 4.13: Comparison of responses of transmitter filter in Band 1 Tx without and with phase correction application (a) magnitude response (b) S_{11} phase response.

coefficients. Figure 4.13 (b) demonstrates the achievement of needed 0° phase at counterpart frequency which accommodates a balanced input port. Figure 4.14 shows phase rotation in Smith Chart for positive passband.

Now both filters are adapted to be included in duplexer presented in Figure 4.15. A common inductor at the antenna $L_{in} = 1.974$ nH is calculated as parallel of both input inductors in Rx and Tx path. Resulted magnitude response is demonstrated in Figure 4.16. It can be noticed a slight influence of loading effect on RL level of transmitter filter and a good adaptation of receiver path of duplexer. Since there is a gap of 130 MHz between two passbands, the phase evaluation in lowpass domain may give an imprecise value at counterpart frequency. Direct bandpass synthesis with phase correction methodology permits to overcome this problem. For the simulation a quality factor of $Q = 2000$ for acoustic resonators at resonance and anti-resonance frequencies, $Q = 25$ for inductors, and $Q = 100$ for capacitors have been taken.

4.5   Chapter Summary

In this chapter a novel phase correction methodology in direct bandpass synthesis has been presented. Phase modification is useful for both stand-alone filters in order to eliminate input/output reactive elements, and for duplexers and multiplexers in order to provide a balanced input port. New coefficients, A and B, are introduced in filtering function for this purpose which lead to purely imaginary roots modification of characteristic polynomials $F(s)$ and $E(s)$ which, in turn, provokes modification of input/output reactive elements and out-of-band mag-
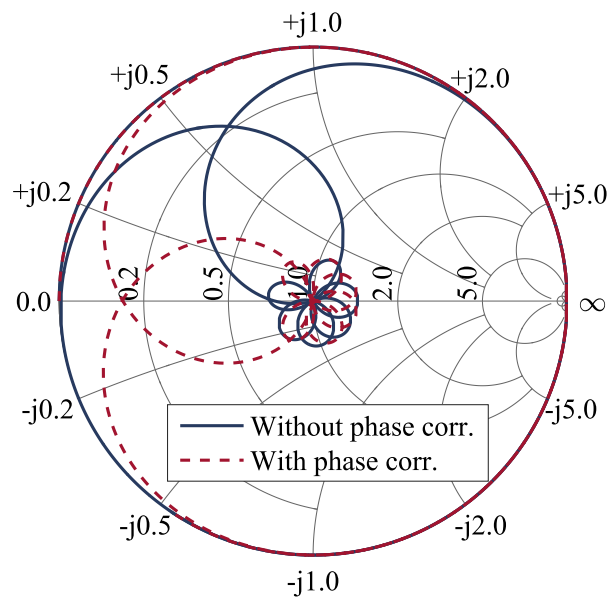
Figure 4.14: S_{11} phase modification represented in Smith Chart for transmitter filter in Band 1 Tx for positive passband.
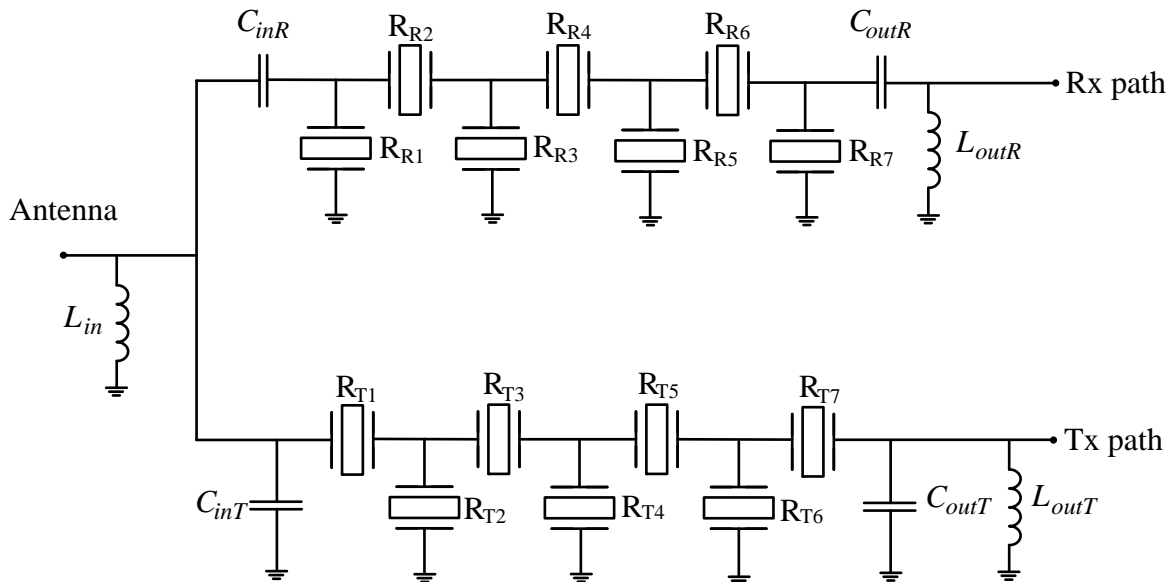
Figure 4.15: Designed duplexer in Band 1.
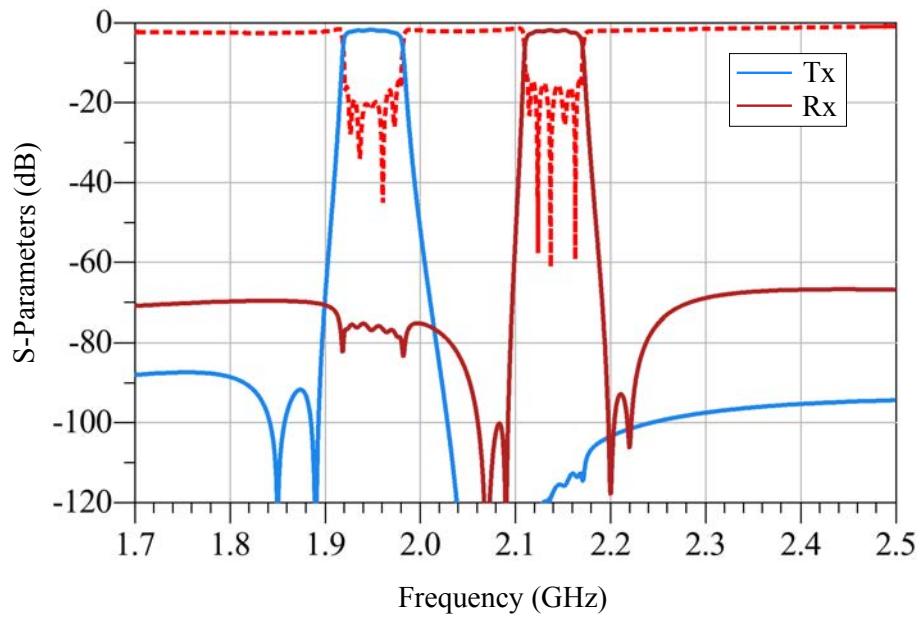
Figure 4.16: Magnitude response of designed duplexer in Band 1.

nitude response of the filter. Different ways of phase correction applications have been shown and accompanying examples have complemented the explanation.

Limitations of the methodology have been outlined as well. A $\pm 90°$ phase correction for networks with capacitive matching elements, and $\pm 130°$ phase modification for topologies with inductors at source and load can be applied without undesirable RZ and transmission pole appearance in the response. However, technological constraints may reduce these values so as to provide a feasible network.

MATLAB nonlinear programming solver *fminsearch* has been implemented in the synthesis routine in order to link A and B coefficients' value with needed phase evaluated at certain frequency. A future work can be done to elaborate a mathematical relation between these parameters. Finally, an example of duplexer in Band 1 has been designed in order to demonstrate the functionalities of the method.

Lossy Acoustic Filter Synthesis by Gradient-Based Optimization Technique

Previous synthesis techniques in lowpass and bandpass domain deal with ideal lossless resonator model with its perfect transmission and reflection response. Resistive elements are added afterwards in order to evaluate the possible negative impact on frequency behavior and make a decision of filter feasibility and fulfillment of mask specifications. Finite quality factor has always been the object of constant improvement by industry since this parameter defines crucial characteristics of filtering networks such as passband edge-rounding, bandwidth, and selectivity.

In this chapter we introduce a lossy synthesis technique which takes into consideration resistive elements of the network from the beginning of the synthesis. This technique allows to rearrange set of quality factor among the resonators, depending on existence of critical resonators. In this case, it is not necessary to have all resonators of high Q but only the indicated ones. The main objective of the synthesis is maintenance of IL level flatness, thus avoiding edge-rounding and loss of spectrum.

The method is based on a gradient-based optimization technique with special cost function. As a result, a coupling matrix of inline lossy filter, providing flat passband IL, is obtained. By imposing optimization restrictions, it allows to avoid edge-rounding, considers losses in resonators only, and it is suitable for acoustic wave technology. This technique works with mixed inline topology, consisting of resonant nodes and NRNs, and operates with source-load coupling or cross-couplings between resonators as well, so it can be suitable for other types of technology. Having the possibility to estimate the lossy filter response at the stage of synthesis helps a designer to make a correct decision of drawbacks correction, appearing because of finite quality factor.
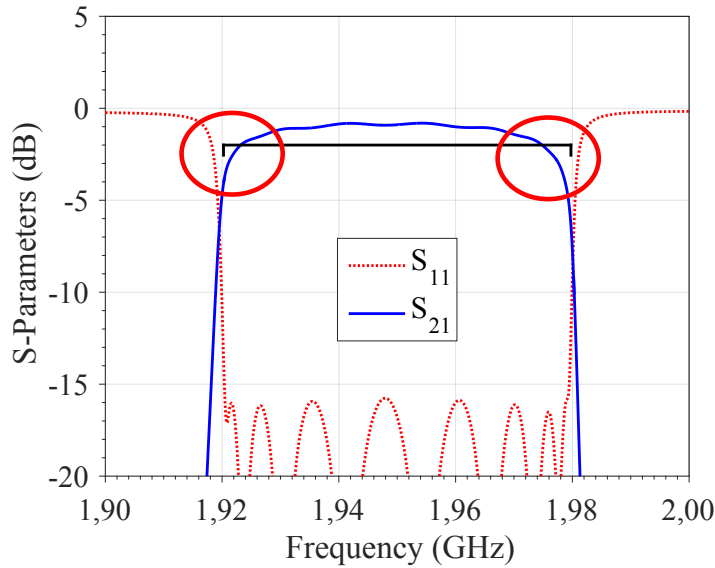
Figure 5.1: Mask breach caused by finite quality factor.

5.1 Lossy Filter Synthesis Techniques

As it has been mentioned in Chapter 2, quality factor is an important parameter which has to be taken into account at the stage of synthesis procedure. When in the lowpass domain lossless resonators are considered, in the bandpass domain finite Q is compensated by bandwidth expanding of the filter response. However, sometimes mask specifications are so strict that it becomes impossible to use this approach. Moreover, bandwidth widening reduces selectivity which will not be acceptable for future demanding applications. Sharp passband corners has always been the reason of high-Q filter structures investigations in acoustic technology.

Inappropriate management of finite quality factor of acoustic resonators may lead to passband rounding and following mask breach and make specifications difficult to fulfill as it is demonstrated in Figure 5.1. Here, it can be observed that the edges of the passband become more rounded and the passband itself results narrower with finite Q consideration. Moreover, passband edges suffer more than the middle of the band which leads to a serious problem for modulations that go right to the edge of the passband, provoking the loss of information. To resolve this drawback, finite quality factor has to be treated by lossy techniques.

Size and mass reduction of the filter and maintenance of flat passband IL level have always been the main reasons to include finite quality factor into the synthesis procedure. Up-to-date lossy techniques include characteristic polynomials' modification, adaptation of admittance parameters, and correction of lossy coupling matrix. Below, we make a brief overview of these techniques.

Method of predistortion

Predistortion is a technique for loss correction in filters due to effects of energy dissipation in such a way that lossy predistored response is not deteriorated by bandedge round-ups and maintains the shape of ideal filter response. The procedure of bandpass network design from lowpass prototype was firstly introduced in [88] and it consists of three steps:

1. Calculation or estimation of Q of the resonator.
2. Definition of $\delta = f_0/BW/Q$, where f_0 is a central frequency and BW represents filter's bandwidth.
3. Synthesis of lowpass filter with its poles shifted toward the $j\omega$ axis by the amount δ.

The method permits to avoid passband edge rounding; however, RL level is heavily deteriorated and only uniform losses can be considered in the synthesis. Afterwards, this technique was extended to filters with cross-couplings and non-uniform quality factors with symmetric and asymmetric realization [89, 90]. Method of predistortion works well for dielectric, coaxial or mixed technologies where resistive cross-couplings can be implemented and RL level compensation can be done by nonreciprocal devices such as isolators and circulators. However, in micro-acoustic technology resistive cross-couplings cannot be implemented, and inclusion of nonreciprocal devices will negatively impact on the total chip size.

Even/Odd Mode Analysis

The method was firstly described in [91] where S-parameters of two-port network are expressed by their even and odd mode of admittance parameters and then are connected in parallel. However, if the network is transformed into ladder-type topology, the losses are presented only in the first and the last resonator, which is equivalent to have attenuators connected at source and load. Hyperbolic rotations can be applied in order to distribute losses among the network but it also provides complex or resistive cross-couplings [92]. This technique allows non-uniform quality factors and it is suitable for parallel connected networks of different technologies providing high level of RL. However, this method cannot be used in acoustic technology either because of impossibility to realize complex and resistive couplings.

Lossy Coupling Matrix

The focus of these techniques is on the circuit synthesis by means of coupling matrix rather than polynomial synthesis. These methods include lossy matrix iteration procedure [93] or lossy matrix optimization [94] where needed losses are introduced directly to networks elements. Up-to-date publications consider network without NRNs and admit resistive cross-couplings.

To sum up, it can be noticed that no lossy technique is suitable for micro-acoustic technology in our best of knowledge. None of them considers NRNs and introduces losses only in resonators. Therefore, in this chapter we implement gradient-based optimization technique [95] in order to obtain a coupling matrix of lossy ladder-type acoustic filter considering NRNs and resistive resonant nodes (RNs), and providing flat passband IL level.

5.2 Lossy Network Realization

As it has been demonstrated in Chapter 2, ladder-type acoustic network is represented by inline nodal configuration. However, in case of lossy filters, RNs have to include resistive elements in accordance with finite Q of acoustic resonator. Thus, updated general inline topology is illustrated in Figure 5.2, where G_S and G_L are normalized conductances at source and load, respectively, and R_i is a resistance characterized finite Q of every RN.

In this chapter a further explanation of the methodology will be based on coupling matrix [96–98]. Since some of the circuit elements have to be optimized and the others are maintained, coupling matrix network description is useful and visual representation of filter's characteristics. Each element in the matrix is identified uniquely with an element of resulting inline topology, and therefore, losses can be directly assigned to the RNs. Thus, general form of lossy inline coupling matrix of acoustic network from Figure 5.2 has the following form:

$$
M_{lossy} =
\begin{array}{c}
\\ S \\ RN_1 \\ \vdots \\ RN_N \\ N_1 \\ \vdots \\ N_N \\ L
\end{array}
\begin{array}{c}
\begin{matrix} S & RN_1 & \cdots & RN_N & N_1 & \cdots & N_N & L \end{matrix} \\
\left[
\begin{matrix}
0 & 0 & \cdots & 0 & j & \cdots & 0 & 0 \\
0 & -j\omega_1 + \delta_1 & & & jJ_{R_1} & & & 0 \\
\vdots & & \ddots & & & \ddots & & \vdots \\
0 & & & -j\omega_N + \delta_N & & & jJ_{R_N} & 0 \\
j & jJ_{R_1} & & & jB_1 & & & 0 \\
\vdots & & \ddots & & & \ddots & & \vdots \\
0 & & & jJ_{R_N} & & & jB_N & -j \\
0 & 0 & \cdots & 0 & 0 & \cdots & -j & 0
\end{matrix}
\right]
\end{array}
\quad (5.1)
$$

where S is source node, L – load, RN_i – RN, and N_i – NRN. Real values of δ_i represent resistance from finite Q of each resonator.

Before optimization proceeding starts, the following constraints have to be taken into account:

1. Unit inverters $1/$–1 ($j/-j$ in matrix representation) among the path between source and load have to be maintained, since it is a necessary condition for further lowpass-to-bandpass elements' transformation.

2. NRN B_i has to be negative for series resonator and positive for resonator connected in shunt in order to correctly obtain finite TZs above and below the passband.
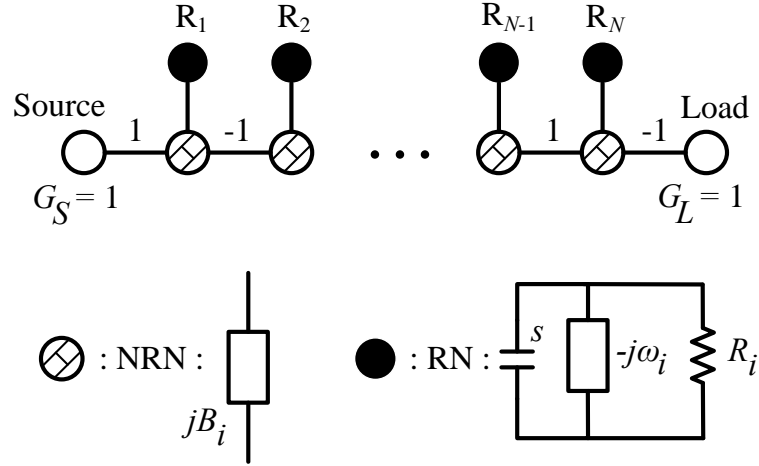
Figure 5.2: Inline lowpass nodal representation of lossy acoustic filter.

3. Self-coupling of each resonator $j\omega_i$ have to be preserved, since it defines the position of normalized finite TZ.

Therefore, the remaining elements to optimize are: NRN of each resonator B_i, taking into account the constraint mentioned above, inverters between RN and NRN J_{R_i}, and IL level value which accommodates flat passband with given distribution of Q of every resonator or δ_i which represents a finite Q values from given IL level by means of

$$Q_i = \frac{f_0}{BW \cdot \delta_i},\tag{5.2}$$

where f_0 is central frequency of the passband and BW represents design bandwidth. It can be noticed that in this approach we apply unloaded quality factor assigned to the frequency of finite TZ instead of Q_s and Q_p. Coupling matrix representation can describe only inline nodal topology, and therefore, only one resistance can be introduced to the matrix element. Thus, we consider one lossy element in mBVD model, namely, inductor L_a which takes part in generating both TZs below and above the passband.

In the process of quality factor distribution it has to be taken into account the nearness of TZ to the passband and the bandwidth of every resonator. Thus, the resonators with narrow bandwidth and closest to passband TZs must have higher quality factor since their transmission characteristics are degraded more because of losses introduction [99].

5.3 Synthesis Procedure

Process of lossy filter synthesis follows the diagram depicted in Figure 5.3. In order to achieve a flat passband IL level two options are possible, depending on input parameters. If there are fixed
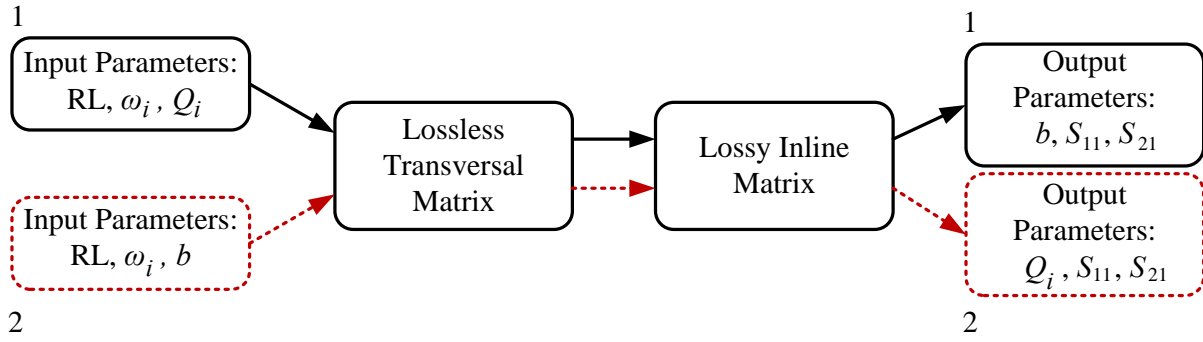
Figure 5.3: Diagram of lossy synthesis procedure with two different options of optimized parameters.

Q values of every resonator, then a parameter b is optimized so as to provide flat IL level inside the passband. In opposite case, when IL level is established by technological constraints, quality factor of each resonator is optimized, taking into account its inherent restrictions. In diagram from Figure 5.3 these two options are indicated by numbers 1 and 2, respectively. Relation between IL level and parameter b is described as

$$IL = 20 \lg(b). \tag{5.3}$$

After input parameters defining, a lossless $N + 2$ transversal coupling matrix is derived by means of characteristic polynomials' synthesis, using recursive technique with further partial fraction expansion of admittance function $[Y_N]$ [54]. Obtained ideal S-parameters will be used as a lossless template in following optimization process.

Next step is lossy inline matrix derivation by using special cost function which is found to be

$$f = w_{r1} \sum_{i=1}^{N} abs(S_{11}(rz_i))^2 + w_{t1} \sum_{j=1}^{N} abs(S_{21}(tz_j))^2 +$$
$$w_{r2} \sum_{k=1}^{N} abs(abs(S_{11}(s_k))^2 - abs(S_{11}^0(s_k))^2) + \tag{5.4}$$
$$w_{t2} \sum_{m=1}^{N} abs(abs(S_{21}(s_m))^2 - abs(bS_{21}^0(s_m))^2),$$

where w_{r1}, w_{t1}, w_{r2}, and w_{t2} are weightings; rz_i is the ith RZ, and tz_j is the jth TZ. S_{11}^0 and S_{21}^0 are template of lossless response. Vector of sampling points s_k is composed by maximums and minimums of S_{11} inside the passband, and s_m contains a distribution of sampling point of S_{21} between the lowest and the highest TZs. Finally, b characterizes flat IL level of lossy response. The first two summands from (5.4) permit to obtain matrix representation of lossless

topologies without NRN [100] and accommodate finite TZ and RZ of the original network. Since inline configuration exhibits presence of NRNs, two summands more are added in order to increase accuracy and introduce losses, providing flat passband IL level. They make the difference between lossless template and lossy response as little as possible. The fourth summand is taken from [101] with modification in sampling points. Optimization process is carries out by MATLAB constrained nonlinear multivariable function *fmincon*, applying SQP algorithm.

Finally, resulting inline matrix describes lossy response with flat passband, providing optimized b parameter from given Q values of every resonator or set of quality factors which accommodates predetermined by technology IL level.

5.4   Numerical Examples

In order to validate the method described above, we present two numerical examples. The first example is a seventh-order acoustic filter with given Q_i distribution. This network is characterized by coupling matrix M_{lossy} from (5.1). Another example is carried out for general mixed inline topology consisted of RNs and NRNs where there are not any technological constraints imposed by micro-acoustic technology so as to demonstrate that the method can be used for equivalent networks of other technologies.

5.4.1   IL Level Optimization

A seventh-order bandpass acoustic filter in Band 25 Tx with passband extending from 1.92 to 1.98 GHz is realized, following the process numbered by 1 in synthesis diagram from Figure 5.3. RL level equals to 22 dB and normalized finite TZs are prescribed at [$3j$, $-2j$, $2j$, $-1.5j$, $2j$, $-2j$, $3j$]. After analysis of critical resonator existence, it has been determined that the first and the last resonators have the narrowest bandwidth, and therefore, they have to be characterized by the highest quality factor. As a result, established Q-vector equals to [1500 1000 1200 1000 1200 1200 1500].

After optimization procedure, the resulting lowpass elements of inline representation, which fulfill requirements mentioned above, are presented in Table 5.1. It can be noticed that although the distribution of finite TZs is symmetric, the final network is asymmetric. This situation is due to Chebyshev function disruption throughout the optimization process by enforcing flat passband IL level. It affects heavily on RL level realization which can be observed in Figure 5.4 (a) and (b). Here, S_{21} Template is ideal S_{21} parameter multiplied by b and it is presented for comparison between lossy and lossless response. Nevertheless, it can be noticed that a flat passband IL level of 2.6536 dB is achieved for lossy acoustic resonators which has been our

Table 5.1: Optimized elements values in lowpass domain for seventh-order lossy filter in Band 1 Tx.

Param.	Res 1	Res 2	Res 3	Res 4	Res 5	Res 6	Res 7
B_i	−0.9618	1.6447	−3.9514	1.3239	−3.8585	2.4979	−3.8020
J_{R_i}	2.2142	1.5092	−2.9361	−1.3337	−2.7519	−1.9920	−3.1053

$b = 0.7367$; $IL = 2.6536$ dB.

(a)   (b)

Figure 5.4: Comparison of lossless and lossy response of seventh-order filter in Band 1 Tx at (a) out-of-band and (b) in-band frequencies. S_{21} Template is a lossless parameter S_{21} multiplied by b and it is presented for comparison.

intention. Resistance values of acoustic branch of every resonator are derived from

$$Q_i = \frac{2\pi f_i L_i}{R_i}, \tag{5.5}$$

and they have been found to be 0.221, 0.713, 2.536, 0.913, 2.744, 0.341, and 1.689 Ohm. This example has been performed in order to demonstrate the method's ability, and therefore, no mask specifications and no technological constraints' adjustment are considered.

5.4.2 Quality Factor Optimization

Second example follows the process numbered by 2 in synthesis diagram from Figure 5.3. General inline network composed by both RNs and NRNs under consideration with passband extending from 1.18 to 1.22 GHz is depicted in Figure 5.5. It is a sixth-order filter with two normalized finite TZs at $[1.9j \; -1.9j]$ and RL level of 20 dB. In this case IL level, which has to be tolerated in fabrication process, is known and equals 2.2 dB. Therefore, a set of Q_i provided flat passband
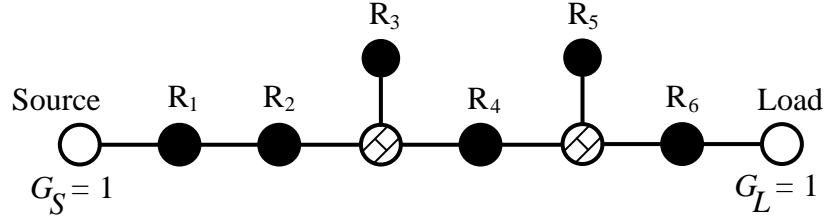
Figure 5.5: Mixed inline topology of sixth-order lossy filter with two finite TZs.
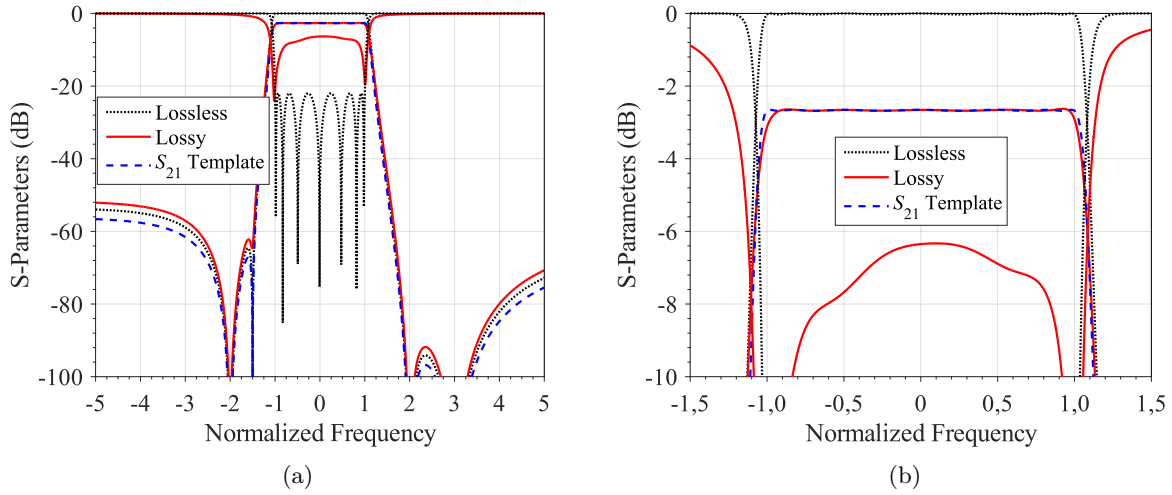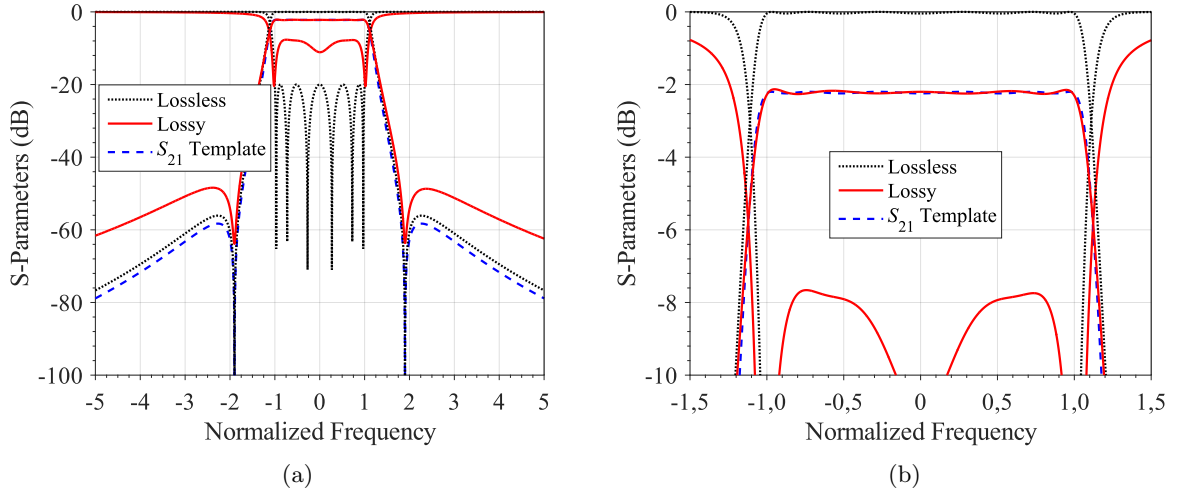

Figure 5.6: Comparison of lossless and lossy response of sixth-order filter with two finite TZs at (a) out-of-band and (b) in-band frequencies. S_{21} Template is a lossless parameter S_{21} multiplied by b and it is presented for comparison.

has to be obtained by optimization process. In this example all elements (except dangling RNs representing finite TZs) are optimized without any constraints inherent to acoustic technology in order to demonstrate the method's capability for other types of technologies which consider NRNs in their equivalent nodal representation.

After optimization procedure the resulting lossy coupling matrix of the network has been obtained where $\delta_i = [0.1000, 0.0250, 0.0258, 0.0265, 0.0270, 0.0269]$ which correspond to $Q_i = [300, 1200, 1163, 1132, 1111, 1116]$. These quality factor values are necessary to implement in fabrication process in order to achieve a flat passband IL level of 2.2 dB. Transmission and reflection response of lossy network at out-of-band and in-band frequencies are shown in Figure 5.6 (a) and (b), respectively. Deterioration of RL level and different slope of S_{21} at higher frequencies can be observed in Figure 5.6 (a) which is due to Chebyshev function disruption. However, flat passband IL level has been achieved which is demonstrated in Figure 5.6 (b).

Two examples have been performed in order to validate the methodology of lossy filter

synthesis for different topologies and technologies. Flat passband IL level has been achieved in both cases; however, a negative impact on RL level inherent for lossy synthesis techniques is presented as well. A change of weighting values can improve RL level, although a situation of finite TZs' movement can be found in this case. For acoustic technology the position of finite TZs is very important since it defines the filter's selectivity. However, for other types of technology their movement can be suitable.

5.5   Chapter Summary

In this chapter lossy synthesis technique for ladder-type acoustic filters has been presented. Existing lossy methods not only provide lossy resonators but also implement resistive or complex couplings and inverters. In acoustic technology lossy inverters cannot be realized since they are not physically implemented and serve to transform inline topology into ladder-type representation. Moreover, up-to-date lossy methodologies do not consider topologies with NRNs.

The proposed technique based on gradient-based optimization and coupling matrix approach resolves these drawbacks, i.e., it deals with NRNs and includes losses only in resonators. The main objective of the optimization is to achieve a flat passband IL level, thus avoiding edge-rounding and maintaining the rectangular passband shape. It has been demonstrated that it is not necessary to implement all high-Q resonators in order to achieve this goal.

Two examples have been provided to demonstrate the possible functionalities of the proposed technique, depending on input parameters. In this approach we do not consider either lossy NRNs or lossy capacitive and inductive external elements. Nevertheless, this technique can be applied for acoustic and any other technology with possibility of cross-coupling application as an initial lossy approximation.

Conclusions and Future Work

Number of mobile devices is constantly growing around the world, including developing countries. In order to provide an outstanding quality of mobile communications, acoustic filters have become object of continuous improvement. 4G and upcoming 5G telecommunication networks require augmented number of filters implemented into the handset front-end with their higher complexity of fabrication. In this competitive environment manufacturers make a lot of effort to provide the best possible filtering solution in terms of chip size, reliability, and frequency performance, investigating materials, structures, topologies, and fabrication processes.

Wide spreading of carrier aggregation technology and implementation of multiplexers have raised the difficulty level of filters' design even more. Indeed, modern filtering networks not only have to exhibit high selectivity, high rejection at stopband frequencies, and flat passband, but also not to load each other, causing interferences. Moreover, acoustic technological constraints have to be considered as well. Thus, filter design procedure becomes a real challenge where time and money resources also play an important role. Numerous optimization methods generally used in industry are good solution for acoustic filters' design; however, they need well-chosen starting seed.

In this work we have provided systematic methodologies which allow to obtain a filtering network, fulfilling mask specifications and acoustic technological constraints. Since here we do not consider either electromagnetic effects or package influence, proposed methodologies can act as starting seed for further optimization process in order to complete full design of the device. Application of mathematical filter synthesis makes the design more efficient compared with traditional optimization techniques and provides better understanding of interdependent behavior of input parameters and technological constraints such as effective coupling coefficient, resonant frequencies, quality factor, power handling, and others. Depending on applications and

required numerical precision, we provide the possibility to synthesize acoustic filters, duplexers, and multiplexers in lowpass domain with further lowpass-to-bandpass transformation or using direct bandpass synthesis methodology.

Thus, Chapter 2 deals with commonly used classical lowpass synthesis approach. In order to be described by mathematical tools, acoustic resonator has to be performed by electrical equivalent BVD circuit able to provide both series and parallel resonant frequencies. For this purpose, lowpass BVD circuit implements FIR elements, thus permitting to establish an equivalence between BVD and dangling resonator representation. Initial set of finite normalized TZs is directly related to inline filter topology consisted of concatenation of dangling resonators. These finite TZs together with RL level and frequency band specifications define Chebyshev filtering function and characteristic polynomials of the network which completely describe frequency behavior of mathematical filtering prototype. Resulting bandpass lumped elements of ladder-type acoustic filter are then obtained by means of extraction procedure. By applying an automatic search engine of input parameters of acoustic filter, it becomes possible to fulfill both mask specifications and technological constraints in fast and precise way. An additional option of input phase correction by means of complementary inductors at source and load ports allows to synthesize duplexers and multiplexers, avoiding loading effect, and thus providing a better overall transmission and reflection response.

Upcoming 5G network standard with stringent specifications and multiplexers implementation may require an advanced methodology for synthesis and design of ladder-type acoustic filters. For this purpose, a direct bandpass synthesis technique has been elaborated in Chapter 3. This alternative method allows to overcome the lack of precision of narrowband lowpass approach and performs perfect magnitude and phase response of transmission and reflection parameters at in-band and out-of-band frequencies. Considering only frequency dependent nodes in dangling resonator model and at source and load complicates derivation of characteristics polynomials and elements' extraction procedure; however, it allows to take into account TZs at the origin and infinity at the beginning of filter's synthesis.

Thus, four basic ladder-type topologies with capacitive and inductive matching elements have been presented and analyzed. Two Chebyshev filtering functions have been proposed in order to mathematically describe complete frequency behavior of acoustic wave filter over the whole frequency range. Unlike existing filtering functions reported by Amari et al. [82] and Zhang et al. [83], the presented two in this work do not introduce additional undesirable RZs over the whole frequency range, exhibit high attenuation level at out-of-band frequencies, and are suitable for ladder-type acoustic wave filters. Recursive technique for characteristic polynomials' calculation has been updated in order to include TZs at the origin and infinity. Finally, bandpass elements' extraction procedure has been elaborated which made possible the obtaining of positive capacitive and inductive elements of the network. Micro-acoustic technological parameters

have been included in the design so as to provide a realistic filtering network. Since the direct bandpass methodology exhibits numerical instabilities, Multiprecision Computing Toolbox was successfully implemented in synthesis routine, thus providing accurate results for design of high-order filters. Position of prescribed finite TZs is maintained since no error of lowpass-to-bandpass transformation has to be considered; therefore, mask specifications' fulfillment can be evaluated prior to the synthesis.

In this work, bandpass methodology has been presented only for four general ladder-type topologies. Every additional TZ appeared because of external ground loop inductor or inclusion of cross-couplings lead to modification of filtering function and have not been considered. This issue makes the methodology difficult to generalize. The problem of method systematization becomes even more complex with following characteristic polynomials' calculation and extraction procedure which still is not resolved even in classical lowpass approach. Nevertheless, the proposed methodology can be a useful tool for designing of challenging filtering ladder-type networks for future applications.

In order to design duplexers and multiplexers devices in direct bandpass methodology, a novel phase correction technique has been developed and described in Chapter 4. Well-known phase application by means of complex term suitable for lowpass approach cannot be implemented in bandpass synthesis technique since it results in complex BVD elements which cannot be physically implemented. Thus, in order to modify input/output capacitors and inductors, two coefficient, A and B, have been introduced into the filtering function. By this way, roots of characteristic polynomials $F(s)$ and $E(s)$ also change, leading to different slopes of transmission response. This is the main difference from lowpass synthesis where phase modification does not provoke any variation in filter's performance. Proposed phase correction method in bandpass domain allows to achieve $0°$ phase for both stand-alone filters and duplexers, leading to modification or even exclusion of input/output matching elements. Multiple choice of phase correction has been proposed in case of networks with inductive matching elements. Nevertheless, not any phase value can be accommodated by this technique. Inherent synthesis and technological limitations reduce the highest possible phase variation to $±130°$. But still, it is enough for design of majority of filtering circuits.

Managements of one of the most important technological constraints, quality factor Q, has been provided in Chapter 5. Implementation of gradient-based optimization technique together with coupling matrix approach allowed to synthesize acoustic filters with losses only in resonators and achieve flat passband without edge-rounding. The method takes into account technological features of inline topology and maintains the position of prescribed finite TZs. Moreover, proposed lossy synthesis technique can be used for any type of technology and topology consisted of resonant and non-resonating nodes with and without cross-couplings. Nevertheless, RL level deterioration inherent for lossy techniques is also obtained since optimization method disrupts

Chebyshev filtering function. Moreover, the process of filter design can be time-consuming, especially for networks of order eight and higher. However, the lossy technique can be useful for study of critical resonators existence and for evaluation of possible quality factor distribution in order to avoid passband edge-rounding and loss of spectrum.

Throughout the Ph.D. program, different software tools have been elaborated in order to accommodate presented in this work theories. They allow to design ladder-type acoustic filters directly in bandpass domain and perform lossy filtering networks suited for micro-acoustic technology and fulfilling mask specifications.

6.1   Future Work

Presented in this work methodologies for synthesis and design of acoustic wave networks provide deep understanding of mathematical and physical behavior of these devices. The most important technological constraints are taken into account in the synthesis routine. However, inclusion of many other processes can provide more realistic filtering model which, in turn, will complicate the synthesis procedure even more. Nevertheless, elaborated techniques can act as basic tools in order to keep investigating more sophisticated topologies or as an initial seed for further optimization processes.

In terms of theoretical work presented in this thesis, some future work lines can be denoted:

1. Direct bandpass methodology presented in this work considers four basic ladder-type topologies. Inclusion of additional TZs appeared from external ground loop inductors into the filtering function can be next step in order to expand the possibilities of the method. Also, bandpass networks with cross-couplings (frequency dependent or not) can be synthesized, simulating electromagnetic effects in the structure. All this leads to a necessity to generalize filtering function, recursive technique of characteristic polynomials, and elements' extraction procedure which can be a challenging task.

2. As a previous step of bandpass methodology systematization, the updating of filtering function, recursive technique, and extraction procedure of networks with external elements can be studied and elaborated in classical lowpass approach.

3. Doubly- and singly-terminated filters of minimum input admittance are useful for duplexer and multiplexer devices, especially in switched configuration, since the loading effect is almost absent in this type of networks. Thus, new procedure of characteristic polynomials calculation for these devices can be elaborated in bandpass domain.

4. Phase correction methodology can be improved by establishing the mathematical relationship between coefficients A and B and modified phase value. Moreover, the possibility to

correct phase value beyond $\pm 130°$ would allow to synthesize any type of networks.

5. Inclusion of losses into NRNs and consideration of both Q_s and Q_p in the lossy synthesis technique will provide more realistic acoustic filter model. However, it will increase the number of optimized variables and make the optimization process very time-consuming. Therefore, other methods by means of lossy characteristic polynomials would be more preferable. But in this case, introduction of losses only into resonators has to be assured.

Wide spreading of current 4G and upcoming 5G network standards motivates the manufacturers to investigate and innovate performance, form factor, and fabrication of acoustic devices. Facing future challenging demands, there is still much to do in order to fulfill the end-user great expectations in terms of data rates, latencies, and capacity. Thus, thanks to its characteristics, micro-acoustic technology will maintain its leading position in mobile segment for at least 10 years more.

Bibliography

[1] GSM Association, "The mobile economy 2018," 2018, [Online]. Available: www.gsma.com/mobileeconomy.

[2] 3GPP: The Mobile Broadband Standard, "Release 15," December 2017, [Online]. Available: www.3gpp.org/release-15.

[3] Ericsson, "Ericsson mobility report," November 2017, [Online]. Available: www.ericsson.com/assets/local/mobility-report/documents/2017/ericsson-mobility-report-november-2017.pdf.

[4] S. Mahon, "The 5G effect on RF filter technologies," *IEEE Transactions on Semiconductor Manufacturing*, vol. 30, no. 4, pp. 494–499, Nov 2017.

[5] F. Jameel, Faisal, M. A. A. Haider, and A. A. Butt, "Massive MIMO: A survey of recent advances, research issues and future directions," in *2017 International Symposium on Recent Advances in Electrical Engineering (RAEE)*, Oct 2017, pp. 1–6.

[6] W. Hong, Z. H. Jiang, C. Yu, J. Zhou, P. Chen, Z. Yu, H. Zhang, B. Yang, X. Pang, M. Jiang, Y. Cheng, M. K. T. Al-Nuaimi, Y. Zhang, J. Chen, and S. He, "Multibeam antenna technologies for 5G wireless communications," *IEEE Transactions on Antennas and Propagation*, vol. 65, no. 12, pp. 6231–6249, Dec 2017.

[7] M. Iwamura, K. Etemad, M. h. Fong, R. Nory, and R. Love, "Carrier aggregation framework in 3GPP LTE-Advanced [WiMAX/LTE update]," *IEEE Communications Magazine*, vol. 48, no. 8, pp. 60–67, August 2010.

[8] A. Bhamri, K. Hooli, and T. Lunttila, "Massive carrier aggregation in LTE-Advanced Pro: impact on uplink control information and corresponding enhancements," *IEEE Communications Magazine*, vol. 54, no. 5, pp. 92–97, May 2016.

[9] M. Amara and A. Feki, "Downlink radio resource allocation with MU-MIMO and carrier aggregation in 5G networks," in *2017 IEEE 28th Annual International Symposium on Personal, Indoor, and Mobile Radio Communications (PIMRC)*, Oct 2017, pp. 1–6.

[10] E. Schmidhammer, T. Metzger, and C. Hoffmann, "Multiplexers: A necessary extension for 4G/5G systems," in _2016 IEEE MTT-S International Microwave Symposium (IMS)_, May 2016, pp. 1–4.

[11] G. G. Fattinger, A. Volatier, M. Al-Joumayly, Y. Yusuf, R. Aigner, N. Khlat, and M. Granger-Jones, "Carrier aggregation and its challenges - or: The golden age for acoustic filters," in _2016 IEEE MTT-S International Microwave Symposium (IMS)_, May 2016, pp. 1–4.

[12] K.-Y. Hashimoto, _Surface Acoustic Wave Devices in Telecommunications: Modelling and Simulation_, Berlin: Springer, 2000.

[13] J. C. Chen, H. Y. Yang, J. W. Wu, S. C. Lin, and S. F. Chang, "Widening the data pipeline: A carrier aggregation BAW quadplexer module," _IEEE Microwave Magazine_, vol. 19, no. 2, pp. 62–69, March 2018.

[14] Yamaji Toru and Goto Rei, "Surface acoustic wave elements with varying electrode finger pitch and connection arrangements," April 2018, European Patent Office, US2018109238 (A1).

[15] M. Solal, J. Gratier, R. Aigner, and K. Gamble, "Piston mode acoustic wave device and method providing a high coupling factor," May 2011, US Patent 7,939,989 B2.

[16] T. Bauer, C. Eggs, K. Wagner, and P. Hagn, "A bright outlook for acoustic filtering: A new generation of very low-profile SAW, TC SAW, and BAW devices for module integration," _IEEE Microwave Magazine_, vol. 16, no. 7, pp. 73–81, Aug 2015.

[17] B. Abbott, A. Chen, T. Daniel, K. Gamble, T. Kook, M. Solal, K. Steiner, R. Aigner, S. Malocha, C. Hella, M. Gallagher, and J. Kuypers, "Temperature compensated SAW with high quality factor," in _2017 IEEE International Ultrasonics Symposium (IUS)_, Sept 2017, pp. 1–7.

[18] T. Takai, H. Iwamoto, Y. Takamine, T. Wada, M. Hiramoto, M. Koshino, and N. Nakajima, "Investigations on design technologies for SAW quadplexer with narrow duplex gap," in _2016 IEEE MTT-S International Microwave Symposium (IMS)_, May 2016, pp. 1–4.

[19] K.-Y. Hashimoto, "Advances in RF SAW devices: What are demanded?," in _2016 European Frequency and Time Forum (EFTF)_, April 2016, pp. 1–4.

[20] K.-Y. Hashimoto, _RF Bulk Acoustic Wave Filters for Communications_, Artech House, 2009.

[21] Christian C Enz and Andreas Kaiser, _MEMS-based Circuits and Systems for Wireless Communication_, Springer, 2013.

[22] Chang Chia-Ta, Chiang Chih-Feng, and Hsieh Tzu-Sheng, "Bulk acoustic wave resonator with a mass adjustment structure and its application to bulk acoustic wave filter," April 2018, European Patent Office, US2018109240 (A1).

[23] R. Ruby, "A decade of FBAR success and what is needed for another successful decade," in *2011 Symposium on Piezoelectricity, Acoustic Waves and Device Applications (SPAWDA)*, Dec 2011, pp. 365–369.

[24] T. Yokoyama, T. Nishihara, S. Taniguchi, M. Iwaki, Y. Satoh, M. Ueda, and T. Miyashita, "New electrode material for low-loss and high-Q FBAR filters," in *2004 IEEE Ultrasonics Symposium*, Aug 2004, vol. 1, pp. 429–432 Vol.1.

[25] J. B. Shealy, R. Vetury, S. R. Gibb, M. D. Hodge, P. Patel, M. A. McLain, A. Y. Feldman, M. D. Boomgarden, M. P. Lewis, B. Hosse, and R. Holden, "Low loss, 3.7GHz wideband BAW filters, using high power single crystal AlN-on-SiC resonators," in *2017 IEEE MTT-S International Microwave Symposium (IMS)*, June 2017, pp. 1476–1479.

[26] T. Yokoyama, M. Hara, M. Ueda, and Y. Satoh, "K-band ladder filters employing air-gap type thin film bulk acoustic resonators," in *2008 IEEE Ultrasonics Symposium*, Nov 2008, pp. 598–601.

[27] M. Hara, T. Yokoyama, T. Sakashita, M. Ueda, and Y. Satoh, "A study of the thin film bulk acoustic resonator filters in several ten GHz band," in *2009 IEEE International Ultrasonics Symposium*, Sept 2009, pp. 851–854.

[28] C. C. W. Ruppel, "Acoustic wave filter technology – a review," *IEEE Transactions on Ultrasonics, Ferroelectrics, and Frequency Control*, vol. 64, no. 9, pp. 1390–1400, Sept 2017.

[29] R. Lanz and P. Muralt, "Bandpass filters for 8 GHz using solidly mounted bulk acoustic wave resonators," *IEEE Transactions on Ultrasonics, Ferroelectrics, and Frequency Control*, vol. 52, no. 6, pp. 938–948, June 2005.

[30] S. Marksteiner, J. Kaitila, G. G. Fattinger, and R. Aigner, "Optimization of acoustic mirrors for solidly mounted BAW resonators," in *IEEE Ultrasonics Symposium, 2005.*, Sept 2005, vol. 1, pp. 329–332.

[31] T. Nishihara, S. Taniguchi, and M. Ueda, "Increased piezoelectric coupling factor in temperature-compensated film bulk acoustic resonators," in *2015 IEEE International Ultrasonics Symposium (IUS)*, Oct 2015, pp. 1–4.

[32] R. Weigel, D. P. Morgan, J. M. Owens, A. Ballato, K. M. Lakin, K. Hashimoto, and C. C. W. Ruppel, "Microwave acoustic materials, devices, and applications," *IEEE Transactions on Microwave Theory and Techniques*, vol. 50, no. 3, pp. 738–749, Mar 2002.

[33] Q. Yang, W. Pang, D. Zhang, and H. Zhang, "A wideband bulk acoustic wave filter with modified lattice configuration," in *2015 IEEE MTT-S International Microwave Symposium*, May 2015, pp. 1–4.

[34] A. A. Shirakawa, J. B. David, P. Vincent, M. El Hassan, E. Kerherve, and A. Cathelin, "A mixed ladder-lattice bulk acoustic wave duplexer for W-CDMA handsets," in *2007 14th IEEE International Conference on Electronics, Circuits and Systems*, Dec 2007, pp. 554–557.

[35] Edén Corrales López, *Analysis and Design of Bulk Acoustic Wave Filters Based on Acoustically Coupled Resonators*, Ph.D. thesis, Universitat Autònoma de Barcelona, 2011.

[36] R. Ruby, S. R. Gilbert, A. Chien, and T. Jamneala, "GPS and WiFi single ended to differential CRF filters using SiOCH as a de-coupling layer," in *2009 IEEE International Ultrasonics Symposium*, Sept 2009, pp. 872–875.

[37] Kun Wang, U. Koelle, J. D. Larson, R. Thalhammer, and S. Martin, "FBAR laterally coupled resonator filter," in *2015 IEEE International Ultrasonics Symposium (IUS)*, Oct 2015, pp. 1–5.

[38] K. Uehara and T. Sato, "Design of a split type filter for wide band cellular system," in *2016 IEEE International Ultrasonics Symposium (IUS)*, Sept 2016, pp. 1–4.

[39] Mercedes Jimenez Blasco and Pedro de Paco, *A coupling matrix vision for mobile filtering devices with micro-acoustic wave technologies. A systematic approach*, Ph.D. thesis, Universitat Autònoma de Barcelona, 2015.

[40] K. M. Lakin, "Bulk acoustic wave coupled resonator filters," in *Proceedings of the 2002 IEEE International Frequency Control Symposium and PDA Exhibition (Cat. No.02CH37234)*, 2002, pp. 8–14.

[41] Jordi Verdú Tirado, *Bulk acoustic wave resonators and their application to microwave devices*, Ph.D. thesis, Universitat Autònoma de Barcelona, 2010.

[42] W.P. Mason, *Piezoelectric Crystals and Their Application to Ultrasonics*, The Bell Telephone Laboratories series. Van Nostrand, 1950.

[43] T. L. Rhyne, "An improved interpretation of mason's model for piezoelectric plate transducers," *IEEE Transactions on Sonics and Ultrasonics*, vol. 25, no. 2, pp. 98–103, March 1978.

[44] D. A. Feld, D. S. Shim, S. Fouladi, and F. Bayatpur, "Advances in nonlinear measurement & modeling of bulk acoustic wave resonators (invited)," in *2014 IEEE International Ultrasonics Symposium*, Sept 2014, pp. 264–272.

[45] D. Karolewski, C. Schaffel, A. Tag, V. Silva Cortes, A. Hagelauer, and G. Fischer, "Modeling of BAW filters for system level simulation," in *2015 German Microwave Conference*, March 2015, pp. 410–413.

[46] M. Solal, M. Gallagher, and A. Tajic, "Full 3D simulation of SAW resonators using hierarchical cascading FEM," in *2017 IEEE International Ultrasonics Symposium (IUS)*, Sept 2017, pp. 1–5.

[47] I. S. Uzunov, M. D. Terzieva, B. M. Nikolova, and D. G. Gaydazhiev, "Extraction of modified Butterworth-Van Dyke model of FBAR based on FEM analysis," in *2017 XXVI International Scientific Conference Electronics (ET)*, Sept 2017, pp. 1–4.

[48] J. Fan, M. Chatras, and D. Cros, "Synthesis method for BAW filters computation," in *2006 13th IEEE International Conference on Electronics, Circuits and Systems*, Dec 2006, pp. 391–394.

[49] J. D. Larson, P. D. Bradley, S. Wartenberg, and R. C. Ruby, "Modified Butterworth-Van Dyke circuit for FBAR resonators and automated measurement system," in *2000 IEEE Ultrasonics Symposium. Proceedings. An International Symposium (Cat. No.00CH37121)*, Oct 2000, vol. 1, pp. 863–868 vol.1.

[50] R. Baum, "Design of unsymmetrical band-pass filters," *IRE Transactions on Circuit Theory*, vol. 4, no. 2, pp. 33–40, Jun 1957.

[51] P. Zhao and K. L. Wu, "An iterative and analytical approach to optimal synthesis of a multiplexer with a star-junction," *IEEE Transactions on Microwave Theory and Techniques*, vol. 62, no. 12, pp. 3362–3369, Dec 2014.

[52] C. Dillon and L. Lind, "Cascade synthesis of polylithic crystal filters containing double-resonator monolithic crystal filter (MCF) elements," *IEEE Transactions on Circuits and Systems*, vol. 23, no. 3, pp. 146–154, Mar 1976.

[53] H. Bell, "Transformed-variable synthesis of narrow-bandpass filters," *IEEE Transactions on Circuits and Systems*, vol. 26, no. 6, pp. 389–394, Jun 1979.

[54] Richard J Cameron, Raafat Mansour, and Chandra M Kudsia, *Microwave filters for communication systems: fundamentals, design and applications*, Wiley-Interscience, 2007.

[55] S. Amari and G. Macchiarella, "Synthesis of inline filters with arbitrarily placed attenuation poles by using nonresonating nodes," *IEEE Transactions on Microwave Theory and Techniques*, vol. 53, no. 10, pp. 3075–3081, Oct 2005.

[56] S. Amari, U. Rosenberg, and J. Bornemann, "Singlets, cascaded singlets, and the nonresonating node model for advanced modular design of elliptic filters," *IEEE Microwave and Wireless Components Letters*, vol. 14, no. 5, pp. 237–239, May 2004.

[57] R. J. Cameron, "Advanced coupling matrix synthesis techniques for microwave filters," *IEEE Transactions on Microwave Theory and Techniques*, vol. 51, no. 1, pp. 1–10, Jan 2003.

[58] A. Gimenez and P. de Paco, "Involving source-load leakage effects to improve isolation in ladder acoustic wave filters," in *2016 IEEE MTT-S International Microwave Symposium (IMS)*, May 2016, pp. 1–4.

[59] F. Z. Bi and B. P. Barber, "Bulk acoustic wave RF technology," *IEEE Microwave Magazine*, vol. 9, no. 5, pp. 65–80, Oct 2008.

[60] P. Warder and A. Link, "Golden age for filter design: Innovative and proven approaches for acoustic filter, duplexer, and multiplexer design," *IEEE Microwave Magazine*, vol. 16, no. 7, pp. 60–72, Aug 2015.

[61] Jia-Shen G Hong and Michael J Lancaster, *Microstrip filters for RF/microwave applications*, vol. 167, John Wiley & Sons, 2004.

[62] R. J. Cameron, "Advanced filter synthesis," *IEEE Microwave Magazine*, vol. 12, no. 6, pp. 42–61, Oct 2011.

[63] Pierre Jarry and Jacques Beneat, *Advanced Design Techniques and Realizations of Microwave and RF Filters*, John Wiley & Sons, 2008.

[64] S. Amari and U. Rosenberg, "Synthesis and design of novel in-line filters with one or two real transmission zeros," *IEEE Transactions on Microwave Theory and Techniques*, vol. 52, no. 5, pp. 1464–1478, May 2004.

[65] Alfred Gimenez Bonastre and Pedro de Paco, *RF Filters and Multiplexers Based on Acoustic Wave Technologies with Ladder-Type and Cross-Coupled Topologies*, Ph.D. thesis, Universitat Autònoma de Barcelona, 2016.

[66] Y. He, G. Wang, and L. Sun, "Direct matrix synthesis approach for narrowband mixed topology filters," *IEEE Microwave and Wireless Components Letters*, vol. 26, no. 5, pp. 301–303, May 2016.

[67] X. Yu, Z. X. Xu, Y. Y. Hu, J. Le-Wei Li, and S. Sun, "Synthesis of dual-band filters with an arbitrary load and asymmetric responses," in *2015 Asia-Pacific Microwave Conference (APMC)*, Dec 2015, vol. 3, pp. 1–3.

[68] J. D. Rhodes and R. J. Cameron, "General extracted pole synthesis technique with applications to low-loss TE011 mode filters," *IEEE Transactions on Microwave Theory and Techniques*, vol. 28, no. 9, pp. 1018–1028, Sep 1980.

[69] Y. Yang, M. Yu, and Q. Wu, "Advanced synthesis technique for unified extracted pole filters," *IEEE Transactions on Microwave Theory and Techniques*, vol. 64, no. 12, pp. 4463–4472, Dec 2016.

[70] R. Ruby, "The "how & why" a deceptively simple acoustic resonator became the basis of a multi-billion dollar industry," in *2017 IEEE 30th International Conference on Micro Electro Mechanical Systems (MEMS)*, Jan 2017, pp. 308–313.

[71] R. Ruby, "11E-2 review and comparison of bulk acoustic wave FBAR, SMR technology," in *2007 IEEE Ultrasonics Symposium Proceedings*, Oct 2007, pp. 1029–1040.

[72] S. Mishin and Y. Oshmyansky, "Improving coupling coefficient distribution on BAW filters manufactured on 200mm wafers," in *2017 Joint Conference of the European Frequency and Time Forum and IEEE International Frequency Control Symposium (EFTF/IFCS)*, July 2017, pp. 542–546.

[73] T. Takai, H. Iwamoto, Y. Takamine, H. Yamazaki, T. Fuyutsume, H. Kyoya, T. Nakao, H. Kando, M. Hiramoto, T. Toi, M. Koshino, and N. Nakajima, "High-performance SAW resonator on new multilayered substrate using LiTaO3 crystal," *IEEE Transactions on Ultrasonics, Ferroelectrics, and Frequency Control*, vol. 64, no. 9, pp. 1382–1389, Sept 2017.

[74] D. A. Feld, R. Parker, R. Ruby, P. Bradley, and S. Dong, "After 60 years: A new formula for computing quality factor is warranted," in *2008 IEEE Ultrasonics Symposium*, Nov 2008, pp. 431–436.

[75] A. Tag, R. Weigel, A. Hagelauer, B. Bader, C. Huck, M. Pitschi, K. Wagner, D. Karolewski, and C. Schaffel, "Influence of temperature distribution on behavior, modeling, and reliability of BAW resonators," in *2014 IEEE International Reliability Physics Symposium*, June 2014, pp. 5C.5.1–5C.5.7.

[76] J. Costa, S. McHugh, N. Rice, P. J. Turner, B. A. Willemsen, N. O. Fenzi, R. B. Hammond, J. D. Ha, C. H. Lee, and T. Sato, "Design and characterization of SAW filters for high power performance," in *2017 IEEE International Ultrasonics Symposium (IUS)*, Sept 2017, pp. 1–4.

[77] A. Tag, V. Chauhan, C. Huck, B. Bader, D. Karolewski, F. M. Pitschi, R. Weigel, and A. Hagelauer, "A method for accurate modeling of BAW filters at high power levels," *IEEE Transactions on Ultrasonics, Ferroelectrics, and Frequency Control*, vol. 63, no. 12, pp. 2207–2214, Dec 2016.

[78] T. Mirea, J. Olivares, M. Clement, J. L. Olivera, J. Sangrador, and E. Iborra, "AlN-solidly mounted resonators sustaining up to 1000C with TCF compensation," in *2017*

Joint Conference of the European Frequency and Time Forum and IEEE International Frequency Control Symposium (EFTF/IFCS), July 2017, pp. 519–522.

[79] S. Dasgupta, B. Block, P. Fischer, H. Then, and M. Radosavljevic, "Film bulk acoustic resonator (FBAR) devices for high frequency RF filters," April 2018, European Patent Office, WO2018063294 (A1).

[80] G. Macchiarella, M. Oldoni, F. Seyfert, and S. Amari, "Synthesis of microwave filters with reactive nodes," in *2012 42nd European Microwave Conference*, Oct 2012, pp. 467–470.

[81] Y. He, G. Macchiarella, G. Wang, W. Wu, L. Sun, L. Wang, and R. Zhang, "A direct matrix synthesis for in-line filters with transmission zeros generated by frequency-variant couplings," *IEEE Transactions on Microwave Theory and Techniques*, vol. 66, no. 4, pp. 1780–1789, April 2018.

[82] S. Amari, F. Seyfert, and M. Bekheit, "Theory of coupled resonator microwave bandpass filters of arbitrary bandwidth," *IEEE Transactions on Microwave Theory and Techniques*, vol. 58, no. 8, pp. 2188–2203, Aug 2010.

[83] R. Zhang and L. Zhu, "Synthesis of dual-wideband bandpass filters with source-load coupling network," *IEEE Transactions on Microwave Theory and Techniques*, vol. 62, no. 3, pp. 441–449, March 2014.

[84] Anatol I Zverev, *Handbook of filter synthesis*, Wiley-Blackwell, 2005.

[85] R. M. Foster, "A reactance theorem," *The Bell System Technical Journal*, vol. 3, no. 2, pp. 259–267, April 1924.

[86] Advanpix, *Multiprecision Computing Toolbox*, [Online]. Available: https://www.advanpix.com.

[87] Matteo Oldoni, Giuseppe Macchiarella, and Fabien Seyfert, *Synthesis and modelling techniques for microwave filters and diplexers: advances in analytical methods with applications to design and tuning*, Scholars' Press, 2014.

[88] R. M. Livingston, "Predistorted waveguide filters for use in communications systems," in *1969 G-MTT International Microwave Symposium*, May 1969, pp. 291–297.

[89] A. E. Williams, W. G. Bush, and R. R. Bonetti, "Predistortion techniques for multicoupled resonator filters," in *1984 IEEE MTT-S International Microwave Symposium Digest*, May 1984, pp. 290–291.

[90] M. Yu and V. Miraftab, "Shrinking microwave filters," *IEEE Microwave Magazine*, vol. 9, no. 5, pp. 40–54, Oct 2008.

[91] B. S. Senior, I. C. Hunter, and J. D. Rhodes, "Synthesis of lossy filters," in *2002 32nd European Microwave Conference*, Sept 2002, pp. 1–4.

[92] A. C. Guyette, I. C. Hunter, and R. D. Pollard, "The design of microwave bandpass filters using resonators with nonuniform Q," *IEEE Transactions on Microwave Theory and Techniques*, vol. 54, no. 11, pp. 3914–3922, Nov 2006.

[93] V. Miraftab and M. Yu, "Generalized lossy microwave filter coupling matrix synthesis and design using mixed technologies," *IEEE Transactions on Microwave Theory and Techniques*, vol. 56, no. 12, pp. 3016–3027, Dec 2008.

[94] Y. Zhao and G. Wang, "Multi-objective optimisation technique for coupling matrix synthesis of lossy filters," *IET Microwaves, Antennas Propagation*, vol. 7, no. 11, pp. 926–933, August 2013.

[95] J. Nocedal and S. J. Wright, *Numerical Optimization*, Springer, 2nd edition, 2006.

[96] R. J. Cameron, "Advanced coupling matrix synthesis techniques for microwave filters," *IEEE Transactions on Microwave Theory and Techniques*, vol. 51, no. 1, pp. 1–10, Jan 2003.

[97] H. C. Bell, "The coupling matrix in low-pass prototype filters," *IEEE Microwave Magazine*, vol. 8, no. 2, pp. 70–76, April 2007.

[98] R. J. Cameron, "Advanced filter synthesis," *IEEE Microwave Magazine*, vol. 12, no. 6, pp. 42–61, Oct 2011.

[99] M. Meng, I. C. Hunter, and J. D. Rhodes, "The design of parallel connected filter networks with nonuniform Q resonators," *IEEE Transactions on Microwave Theory and Techniques*, vol. 61, no. 1, pp. 372–381, Jan 2013.

[100] S. Amari, "Synthesis of cross-coupled resonator filters using an analytical gradient-based optimization technique," *IEEE Transactions on Microwave Theory and Techniques*, vol. 48, no. 9, pp. 1559–1564, Sep 2000.

[101] Meng Meng, *Design and Synthesis of Lossy Microwave Filters*, Ph.D. thesis, 2014.